BEHAVIORAL ENGINEERING LABORATORY
Department of Psychology
New Mexico State University

May 1985

AD-A161 364

A MULTIPLE-REGRESSION MODEL OF PILOT PERFORMANCE IN VERTICAL AND TRANSLATIONAL FLIGHT

John Wiedemann and
Stanley N. Roscoe

NOV 1 3 1985

85 11 12 021

REPORT DOCUMENTATION PAGE	READ INSTRUCTIONS BEFORE COMPLETING FORM

1. REPORT NUMBER BEL-85-2/ONR-85-2 ✓	2. GOVT ACCESSION NO. AD-A16136 4	3. RECIPIENT'S CATALOG NUMBER

4. TITLE (and Subtitle) A Multiple-Regression Model of Pilot Performance in Vertical and Translational Flight	5. TYPE OF REPORT & PERIOD COVERED Technical Report
	6. PERFORMING ORG. REPORT NUMBER

7. AUTHOR(s) John Wiedemann and Stanley N. Roscoe	8. CONTRACT OR GRANT NUMBER(s) N00014-81-K0439

9. PERFORMING ORGANIZATION NAME AND ADDRESS Behavioral Engineering Laboratory New Mexico State University, Box 5095 Las Cruces, NM 88003	10. PROGRAM ELEMENT, PROJECT, TASK AREA & WORK UNIT NUMBERS NR 196-170

11. CONTROLLING OFFICE NAME AND ADDRESS Engineering Psychology Programs Office of Naval Research 800 N. Quincy Street, Arlington, VA 22217	12. REPORT DATE May 1985
	13. NUMBER OF PAGES 92

14. MONITORING AGENCY NAME & ADDRESS(if different from Controlling Office)	15. SECURITY CLASS. (of this report) Unclassified
	15a. DECLASSIFICATION/DOWNGRADING SCHEDULE

16. DISTRIBUTION STATEMENT (of this Report)

This document has been approved for public release and sale; its distribution is unlimited

17. DISTRIBUTION STATEMENT (of the abstract entered in Block 20, if different from Report)

18. SUPPLEMENTARY NOTES

19. KEY WORDS (Continue on reverse side if necessary and identify by block number)

Helicopter flight instrumentation,	Predictor displays,
VTOL flight instrumentation,	Horizontal situation displays,
Computer graphic displays,	Vertical situation displays,
Contact analog displays,	Translational flight,
Frequency-separated displays,	Vertical flight.

20. ABSTRACT (Continue on reverse side if necessary and identify by block number)

An experiment was conducted to advance the development of a multiple-regression model of VTOL pilot performance as a function of various control/display system and flight mission variables. Second-order response surfaces as a function of two control system design variables (translational control order and vertical control gain reduction factor) and three downward-looking display design variables (horizontal position error magnification, translational prediction time, and translational tracking mode) were derived from

Pilot performances on each of three mission scenarios. The optimum values
for each of the five system design variables were determined for each
scenario independently using the same central composite experimental design
with three groups of four subjects each. Comprehensive analyses of
variance and canonical analyses were used to refine the fitted surfaces to
determine the true nature of the pilot performance effects for each flight
scenario and to select a single set of system design parameters that would
yield near-optimum performances on all three scenarios.

CONTENTS

LIST OF FIGURES

LIST OF TABLES

SUMMARY

An Office of Naval Research (ONR) project at the Behavioral
Engineering Laboratory (BEL) of New Mexico State University has led
to the development of a horizontal display for all-weather vertical
and translational flight in vertical takeoff and landing (VTOL)
aircraft (Roscoe, Hull, Simon, and Corl, 1981; Roscoe, 1982; Roscoe,
Tatro, and Trujillo, 1984; Tatro, Corl, and Roscoe, 1983). This
HOVERING display provides the pilot with information critical in
taking advantage of the VTOL's inherent ability to fly missions
totally beyond the capabilities of fixed-wing airplanes.

Before attempting to make the HOVERING display operational, the
critical elements for pilot performance must be experimentally
identified and optimized across various mission scenarios. To
achieve this goal, a holistic experimental philosophy has been
adopted by BEL whereby as many potentially critical real-world
variables as possible are experimentally tested to evaluate their
absolute contributions to the total variance in system performance.
To the extent the goal of a holistic investigation is achieved, the
potential for biased data will be reduced to a minimum and
predictability to real-world situations will be achieved (Simon,
1977).

This approach is not without precedent, with problems in
research, development, and manufacturing frequently necessitating the
screening of multiple variables to identify the critical factors
(Blodgett, 1957; Cragle, Myers, Waugh, Hunter, and Anderson, 1955;
Day, 1949; Davies and Hay, 1950; Wilburn, 1963). To date, however,
human factors investigators have been slower to adopt this philosophy
along with its numerous benefits, depending instead on traditional
factorial analysis of variance methods. Among notable examples,
however, a multifactor study was conducted to identify those display
dynamic characteristics critical to pilot performance with the
HOVERING display (Tatro et al., 1983; Tatro and Roscoe, 1985).

Tatro and his associates screened eight potentially critical
factors in a 30-second standard instrument departure (SID) procedure.
Pilot performance was evaluated in terms of crosscourse, alongcourse,
and vertical tracking error with magnification factor (MF), control
gain (CG), control order (CO), altitude control gain reduction factor
(GR), tracking mode (TM), flight-path prediction time (PT),
prediction order (PO), and initial position error (IP) as independent
experimental variables. CO and PT accounted for 45 percent of the
crosscourse tracking variance. For alongcourse tracking, MF, CO, CG,
and TM accounted for 54 percent of the error variance. And finally,
CO, PT, and TM along with various interactions accounted for 60
percent of the variance in altitude tracking.

Thus, five factors (CG, CO, MF, PT, and TM) accounted for most of
the performance variance. Once the most critical factors have been
identified, the optimization process can start, the end product of
which is a multiple regression model, or set of models for the

various dependent variables in different flight scenarios. Such a model indicates not only where optimum performance occurs but also how performance deteriorates with departures from optimum. In the present study, this model optimization process was carried out in the following way. The first step was to settle on a general display and control system configuration in which the numerical values of the independent variables had not been fixed.

For the HOVERING display, the function can be expressed as

$$P = f(CG, CO, MF, PT, TM)$$

where P is an index of pilot performance as a function of the five previously identified critical factors. This function is then minimized (tracking error near null) by a computational search for the optimum variable levels. Before evaluating any relationsnip, an experimental strategy must be employed that will economically and holistically estimate pilot performance. Only after the function is empirically derived can classical optimization techniques be used to evaluate the function.

This has been accomplished through the use of Response Surface Methodology (RSM) techniques to develop a multiple-regression model of VTOL pilot performance for each of three flight tasks, or scenarios, composed of different combinations of representative vertical and translational flight maneuvers. Once empirical models were estimated, the functions could be evaluated using classical optimization techniques such as canonical analysis, computational searches, and graphical analysis to obtain the optimum operating conditions for each of the critical factors.

INTRODUCTION

Background

A conceptual analysis and review of instrument flight problems in piloting VTOL aircraft, including helicopters, preceded the development of a generic VTOL simulation and the initiation of an experimental investigation of critical design variables in forward- and sideward-looking vertical situation displays and downward-looking horizontal situation displays (Figure 1). The vertical displays are large, flat plasma screens on which computer-animated contact analog symbology is presented in real time, and in the case of the downward-looking display, altitude and vertical rate information are effectively integrated with horizontal positions and rates to achieve accuracy and stability of vertical and transitional flight control.

In the BEL MicroGraphic VTOL Simulator, alongcourse and crosscourse translational rates and/or accelerations (depending on the mode in effect) are controlled by a three-axis, spring-centered control stick mounted on the right-hand arm rest (see Figure 1). Alongcourse tracking is controlled by fore and aft stick displacement from a center detent, and crosscourse tracking by left and right stick displacement. Rotating (twisting) the stick about its vertical axis controls the vehicle's yaw (crab) angle relative to the
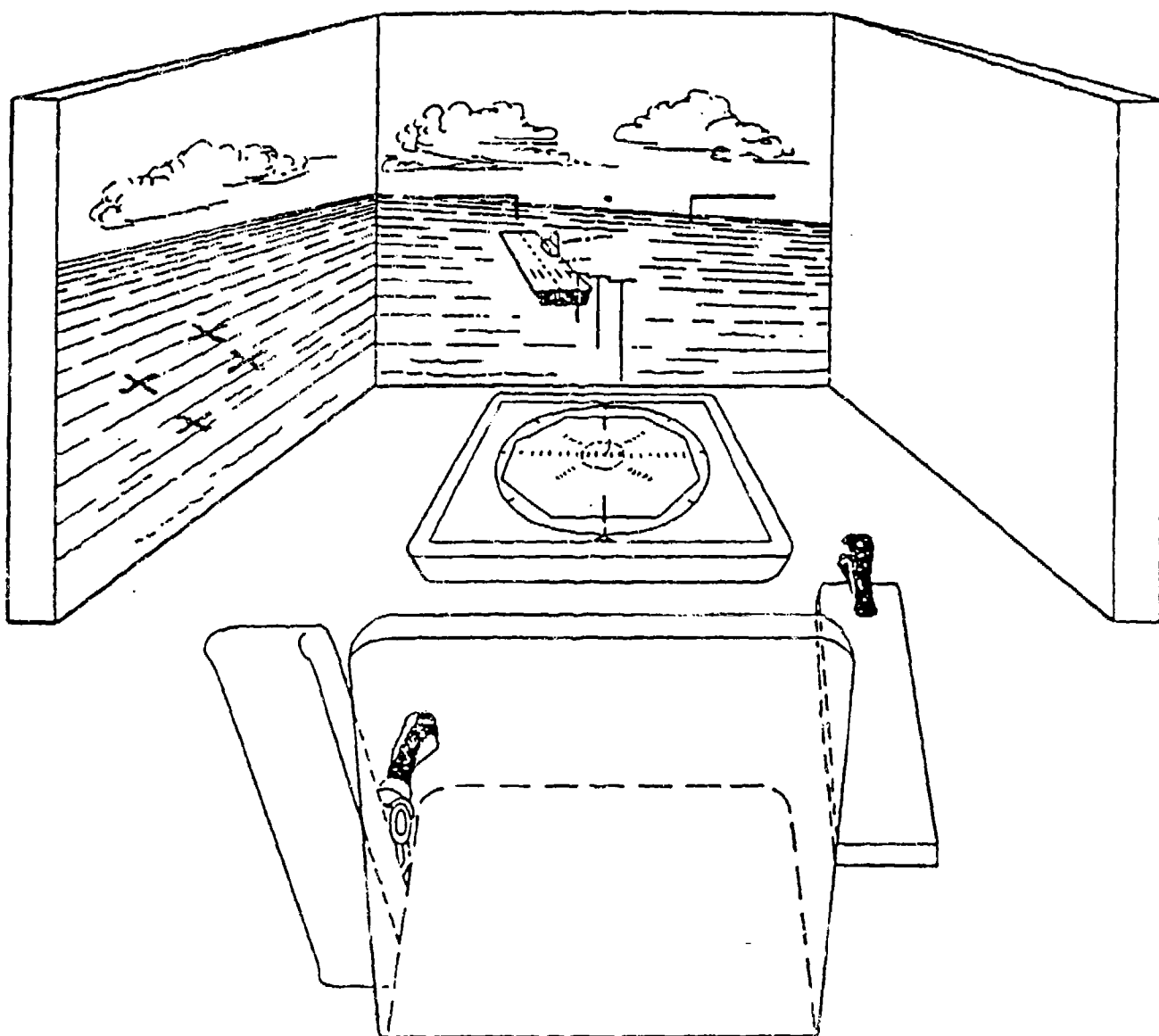
Figure 1. Configuration of BEL's MicroGraphic VTOL Simulator,
            including the centrally located HOVERING display.

horizontal velocity vector. Vertical flight is regulated by a vertical speed control (VSC) operated by the pilot's left hand. The vertical speed control is spring-centered, viscously damped, and is operated by displacing the stick upward to ascend and downward to descend, similar to a collective control in a helicopte.·.

The vehicle's heading in the horizontal plane is displayed by a rotating compass rose that responds to both crosscourse control inputs and weather-vaning of the vehicle due to the effects of relative wind (Figure 2). A turn-rate index line is shown relative to top-dead-center of the display so that a desired heading can be captured by matching this index with the desired position on the rotating compass rose. Crosscourse and alongcourse rates and/or accelerations are displayed by a position predictor. For vertical flight control, the information provided by the HOVERING display includes a present altitude indicator, imminent altitude predictors, desired altitude goal bars, and both desired and actual vertical rate indicators (Figure 3).
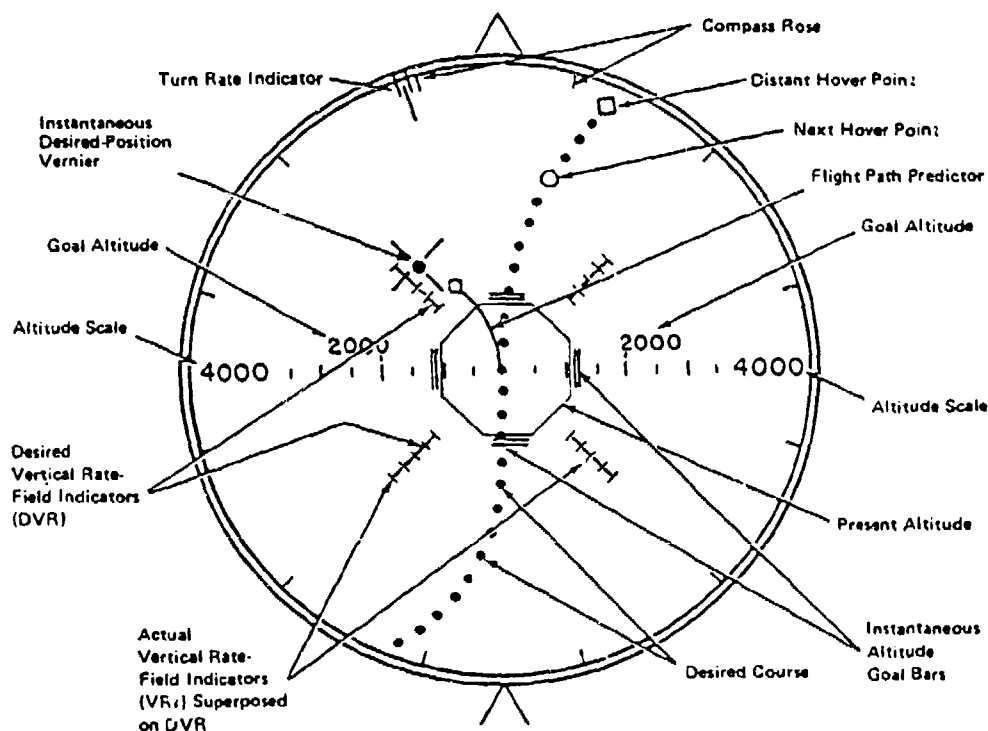
Figure 2. Present configuration of the HOVERING display.

For lateral and longitudinal control, the pilot is presented with symbology representing a desired flight path, next hover point, and distant hover point, shown in Figure 4. This presentation allows

the pilot a view of where the aircraft has been and where it's going.
The "big picture" essentially provides a backdrop against which more
precise tracking takes place. The precise translational tracking
symbols consist of a vehicle target cross, a kite-like flight-path
closing-rate predictor, and a sensitive instantaneous desired position
vernier (magnified) indicator. The pilot's task in translational
control is to align the vehicle with the vernier target cross
using the closing-rate predictor as a guide for control inputs.
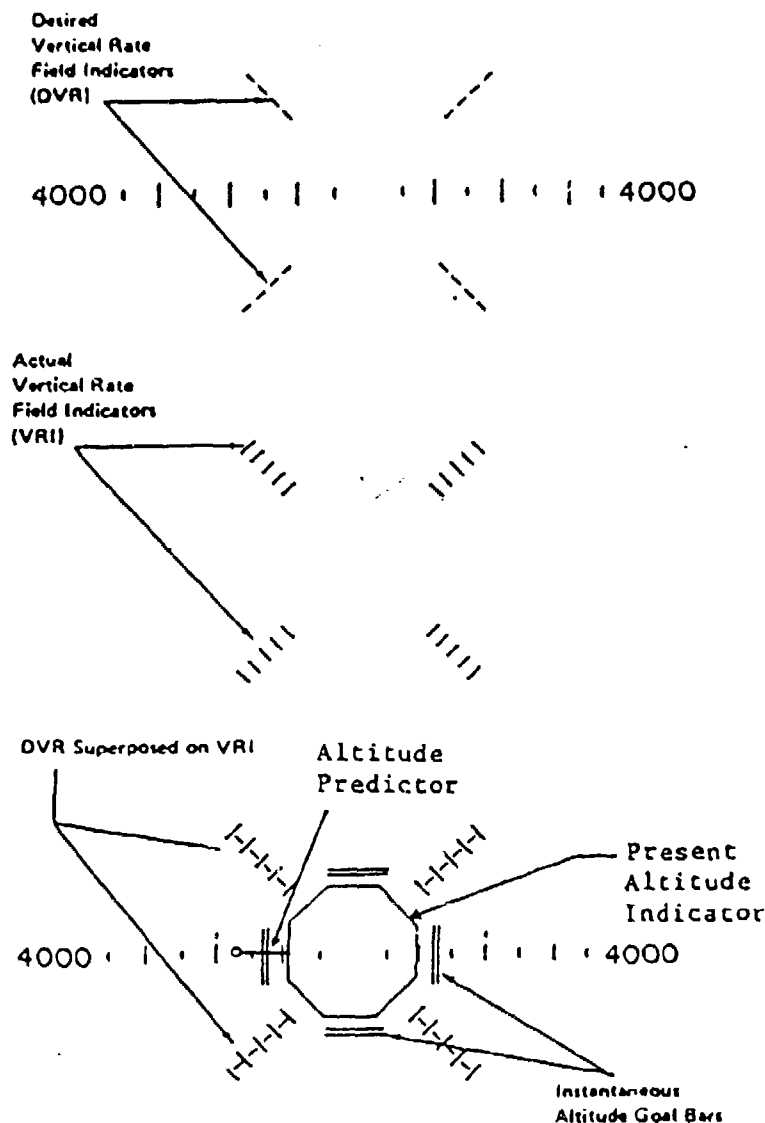
Figure 3. Vertical flight information provided by the HOVERING
display.
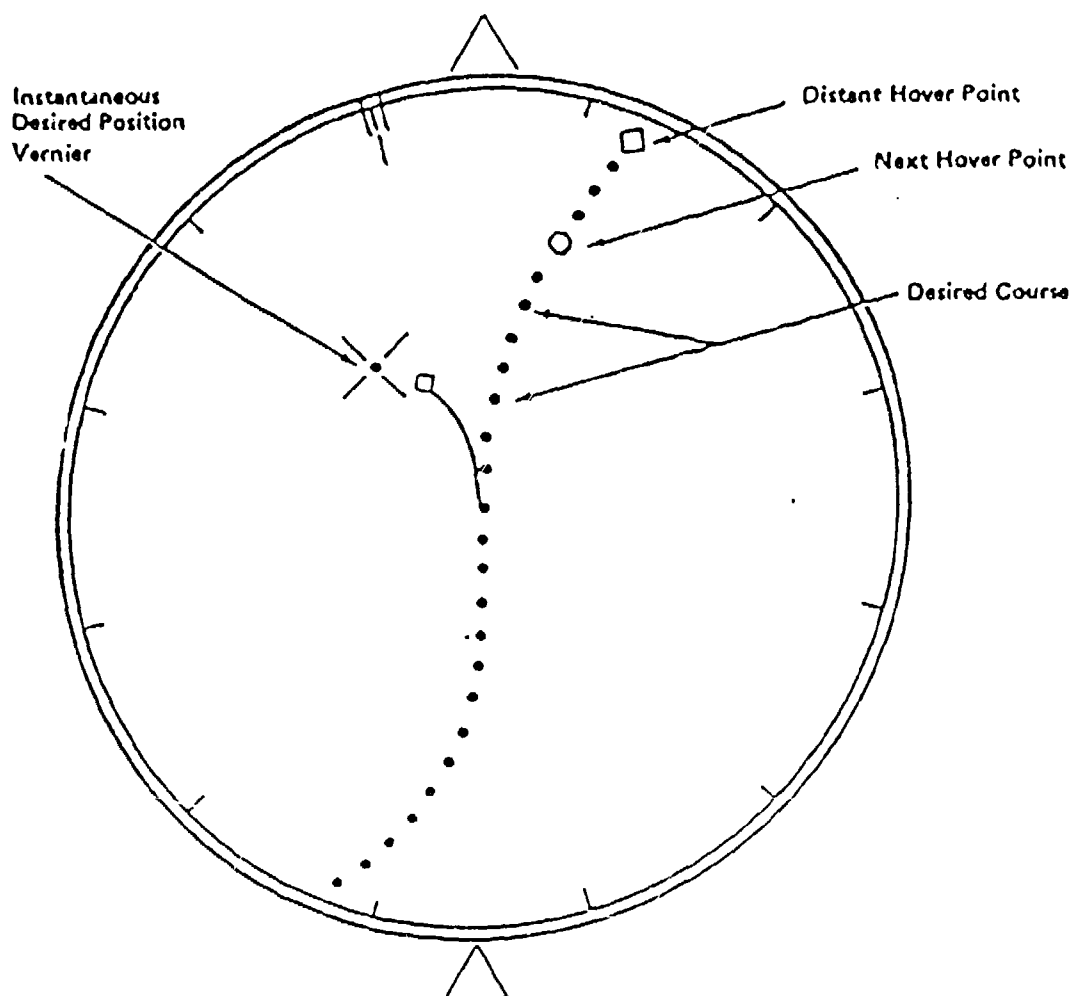
Figure 4. The big picture and the precise tracking symbols in the HOVERING display.

The present altitude indicator is an octagonal box that dilates as altitude increases and constricts as altitude decreases, as shown in Figure 3. Altitude (size of the octagonal box) is read against a fixed scale emanating from the center of the display left and right to the momentary limits of the scale at the display's outer edge. The scale limits automatically change by a ratio of 4 to 1 as the simulated aircraft ascends through the momentary limits and as it decends within the limits of the next larger scale, as depicted in Figure 5. Altitude goal bars (AGBs) provide an indication of instantaneous desired altitude. The pilot's task is to keep the octagonal box aligned within the altitude goal bars. The altitude goal bars and the octagonal altimeter move independently; hence, altitude control reduces to a basic pursuit tracking task.

Altitude Scale 60 | | | | | | | | | | 60

Altitude Scale 250 | | | | | | | 250

Altitude Scale 1000 | | | | | | | | | | | | | | | | | | 1000

Altitude Scale 4000 | | | | | | | | | | | | | | | | 4000
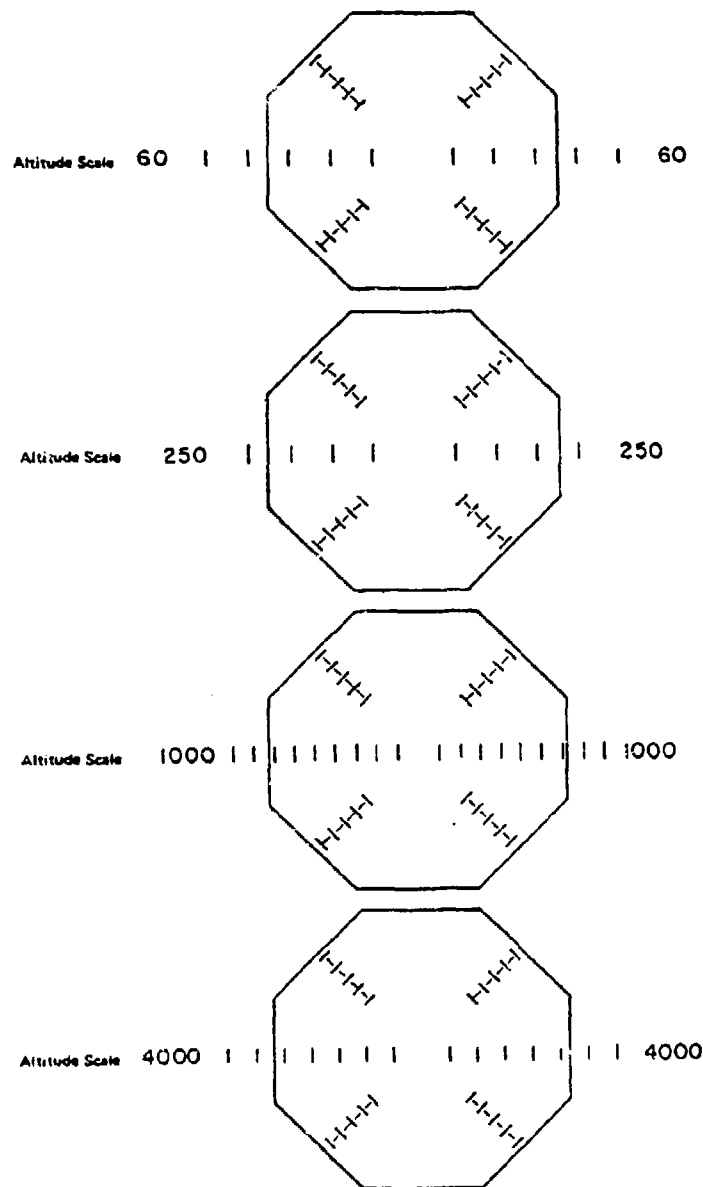
Figure 5. Example of altitude scale changes in the HOVERING display.

Desired vertical rate-field indicators (DVRs) consist of four sets of bars that flow outward to display desired rate cf climb and inward for desired rate of descent. The actual vertical rate indicators (VRIs) consist of four sets of bars superposed on, but perpendicular to, the DVRs. The flow of both the desired and actual vertical rate indicators matches that of the octagonal altimeter; outward flow indicates a desired or actual rate of climb, and inward movement indicates desired or actual rate of descent.

Experimental Variables

Those five variables found to be critical in the screening study had a direct influence on the usefulness of the aforementioned aspects of the HOVERING display. The magnification factor of the vernier deviation indicator had the largest single effect, accounting for 25 percent of the variance in both alongcourse and crosscourse tracking. As magnification increased, tracking became more precise. However, as magnification increases, a tradeoff in the acceptable control/display ratio occurs. At higher magnifications, control gain must be reduced to maintain an acceptable ratio. Thus an optimum combination between control gain and magnification must be found for the various flight tasks.

Control gain is of major importance in the optimization procedure. High control gain results in faster target acquisition but less time on target. Low control gain accommodates the fine adjustments needed for keeping on target but causes slower target acquisition. Thus a compromise is needed between the two extremes. In a flight task such as an intercept approach, high gain would be preferable; while in a sea-rescue mission, low gain would help the pilot. Thus the optimum sensitivity of control needs to be a compromise between the high gain required to reduce acquisition time and the low gain required for accurate fine adjustments (Poulton, 1974), yet at the same time being compatible with the magnification factor in use.

Control order proved to be important in the screening study for all three dimensions, with second-order control being most effective. In the literature on tracking experiments involving control order, some experiments show first-order control superior, while other studies indicate second-order control to be easier (Poulton, 1974). These contradictory results are most likely task-related, and such being the case, control order needed to be optimized across various flight scenarios.

Prediction time was also found to be a significant contributor to the observed performance variance. Optimum prediction time has been found to vary from task to task (Roscoe, 1980; Tatro et al., 1983). However, according to Beringer, Williges, and Roscoe (1975), short prediction times produce a tendency for overcontrolling the vehicle; the longer the prediction time, the smoother and slower the control inputs. Hence, short prediction times were better with large errors, and long prediction times with small errors. Thus prediction time needed to be evaluated across mission scenarios, especially with the addition of an altitude predictor since the completion of the screening phase.

The last critical variable in the screening study was tracking mode. Pursuit tracking has consistently been shown to be superior to compensatory tracking; however, practical limitations have dictated the use of compensatory presentations. In pursuit tracking, independent indices of both target and vehicle movement are presented

8

against a common fixed frame of reference, whereas in compensatory tracking only the relative position of target to vehicle (or vice versa) is displayed, thereby resulting in a single index of error. Based on the work of Bauerschmidt and Roscoe (1960), the HOVERING display has a feature that transforms the compensatory tracking presentation into what has been termed a quasi-pursuit display.

In the quasi-pursuit tracking presentation, the position error is allotted to both the target and vehicle (instead of the standard single-error compensatory configuration), creating an appearance of independent movement. In the screening study, a target-referenced compensatory (TRC) presentation, a vehicle-referenced compensatory (VRC) presentation, and a 50-percent-TRC/50-percent-VRC (quasi-pursuit) presentation were compared. The 50/50 mode resulted in significant improvement in translational tracking. Since the fraction of error allotted to either the target or vehicle can be manipulated, and because this display innovation has not been systematically investigated, tracking mode was included as an experimental variable.

Response Surface Methodology

In the optimization of a given system, an investigator's prime concern is the establishment of a quantitative relationship between human performance and a set of system parameters. Once the quantitative relationship has been established, the investigator is able to determine the level of performance expected for given levels of the system parameters and, conversely, to determine the levels of the system parameters required to maintain performance at a prescribed level. The estimated function of system parameter levels to levels of performance is known as the response surface.

The procedures used to investigate response surfaces were originally developed by Box and Wilson (1951) for use in chemical research to determine the optimum combination of variables to produce the maximum yield of a chemical process. Response surface methodology (RSM) has since been shown to be practical in psychological research, especially in studies pertaining to human performance (Beringer, 1979; Clark, 1976; Clark and Williges, 1972, 1973; Meyer, 1963; Randle, Roscoe, and Petitt, 1980; Roscoe and Eisele, 1980; Scanlan, 1975a, 1975b; Scanlan and Roscoe, 1980; Simon, 1970; Williges and Simon, 1971).

Among the numerous benefits from the use of RSM, the most notable is its sampling economy (Simon, 1970). Response surface designs are planned to minimize redundancy and to limit data collection to that really necessary (Simon, 1973). This is accomplished by collecting the fewest data sufficient to estimate the coefficients of the lowest-degree polynomial that yields an acceptable fit. For most behavioral response surfaces, a second-degree polynomial seems to be adequate (Clark, 1976). Since results from the screening study indicated a bow in the data, this assumption would seem to be appropriate here.

9

In the current experiment with five factors, following traditional psychological methodology, a 3^5 factorial design with a resulting 243 data points would be required to estimate the second-order polynomial. Response surface designs, on the other hand, are built on the theoretical assumption that a minimum of N data collection points are required to write a polynomial of N coefficients (Simon, 1970). Thus with five factors, a minimum of 21 observations are required to estimate a second-order function, an enormous saving in time, cost, and resources. The loss of information in the response surface design, due to fewer observations, is limited to those interactions involving more than two factors that generally are negligible (Box and Hunter, 1957).

As an alternative to the 3^K factorial designs, Box and Wilson (1951) have devised a class of composite designs, of which the most pertinent to human factors research is the central-composite design (CCD). The central-composite design is a 2^K factorial or fractional factorial ($K \geq 5$) augmented by additional strategic points to allow estimation of the second-order coefficients. For the sake of simplicity, the building of a central-composite design in three variables will serve as an example.

If instead of the five factors to be evaluated, we were to investigate just magnification factor, prediction time, and control order, a full 3^3-factorial experiment consisting of 27 data points would normally be conducted. As an alternative, a 2^3-factorial experiment, depicted as a design matrix in Table 1, could be augmented with seven additional data points, shown in Table 2, to construct the central-composite design. The result, illustrated in Figure 6, is a cube consisting of the factorial portion of the design, a center point, and six axial or star points.

TABLE 1
Coded-Value Coordinates of Data
Points in a Full 2^3 Factorial

X_1	X_2	X_3
+1	+1	+1
-1	+1	+1
+1	-1	+1
-1	-1	+1
+1	+1	-1
-1	+1	-1
+1	-1	-1
-1	-1	-1
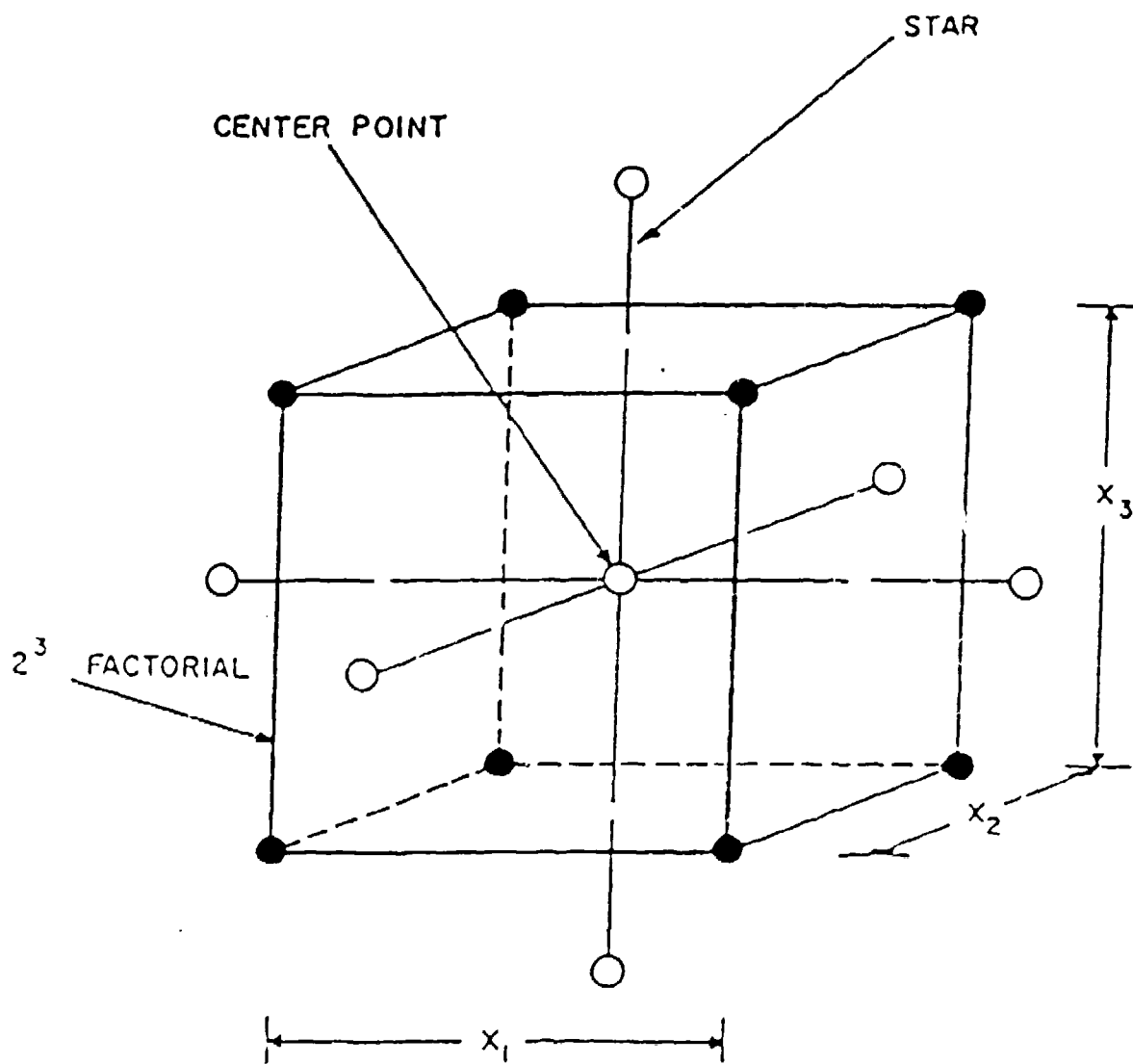
Figure 6.   Three-factor, central-composite design
(Clark and Williges, 1972).

TABLE 2
Coded-Value Coordinates of Data
Points to Augment the 2^3 Factorial

X_1	X_2	X_3
$-\alpha$	0	0
$+\alpha$	0	0
0	$-\alpha$	0
0	$+\alpha$	0
0	0	$-\alpha$
0	0	$+\alpha$

The formula for the number of data points in a basic CCD is:

$$2^K + (2*K + 1), \text{ for } K \leq 4$$

and

$$2^{K-1} + (2*K + 1), \text{ for } K \geq 5.$$

Each factor is now sampled at five levels with an enormous reduction in data collection. This saving is magnified as the number of factors increases, as shown in Table 3. For studies involving five or more factors, a fractional factorial sampling is used instead of the full factorial, thereby yielding even more economy.

TABLE 3
Comparison of the Number of Data Points Required Between a
Three-Level Full Factorial and a Basic Central-Composite Design

	Number of Data Points		
Number of Factors, K	Full Factorial	Basic CCD	Saving
2	9	13	-4
3	27	20	7
4	81	31	50
5	243	32*	211
6	729	53*	676
7	2187	92*	2095

CCD designs marked with * indicate a fractional factorial is used.

A second-order polynomial can now be estimated. If repeated observations are taken at the center point, as illustrated in Figure 7, an estimate of experimental error variance can be calculated to test the significance of the derived polynomial and each of its components. The final step in the construction of a central composite design is the selection of α to establish the positions of the axial star points.

The value of α should be selected with the design property of rotatability. A design is said to be rotatable when the variance of the estimated response ($\hat{Y}$) is a function of the distance from the center of the design, regardless of the direction (Box and Hunter, 1957). Thus the information obtained from two points equidistant from center will be equal. This feature is highly desirable because, until the response surface is evaluated, the importance of each point in the experimental design is unknown. The values of α that result in a rotatable CCD are given in Table 4.

TABLE 4
Rotatable, Second-Order Central-Composite Design Statistics

| Number of Factors, K | Number of Observations in: | | | | |
	2^K Factorial Portion	2K Star Portion	Center Points	Total Design	α Value for Rotatability
2	4	4	5	13	1.414
3	8	6	6	20	1.682
4	16	8	7	31	2.000
5	16 (1/2 replicate)	10	6	32	2.000
6	32 (1/2 replicate)	12	9	53	2.378
7	64 (1/2 replicate)	14	14	92	2.828

A second important feature of the CCD is the number of repeated center-point observations. This number is selected to obtain uniform or near-uniform precision. Uniformity refers to the idea that the quality of information (the reciprocal of the variance) at any point from the center of the design to the vertices of the hypercube portion of the experimental space should be equal (Simon, 1970). The number of center points has a direct effect on the information profile of the experiment. The appropriate number of center points to obtain near-uniform precision is given in Table 4. For a more comphrehensive review of uniform precision and rotatability in the CCD, see Box and Wilson (1951) and Box and Hunter (1957).

To obtain the maximum benefits from the CCD, independent and dependent variables must be continuous, quantitative factors. In this way a polynomial model can be derived through the use of least-squares techniques. Once the regression equation has been estimated,

13

an analysis of variance is conducted on the adequacy of the model to fit the data and the significance of the contributions of the individual coefficients. To explore the estimated function further, graphical analyses, canonical reduction, and various optimizational searches can then be employed.
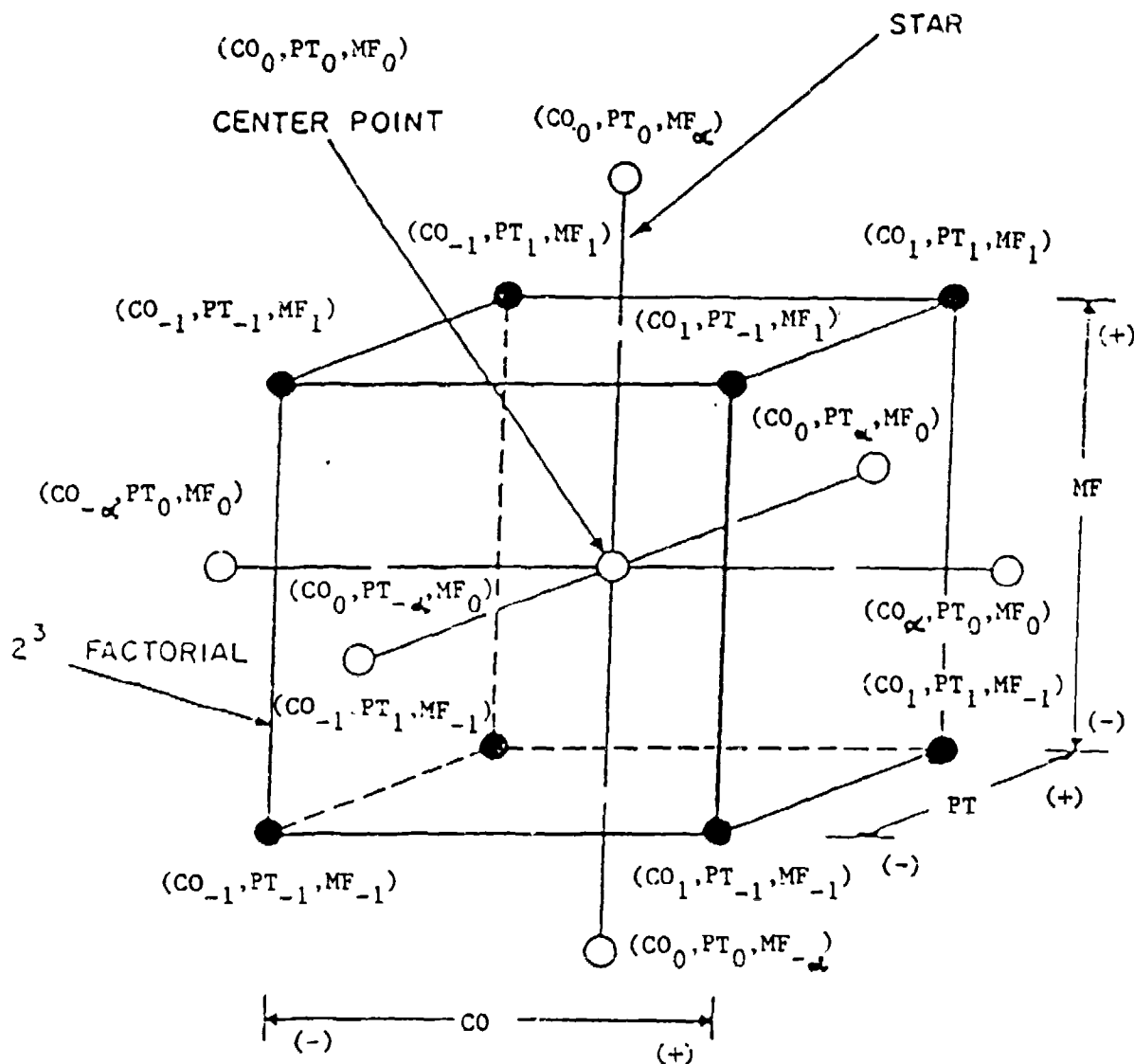

Figure 7. Three-factor, central-composite design with labeled data collection points.

METHOD

Mission Scenarios

Five critical variables affecting pilot performance in three flight tasks or scenarios were experimentally manipulated. Each flight was to be completed in 35 seconds.

In Scenario 1, subjects were presented with a VTOL takeoff task involving precise altitude control with some crosscourse manuevering. For the altitude profile of the flight, subjects initially started from a stationary point on an aircraft carrier. During the first four seconds, the aircraft was to ascend to 15 feet and fly level for five seconds. During the last 26 seconds of flight, the aircraft was to ascend rapidly from 15 feet to 400 feet, holding a constant heading away from the ship.

Scenario 2 involved a terrain-following and landing task calling for precise control in three dimensions. The altitude subtask involved a level-descend-level-descend sequence starting at 100 feet, dipping below 60 feet, and then descending to zero feet. In this sequence the pilot had to negotiate one scale change when descending through the 60-foot altitude. For the translational subtask, a cruise-bank-cruise-bank-cruise sequence was followed, calling for precise crosscourse and alongcourse tracking.

Finall', in Scenario 3, the standard instrument departure task used in the screening study (Tatro et al., 1983) was reevaluated to confirm or refine the previous results and estimate the quadratic components of the response surfaces. The task involved a climbing turn to the right from 400 to 950 feet in altitude and 0 to 35 degrees in heading.

Subjects

Twelve right-handed male Introductory Psychology students were selected from a larger number who were first pretested on the HOVERING display in the following manner: Altitude symbology was turned off, resulting in a two-dimensional translational task. A 35-second course consisted of a left turn at a rate of 1 degree per second. Potential subjects flew ten trials, with the average of the three best consecutive trials serving as a baseline matching score.

Of the 20 potential subjects tested, 12 were selected to form four stratified groups of three subjects each, respectively matched to minimize within-group and maximize between-group variances. One subject from each group was then assigned to each of the three experiments, one experiment for each of the three scenarios. This matching procedure was designed to reduce bias due to subject differences in initial tracking and time-sharing ability.

15

Experimental Design

For each of the three flight scenarios, the same five-factor central-composite design was used. A Resolution-V (2^{5-1}) fractional factorial sampling (Simon, 1973) was augmented with axial and center points to complete the CCD. With Resolution-V, main effects are confounded with third-order (four-factor) interactions, and first-order (two-factor) interactions are confounded with second-order (three-factor) interactions. Because three-factor and higher interactions are usually negligible, main effects and first-order terms are essentially unconfounded. The defining contrast for the fractional factorial is: $I = abcde$, which is selected to create the fractional and to identify the aliasing (confounding) of the estimated effects.

The fractional factorial samples along with the aliases for each effect are given in Table 5. The value of α chosen to identify the axial points in the CCD was 2.0, which results in a rotatable design. To obtain near-uniform precision in the CCD, six center points were added to the fractional factorial. Thus, for each of the optimization experiments, there were 32 distinct observation points, allowing estimation of second-order regression equations for each dependent measure for each flight scenario. The total design in matrix form is given in Table 5.

Variable Levels

One advantage of the CCD is that the data obtained are readily transformed for ease of interpretation and analysis. Each of the five variables (tracking mode, magnification factor, prediction time, control order, and control gain) were transformed and assigned to five coded levels (-2, -1, 0, +1, +2). For the spacing between levels of control order to be equal in terms of effects, a logrithmic transformation was deemed appropriate based on the screening study (Tatro et al., 1983), while the other four variables were linearly transformed. The real-world ranges and transformations are provided in Table 6. Experimental variable real-world levels and their association with the five-level experimental design are shown in Table 7.

Performance Measures

There are four dependent measures of pilot performance for each flight task. As in previous studies, log RMS error was used to evaluate altitude (vertical), crosscourse (lateral), and alongcourse (longitudinal) tracking. The log RMS error distribution has been empirically shown to yield a good approximation of a normal distribution and homogeneous variances (Tatro et al., 1983) and hence justifies the assumptions inplicit with least-squares regression techniques.

TABLE 5
Design Matrix for the Five-Factor Central-Composite Design

Condition	Variable a	b	c	d	e	Effect	Alias
1	−	−	−	−	−	(1)	abcde
2	+	+	+	+	−	abcd	e
3	−	−	−	+	+	de	abc
4	+	+	+	−	+	abce	d
5	+	+	−	−	−	ab	cde
6	−	−	+	+	−	cd	abe
7	+	+	−	+	+	abde	c
8	−	−	+	−	+	ce	abd
9	+	−	+	−	−	ac	bde
10	−	+	−	+	−	bd	ace
11	+	−	+	+	+	acde	b
12	−	+	−	−	+	be	acd
13	−	+	+	−	−	bc	ade
14	+	−	−	+	−	ad	bce
15	−	+	+	+	+	bcde	a
16	+	−	−	−	+	ae	bcd
17	0	0	0	0	0	center point	
18	0	0	0	0	0	center point	
19	0	0	0	0	0	center point	
20	0	0	0	0	0	center point	
21	0	0	0	0	0	center point	
22	0	0	0	0	0	center point	
23	−2	0	0	0	0	axial point	
24	0	−2	0	0	0	axial point	
25	0	0	−2	0	0	axial point	
26	0	0	0	−2	0	axial point	
27	0	0	0	0	−2	axial point	
28	2	0	0	0	0	axial point	
29	0	2	0	0	0	axial point	
30	0	0	2	0	0	axial point	
31	0	0	0	2	0	axial point	
32	0	0	0	0	2	axial point	

TABLE 6
Real-World Variable Ranges and Transformations

Experimental Variable	Range	Transformation
Tracking mode (percent VRC)	25 to 75	(X-50)/12.5
Magnification factor	50 to 150	(X-100)/25
Prediction time (sec)	0.5 to 2.5	(X-1.5)/0.5
Control order	1.2 to 2.0	(X-1.6)/0.2
Control gain (unitless ratios)		
longitudinal (1st order)	-6000 to -10000	(X+8000)/-1000
longitudinal (2nd order)	-100 to -250	(X+175)/-37.5
lateral (1st order)	13000 to 20000	(X-16500)/1750
lateral (2nd order)	600 to 900	(X-750)/75
azimuth (1st order)	0.40 to 1.20	(X-0.8)/0.2
azimuth (2nd order)	0.20 to 0.60	(X-0.4)/0.1
vertical (1st order)	-1500 to -2500	(X-1000)/250
vertical (2nd order)	-50 to -120	(X-60)/17.5

TABLE 7
Experimental Variable Levels

Experimental Variable	Variable Levels				
	(-2)	(-1)	(0)	(+1)	(+2)
(a) Tracking mode (percent VCR)	25	37.5	50	62.5	75
(b) Magnification factor	50	75	100	125	150
(c) Prediction time (sec)	0.5	1.0	1.5	2.0	2.5
(d) Control order	1.2	1.4	1.6	1.8	2.0
(e) Control gain (unitless ratios)					
longitudinal (1st order)	-6000	-7000	-8000	-9000	-10000
longitudinal (2nd order)	-100	-137.5	-175	-212.5	-250
lateral (1st order)	13000	14750	16500	18250	20000
lateral (2nd order)	600	675	750	825	900
azimuth (1st order)	0.40	0.60	0.80	1.00	1.20
azimuth (2nd order)	0.20	0.30	0.40	0.50	0.60
vertical (1st order)	-500	-750	-1000	-1250	-1500
vertical (2nd order)	-25	-42.5	-60	-77.5	-95

The fourth dependent variable consisted of a log composite error vector score of the form:

$$\log \frac{\Sigma \sqrt{X^2 + Y^2 + Z^2}}{N}$$

in which X, Y, and Z are position errors and N is the number of position error samples taken. This composite score served as an overall index of display performance, whereas the other three measures served to isolate effects of the various configurations on the specific subtasks (altitude, crosscourse, and alongcourse tracking).

Procedure

For each experiment, subjects flew ninety-six 35-second flight trials on each of three consecutive days. Each flight was followed by a 10-second intertrial interval. The first two 72-minute sessions served as training sessions, followed on the third day by a 72-minute testing session. Each subject was tested in a different (partially counterbalanced) serial sequence as seen in Table 8.

In the within-subject design used in each of the three scenario experiments, careful attention was given to possible biases that might result from intraserial transfer effects due to the testing sequences. The fractional factorial sampling used in this design has been found by Simon (1977) to be orthogonal to intraserial trends in the first- and second-order effects, thus effectively counter-balanced.

Traditional counterbalancing, though, has been shown by Poulton (1974) to be generally ineffective as a way to reduce or eliminate sequence effects in tracking studies. Thus, to minimize any remaining possibility of biases as a result of asymmetrical transfer, highly trained subjects were used, and two buffer trials were flown before the test trial with each system configuration. An unreported experiment at this laboratory has demonstrated the effectiveness of this procedure.

Analysis of Results

The first step in the estimation of the true functional relationship between experimental variables and response variables is a least-squares multiple-regression analysis. From this analysis, multiple-regression equations were derived for the various performance measures and flight scenarios and subsequently used to determine the true nature of the response surfaces. To evaluate the adequacy of the multiple-regression models, analyses of variance were conducted on the models as well as the individual regression coefficients. These analyses provided information as to the amount of variance accounted for by each whole model as well as the contributions of each of the individual experimental factors.

TABLE 8
Order of Presentation for Each Subject

	Order of Conditions			
Trials	Subject 1	Subject 2	Subject 3	Subject 4
1 - 3	17 (c)	22 (c)	22 (c)	17 (c)
4 - 6	18 (c)	21 (c)	21 (c)	18 (c)
7 - 9	1 (f)	16 (f)	16 (f)	1 (f)
10 - 12	2 (f)	15 (f)	15 (f)	2 (f)
- 15	3 (f)	14 (f)	14 (f)	3 (f)
1o - 18	4 (f)	13 (f)	13 (f)	4 (f)
19 - 21	23 (a)	30 (a)	28 (a)	31 (a)
22 - 24	24 (a)	29 (a)	27 (a)	32 (a)
25 - 27	25 (a)	12 (f)	26 (a)	5 (f)
28 - 30	5 (f)	11 (f)	12 (f)	6 (f)
31 - 33	6 (f)	10 (f)	11 (f)	7 (f)
34 - 36	7 (f)	9 (f)	10 (f)	8 (f)
37 - 39	8 (f)	25 (a)	9 (f)	29 (a)
40 - 42	26 (a)	24 (a)	32 (a)	30 (a)
43 - 45	27 (a)	23 (a)	31 (a)	19 (c)
46 - 48	28 (a)	20 (c)	20 (c)	20 (c)
49 - 51	19 (c)	19 (c)	19 (c)	26 (a)
52 - 54	20 (c)	32 (a)	25 (a)	27 (a)
55 - 57	29 (a)	31 (a)	24 (a)	28 (a)
58 - 60	30 (a)	8 (f)	23 (a)	9 (f)
61 - 63	9 (f)	7 (f)	8 (f)	10 (f)
64 - 66	10 (f)	6 (f)	7 (f)	11 (f)
67 - 69	11 (f)	5 (f)	6 (f)	12 (f)
70 - 72	12 (f)	28 (a)	5 (f)	23 (a)
73 - 75	31 (a)	27 (a)	30 (a)	24 (a)
76 - 78	32 (a)	26 (a)	29 (a)	25 (a)
79 - 81	13 (f)	4 (f)	4 (f)	13 (f)
82 - 84	14 (f)	3 (f)	3 (f)	14 (f)
85 - 87	15 (f)	2 (f)	2 (f)	15 (f)
88 - 90	16 (f)	1 (f)	1 (f)	16 (f)
91 - 93	21 (c)	18 (c)	18 (c)	21 (c)
94 - 96	22 (c)	17 (c)	17 (c)	22 (c)

f = factorial point; c = center point; a = axial point

The analyses of the fitted surfaces were further enhanced by graphically depicting the response surfaces generated by each experimental factor (linear and quadratic). In this way, regions of optimum response for each factor could be deduced and used to conduct further experiments to locate an area of minimum error precisely. Because of the complex nature of a surface consisting of five factors, the graphical representation of individual factor response surfaces is a gross simplification of the overall surface. To take into account the many interactions along with the linear and quadratic effects, multiple-regression equations must be reduced to a simpler form for interpretation. This reduction is called a canonical analysis of a fitted surface.

The goal of canonical analysis is to restate the original multiple-regression equation in an easily interpretable form. A canonical analysis takes place in four stages. The analysis begins with a translation of the response surface from the experimental design origin (CCD center point) to the stationary point of the response surface. The stationary or near-stationary point is determined by taking the K partial derivatives with respect to each factor and then solving the K equations. In the present study, five equations in five unknowns had to be solved to determine the stationary point of each response surface.

Upon determination of the stationary point, the reponse function is transformed into an equation expressed in K new variables (W's), whose axes correspond to the principal axes of the response surface. This new equation provides a clear picture of the nature of the response surface as one moves away from the stationary point. The new response surface equation is called the canonical equation. The canonical equation is determined by finding the characteristic roots or eigenvalues of the second-order symmetrical matrix, consisting of the quadratic and linear-by-linear interaction terms of the original multiple-regression model.

With five experimental factors, expansion of the second-order matrix yields five characteristic roots. These characteristic roots are arranged in ascending order to determine the coefficients of the five new variables (W's), with the estimated response at the stationary point determining the mean of the canonical equation. The signs and magnitudes of the various coefficients then reveal the nature of the response surface. Since the response surface is now expressed in terms of new variables, it becomes beneficial to ascertain the relationship between the old variables and the new canonical variables.

This relationship takes the matrix form: $W = MZ$, where M represents the 5 X 5 matrix of normalized eigenvectors corresponding to each characteristic root; Z represents the 5 X 1 matrix of x-values minus the corresponding stationary point x-values; and W represents the 5 X 1 matrix of W values to be determined. In the fourth stage of the canonical analysis, the canonical equation and the x to W transformations are used to find either the values of the x-variables that result in a given operating condition or those that result in an optimum operating condition.

Takeoff Scenario

Each of the four dependent variables (lateral, longitudinal, vertical, and radial errors) was analyzed separately.

The regression analyses yielded equations that relate the dependent variables to the second-order combination of the coded values of the five independent variables. The equations together with summaries of their associated analyses of variance and graphic illustrations are presented in the APPENDIX. The illustrations depict the error values predicted by the regression equations as a function of each of the significant independent variables when all other variables are at their center-point values, including pseudo three-dimensional plots of the significant two-way interactions.

The F-ratios indicate that the overall model is reliable for each dependent variable, with R^2's of 0.44, 0.42, 0.39, and 0.46, respectively. In addition, tests were made on the individual coefficients of each regression equation. For lateral log RMS error, the significant terms are CO, PT^2, CO^2, CG^2 and PTxCG; for longitudinal log RMS error, significant terms are CO, MF^2, PT^2, CO^2, CG^2, TMxCG, and PTxCG; for vertical log RMS error, CO, CO^2, PTxCG, and COxCG were significant; while for radial log RMS error, CO, PT, CO^2, TMxCG, and PTxCG reached significance.

The Residual sum-of-squares was partitioned into Replications, Lack-of-Fit, and Subjects terms. Replications was used as an estimate of experimental error for all F-tests. The reliable Subjects effect for all four dependent variables indicates that the behavior of at least one of the subjects differed from that of the others. The existence of a significant Lack-of-Fit term means that either higher-order models would better approximate the response surfaces or that an additional factor or factors should be included in the models.

The canonical analysis of each fitted surface was then conducted to describe the nature of the response surfaces more intelligibly. The stationary point for each of the four systems is given in Table 9. The canonical analyses yielded the following four equations that relate the dependent variables to five new canonical variables:

$$\log RMSE, lat = 1.17 - 0.03W1^2 + 0.03W2^2 + 0.03W3^2 + 0.14W4^2 + 0.23W5^2.$$

$$\log RMSE, lon = 1.29 - 0.05W1^2 - 0.02W2^2 + 0.06W3^2 + 0.08W4^2 + 0.15W5^2.$$

$$\log RMSE, ver = 1.16 - 0.10W1^2 - 0.00W2^2 + 0.03W3^2 + 0.03W4^2 + 0.11W5^2.$$

$$\log RMSE, rad = 1.63 - 0.02W1^2 + 0.01W2^2 + 0.04W3^2 + 0.10W4^2 + 0.14W5^2.$$

TABLE 9
Response Surface Stationary Points for the Takeoff Scenario

log RMSE	TM	MF	PT	CO	CG	Y
Lateral	0.21	0.42	-0.03	0.55	-0.35	1.17
Longitudinal	-0.79	0.39	0.63	-0.48	0.62	1.29
Vertical	0.03	-0.65	0.57	-0.25	0.01	1.16
Radial	-0.07	1.54	1.44	-0.47	0.94	1.63

As indicated by the signs of the coefficients of the canonical equations, all four response surfaces are of the saddle-point type. For lateral and radial log RMS error, moving along the W1 axis results in decreases in Y, while moving along the W2, W3, W4, and W5 axes results in increases in Y. For longitudinal and vertical log RMS error, moving along the W1 and W2 axes results in decreases in Y, while moving along the W3, W4, and W5 axes results in increases in Y. The magnitudes of the W coefficients reveal that, for lateral and radial log RMS error, the surface is attenuated along the W1, W2, and W3 axes; for longitudinal log RMS error, the surface is attenuated along the W2 axis; whereas for vertical log RMS error, attenuation occurs along the W2, W3, and W4 axes.

Once the surfaces have been described in terms of the new canonical variables (W's), the relationship between the old x-variables and the new W-variables is needed. The four matrix equation transformations are given in Table 10. With the response surfaces thus described, it becomes possible to locate those values of the coded independent variables that result in an optimum operating condition.

For lateral log RMS error, these coded-values are: TM = 0.2, MF = 0.4, PT = 2.0, CO = 0.5, CG = -0.3, with a predicted error of 1.11 or 12.88 feet. For longitudinal log RMS error, the optimum operating condition results at the coded values: TM = -0.8, MF = 2.0, PT = 2.0, CO = -0.5, CG = 0.6, with a predicted error of 1.08 or 12.12 feet. For vertical log RMS error, an optimum condition occurs at the points: TM = 0.1, MF = 2.0, PT = 2.0, CO = -0.2, CG = 0.0, with a predicted error of 0.40 or 2.52 feet. Finally, for radial error, the optimum values are: TM = -0.1, MF = 1.5, PT = 1.4, CO = -0.5, CG = 0.9, with a predicted error of 1.63 or 42.29 feet.

TABLE 10
X to W Transformation Matrix Equations for the Takeoff Scenario

Lateral

W1		0.27	-0.01	-0.89	0.29	0.21	x1 - 0.21
W2		-0.63	0.75	-0.13	0.16	0.08	x2 - 0.42
W3	=	-0.44	-0.30	-0.39	-0.31	-0.69	x3 + 0.03
W4		0.00	-0.10	0.18	0.87	-0.45	x4 - 0.55
W5		-0.58	-0.59	0.02	0.20	0.53	x5 + 0.35

Longitudinal

W1		-0.25	0.91	-0.01	-0.27	0.20	x1 + 0.79
W2		0.02	-0.02	0.99	-0.10	0.07	x2 - 0.39
W3	=	0.84	0.38	0.04	0.37	-0.15	x3 - 0.63
W4		0.07	-0.09	-0.04	0.31	0.94	x4 + 0.48
W5		0.48	-0.17	-0.11	-0.83	0.22	x5 - 0.62

Vertical

W1		-0.15	-0.80	-0.47	0.33	0.07	x1 - 0.03
W2		0.01	-0.58	0.71	-0.39	-0.08	x2 + 0.65
W3	=	0.38	-0.09	-0.51	-0.77	-0.05	x3 - 0.57
W4		0.13	-0.02	-0.04	0.15	-0.98	x4 + 0.25
W5		0.90	-0.09	0.13	0.35	0.17	x5 - 0.01

Radial

W1		-0.59	-0.63	0.35	0.36	0.06	x1 + 0.07
W2		0.30	-0.55	-0.74	0.23	-0.00	x2 - 1.54
W3	=	0.30	-0.53	0.30	-0.70	-0.21	x3 - 1.44
W4		0.11	0.06	0.11	0.33	-0.93	x4 + 0.47
W5		0.68	0.08	0.47	0.46	0.30	x5 - 0.94

Landing Scenario

For the landing scenario, the regression equations, analysis of variance summaries, and graphic illustrations are also presented in the APPENDIX. The F-ratios indicate that the overall model for each dependent variable was significant with R^2's of 0.38, 0.32, 0.29, and 0.43, respectively. F-tests on the individual coefficients of the four regression equations indicate that, for lateral log RMS error, MF, CO, and CO^2 were significant; for longitudinal log RMS error, CO, PT, and CO^2 reached significance; significant terms for vertical log RMS error were PT, CO, PT, and CO; while for radial log RMS error, CO, MF^2, PT^2, and CO^2 were significant.

The partitioned Residual sum-of-squares indicates a reliable Subjects effect for all four dependent variables, meaning that the

behavior of at least one subject differed from that of the others. The significant Lack-of-Fit term for lateral, longitudinal, and radial log RMS error would indicate the inclusion of additional terms is needed in the models, either higher-order terms or additional factors. For vertical log RMS error, the model seems to account for all the variance possible, excluding subject factors.

The stationary point for each of the four response surfaces is given in Table 11. The nature of the systems around the stationary points is determined by the four canonical equations:

$$\log \text{RMSE,lat} = 1.16 - 0.03W1^2 - 0.02W2^2 + 0.02W3^2 + 0.04W4^2 + 0.13W5^2.$$

$$\log \text{RMSE,lon} = 1.34 - 0.05W1^2 - 0.02W2^2 + 0.02W3^2 + 0.04W4^2 + 0.09W5^2.$$

$$\log \text{RMSE,ver} = 0.96 - 0.02W1^2 - 0.00W2^2 + 0.02W3^2 + 0.03W4^2 + 0.06W5^2.$$

$$\log \text{RMSE,rad} = 1.40 - 0.04W1^2 - 0.02W2^2 + 0.02W3^2 + 0.04W4^2 + 0.11W5^2.$$

TABLE 11
Response Surface Stationary Points for the Landing Scenario

log RMSE	TM	MF	PT	CO	CG	Y
Lateral	0.42	0.66	0.04	-0.39	0.39	1.15
Longitudinal	0.68	0.06	0.21	-0.41	-0.35	1.34
Vertical	0.06	-0.07	-0.51	-1.22	-1.89	0.96
Radial	0.28	0.15	0.25	-0.53	0.02	1.40

The signs of the W coefficients of the canonical equations reveal that all four surfaces are saddle-point type. For all four response surfaces, moving along the W1 and W2 axes results in decreases in Y, while moving along the W3, W4, and W5 axes results in increases in Y. For lateral and longitudinal log RMS error, the magnitude of the W coefficients shows that the surface is attenuated along the W2 and W3 axes, whereas for vertical and radial log RMS error, the surfaces appear to be relatively uniform.

To transform the old x's to the new canonical W variables, the matrix equations given in Table 12 were solved. Once the x to W relationships and the nature of the response surfaces are known, optimum operating conditions can be found.

For lateral log RMS error, the coded values are: TM = 0.4, MF = 0.7, PT = 0.1, CO = -0.4, CG = 0.3, with a predicted error of 1.16 or 14.40 feet. For longitudinal log RMS error, the optimum operating condition results at the coded values: TM = 0.0, MF = 1.0, PT = 0.2,

CO = -1.0, CG = -0.5, with a predicted error of 1.30 or 19.79 feet. For vertical log RMS error, an optimum condition occurs at the points: TM = 0.1, MF = -0.1, PT = -0.5, CC = -1.2, CG = -1.8, with a predicted error of 0.96 or 9.12 feet. Finally, for radial log RMS error, the optimum values are: TM = 0.3, MF = 0.1, PT = -1.0, CO = 1.0, CG = 0.0, with a predicted error of 1.28 or 18.90 feet.

TABLE 12
X to W Transformation Matrix Equations for the Landing Scenario

---

Lateral

W1		0.81	0.51	-0.26	0.08	0.09	x1 - 0.42
W2		0.11	0.15	0.44	-0.86	0.19	x2 - 0.66
W3	=	-0.14	-0.12	-0.86	-0.48	-0.03	x3 - 0.04
W4		0.10	0.09	0.09	-0.14	-0.98	x4 + 0.39
W5		-0.55	0.83	-0.06	0.05	0.00	x5 - 0.28

Longitudinal

W1		0.72	-0.57	-0.39	0.01	0.06	x1 - 0.68
W2		-0.06	-0.23	0.21	-0.95	-0.05	x2 - 0.06
W3	=	-0.17	0.34	-0.85	-0.24	-0.27	x3 - 0.21
W4		0.09	-0.13	0.20	0.12	-0.96	x4 + 0.41
W5		0.67	0.70	0.20	-0.17	-0.02	x5 + 0.35

Vertical

W1		0.73	-0.38	-0.43	-0.37	-0.03	x1 - 0.05
W2		-0.54	0.16	-0.72	-0.36	-0.19	x2 + 0.07
W3	=	0.07	-0.17	-0.39	0.81	-0.39	x3 + 0.51
W4		0.05	0.18	-0.37	0.27	0.87	x4 + 1.22
W5		0.42	0.88	-0.05	0.01	-0.23	x5 + 1.89

Radial

W1		0.82	0.54	-0.14	-0.08	0.08	x1 - 0.28
W2		-0.03	0.08	0.63	-0.76	0.15	x2 - 0.15
W3	=	-0.09	-0.12	-0.74	-0.64	-0.14	x3 - 0.25
W4		0.08	0.06	0.20	-0.03	-0.97	x4 + 0.53
W5		0.56	-0.82	0.09	-0.03	0.02	x5 - 0.02

Standard Instrument Departure

For the standard instrument departure scenario, the regression equations, analysis of variance summaries, and graphic illustrations are presented in the APPENDIX.

The F-ratios for the SID scenario indicate that the overall model for each dependent measure except vertical log RMS error was significant, with R^2's of 0.40, 0.38, 0.17, and 0.38, respectively.

F-tests on the individual coefficients of the four regression
equations indicated that for lateral log RMS error, TM, MF, PT, CO,
CO^2, TMxMF, and MFxPT were significant; for longitud'.al log RMS
error, TM, MF, PT, PT^2, CO^2, MFxPT, PTxCO, and PTxCG reached
significance; the only significant term for vertical log RMS error
was CO^2; while for radial log RMS error, MF, PT, CO, CO^2, MFxPT, and
PTxCO were significant.

The partitioned Residual sum-of-squares indicates a reliable
Subjects effect for lateral and vertical log RMS error, meaning the
behavior of at least one of the subjects differed from that of the
rest. The significant Lack-of-Fit term for each model indicates the
equations would better approximate the response surfaces with the
addition of higher-order terms or additional factors, especially in
the case of vertical log RMS error.

The stationary point for each of the four systems is given in
Table 13. The four canonical equations describing the nature of the
response surfaces surrounding the stationary points are:

$$\log RMSE, lat = 0.99 - 0.06W1^2 - 0.01W2^2 + 0.02W3^2 + 0.06W4^2 + 0.10W5^2.$$

$$\log RMSE, lon = 1.29 - 0.03W1^2 - 0.00W2^2 + 0.01W3^2 + 0.05W4^2 + 0.10W5^2.$$

$$\log RMSE, ver = 1.09 - 0.03W1^2 - 0.01W2^2 + 0.01W3^2 + 0.03W4^2 + 0.09W5^2.$$

$$\log RMSE, rad = 1.32 - 0.03W1^2 + 0.00W2^2 + 0.01W3^2 + 0.04W4^2 + 0.10W5^2.$$

TABLE 13
Response Surface Stationary Points for the SID Scenario

log RMSE	TM	MF	PT	CO	CG	Y
Lateral	-0.49	0.05	1.72	-0.23	0.81	0.99
Longitudinal	0.34	-2.37	0.53	-0.54	-1.88	1.29
Vertical	-0.33	-0.42	-0.56	-0.20	-0.82	1.09
Radial	-0.96	-0.69	1.46	-0.05	-0.49	1.32

All four systems, upon examination of the signs of the canonical
coefficients, seem to be saddle-point type surfaces. For lateral,
longitudinal, and vertical log RMS errors, moving along the W1 and W2
axes results in decreases in Y, while moving along the W3, W4, and W5
axes results in increases in Y. For radial log RMS error, decreases
in Y occur when moving along the W1 axis, whereas increases in Y
occur when moving along the W2, W3, W4, and W5 axes. The magnitudes
of the W coefficients reveal that the surfaces for lateral and radial

log RMS error are attenuated along the W2 and W3 axes, whereas for longitudinal and vertical log RMS error, attentuation occurs along the W1, W2, and W3 axes.

The matrix equations relating the old x's to the new W variables are given in Table 14. Optimum operating conditions, as determined by the x to W relationships and the canonical equations, are as follows: for lateral log RMS error, TM = -1.0, MF = 0.5, PT = -1.0, CO = 1.0, CG = 0.5, with a predicted error of 0.69 or 4.84 feet; for longitudinal log RMS error, TM = 0.3, MF = 2.0, PT = 0.5, CO = -0.5, CG = -1.8, with a predicted error of 1.30 or 19.85 feet; for vertical log RMS error, TM = 2.0, MF = 2.0, PT = -0.6, CO = -1.0, CG = -0.8, with a predicted error of 0.89 or 7.78 feet; and finally, for radial log RMS error, TM = -1.0, MF = 2.0, PT = 1.4, CO = -0.1, CG = - 0.5, with a predicted error of 1.31 or 19.91 feet.

TABLE 14
X to W Transformation Matrix Equations for the SID Scenario

Lateral

W1		-0.69	0.06	-0.58	0.41	0.00	x1 + 0.49
W2		0.60	0.25	-0.18	0.73	0.03	x2 - 0.05
W3	=	-0.31	-0.31	0.72	0.54	0.01	x3 - 1.72
W4		0.05	0.17	0.12	-0.02	-0.98	x4 + 0.23
W5		-0.24	0.90	0.31	-0.04	0.18	x5 - 0.81

Longitudinal

W1		-0.63	-0.15	-0.74	0.08	-0.15	x1 - 0.34
W2		0.55	0.55	-0.49	0.29	-0.28	x2 + 2.37
W3	=	-0.43	0.32	0.46	0.51	-0.49	x3 - 0.53
W4		-0.16	0.29	-0.03	0.49	0.81	x4 + 0.54
W5		-0.30	0.70	0.03	-0.64	0.08	x5 + 1.88

Vertical

W1		-0.46	-0.66	0.06	-0.57	-0.15	x1 + 0.33
W2		-0.48	-0.33	-0.07	0.80	-0.11	x2 + 0.42
W3	=	0.74	-0.62	0.04	0.17	-0.19	x3 + 0.55
W4		0.02	-0.27	-0.05	0.03	0.96	x4 + 0.20
W5		-0.04	0.03	0.99	0.08	0.06	x5 + 0.82

Radial

W1		-0.56	0.62	-0.51	0.21	-0.06	x1 + 0.96
W2		0.64	0.54	0.18	0.48	-0.19	x2 + 0.69
W3	=	-0.47	-0.25	0.50	0.61	-0.29	x3 - 1.46
W4		-0.06	0.07	0.16	0.30	0.94	x4 + 0.05
W5		-0.23	0.50	0.66	-0.51	0.00	x5 + 0.49

DISCUSSION

As seen in the analyses of variances, the relative importance of the five manipulated control and display factors varied greatly as a function of flight task. This result was anticipated, since the three flight task profiles imposed vastly different control and attentional demands. The landing and takeoff scenarios consisted of complex sequences of banks and cruises, ascents and descents, resulting in the emergence of control order (linear and quadratic components) as the dominant factor. Decreasing the acceleration component of the control-order fraction resulted in more precise tracking.

The other major factor in the landing and takeoff scenarios was the quadratic prediction-time component. As seen in the figures graphically depicting the response surfaces for prediction time, a U-shaped surface emerges with short and long prediction times resulting in increases in tracking error. Again the nature of the flight tasks would seem to be the major reason for the shape of the functions. Short prediction times resulted in overcontrol of the vehicle when precise tracking was required, while long prediction times resulted in undercontrol of the vehicle.

The relative insignificance of the other three experimental factors can be attributed directly to the dominance of control order. When subjects were presented with a display and control configuration with pure acceleration (second-order) control, performance deteriorated such that the levels of the other factors became unimportant. It is believed that if control order were kept at a fixed optimum level, the other factors would emerge as significant. This finding reiterates the need for multifactor experimentation. The interactions among numerous variables are so complex that a reductionist study would only give an incomplete and possibly biased account of the response surface.

Results from the standard instrument departure scenario confirmed the results found in the previous screening study. (Tatro et al., 1983). All five experimental factors were significant. An interesting result from this scenario was the fact that the linear terms of the model accounted for the majority of the variance, whereas the quadratic components of the regression models emerged significant in the more complex flight tasks. This would indicate the need for estimating second-order models in approximating surfaces for complex tasks, which are the norm for VTOL flight.

All three flight scenarios, upon examination of the fitted surfaces, revealed optimum operating conditions in approximately the same variable ranges as seen in Table 15. It appears the selection of the experimental variable ranges and center-point values of the central composite design provided a good sampling for interpolating optimum conditions as indicated by the optimum variable ranges and the minimums of the U-shaped functions for the various factors.

TABLE 15
Summary of the Optimum Operating Condition Ranges
Across All Three Flight Scenarios

Variable	Optimum Coded Range	Optimum Transformed Range
Takeoff		
Tracking Mode (TM)	-0.8 to 0.2	40% to 53% VRC
Magnification Factor (MF)	0.4 to 2.0	100 to 125
Prediction Time (PT)	1.4 to 2.0	2.2 to 2.5 sec
Control Order (CO)	-0.5 to 0.5	1.5 to 1.7
Control Gain (CG)		
longitudinal (1st order)	-0.3 to 0.9	-7700 to -8900
longitudinal (2nd order)	-0.3 to 0.9	-164 to -209
lateral (1st order)	-0.3 to 0.9	15975 to 18075
lateral (2nd order)	-0.3 to 0.9	728 to 818
vertical (1st order)	-0.3 to 0.9	-925 to -1225
vertical (2nd order)	-0.3 to 0.9	-55 to -76
azimuth (1st order)	-0.3 to 0.9	0.7 to 1.0
azimuth (2nd order)	-0.3 to 0.9	0.4 to 0.5
Landing		
Tracking Mode (TM)	0.0 to 0.4	50% to 55% VRC
Magnification Factor (MF)	-0.1 to 1.0	75 to 125
Prediction Time (PT)	-1.0 to 0.2	1.0 to 1.7 sec
Control Order (CO)	-1.2 to 1.0	1.4 to 1.8
Control Gain (CG)		
longitudinal (1st order)	-1.8 to 0.3	-6200 to -8300
longitudinal (2nd order)	-1.8 to 0.3	-108 to -186
lateral (1st order)	-1.8 to 0.3	13350 to 17025
lateral (2nd order)	-1.8 to 0.3	615 to 773
vertical (1st order)	-1.8 to 0.3	-550 to -1075
vertical (2nd order)	-1.8 to 0.3	-29 to -65
azimuth (1st order)	-1.8 to 0.3	0.4 to 0.9
azimuth (2nd order)	-1.8 to 0.3	0.2 to 0.4

TABLE 15, Continued

Standard Instrument Departure

Tracking Mode (TM)	-1.0 to 2.0	38% to 75% VRC
Magnification Factor (MF)	0.5 to 2.0	112 to 125
Prediction Time (PT)	-1.0 to 1.0	1.0 to 2.0 sec
Control Order (CO)	-1.0 to 1.0	1.4 to 1.8
Control Gain (CG)		
longitudinal (1st order)	-1.8 to 0.5	-6200 to -8500
longitudinal (2nd order)	-1.8 to 0.5	-108 to -194
lateral (1st order)	-1.8 to 0.5	13350 to 17375
lateral (2nd order)	-1.8 to 0.5	615 to 788
vertical (1st order)	-1.8 to 0.5	-550 to -1125
vertical (2nd order)	-1.8 to 0.5	-29 to -69
azimuth (1st order)	-1.8 to 0.5	0.4 to 0.9
azimuth (2nd order)	-1.8 to 0.5	0.2 to 0.5

Overall, it appears an optimum operating condition occurs when tracking mode (TM) = 50% VRC, magnification factor (MF) = 110, prediction time (PT) = 1.7 seconds, control order (CO) = 1.6, and control gain (CG) longitudinal first-order = -7630, longitudinal second-order = -162, lateral first-order = 15858, lateral second-order = 631, vertical first-order = -908, vertical second-order = -54, azimuth first-order = 0.7, azimuth second-order = 0.4, all of which are very close to the CCD center-point condition.

Finally, further experimentation should explore a very limited range surrounding the optimum operating conditions. In this way the values can be refined to achieve even more precise tracking. In addition, other flight scenarios should be evaluated because the nature of the flight task dictates which variables affect performance critically. Because of the significant Lack-of-Fit found in all but one of the regression equations, other variables may have to be screened to assess their importance. It is believed, though, that the inclusion of a hypothetical time-sharing "factor" in the model will account for a majority of the still unaccounted for variance.

Indirect evidence from this experiment supports the existence of such an intervening variable. Although performance data for the three flight scenarios were not analyzed collectively, it is evident that, as task complexity increased from the standard instrument departure to terrain following and landing to the instrument takeoff, the ranges of scores increased as a function of subject ability levels. The increasing complexity of the flight tasks called for increasing time-sharing of attention, and time-sharing ability no doubt contributed heavily to the subjects' pretest matching scores.

The multiple-regression prediction equations for the various
dependent performance measures on the three task scenarios serve as
reasonably comphrehensive models of pilot performance in
representative vertical and translational flight maneuvers. Because
the more complex scenarios for terrain following and landing and for
takeoff impose greater time-sharing demands than the standard
instrument departure, a composite model based on radial tracking
errors for those scenarios would be the indicated choice as a guide
in system design. For all variables except prediction time, a single
value can be selected that falls within the optimum range shown in
Table 15. As in the case of vertical control gain, prediction time
should be adjusted automatically with changes in altitude scale
factor.

THIS
PAGE
IS
MISSING
IN
ORIGINAL
DOCUMENT

TABLE A-1
Summary of the Analysis of Variance for the Regression
Equation of Lateral Log RMS Error in the Takeoff Scenario

$$\log \text{RMSE,lat} = 1.06 - 0.02\text{TM} - 0.03\text{MF} - 0.02\text{PT} + 0.20\text{CO} + 0.07\text{CG}$$
$$+ 0.05\text{TM}^2 + 0.01\text{MF}^2 + 0.12\text{PT}^2 + 0.16\text{CO}^2 + 0.07\text{CG}^2 + 0.04\text{TMxMF}$$
$$- 0.06\text{TMxPT} + 0.02\text{TMxCO} + 0.08\text{TMxCG} - 0.07\text{MFxPT} + 0.02\text{MFxCO}$$
$$- 0.02\text{MFxCG} + 0.06\text{PTxCO} - 0.10\text{PTxCG} - 0.05\text{COxCG}.$$

Source	df	Mean Square	F
Regression	20	.5921	4.2720**
TM	1	.0461	.3324
MF	1	.0991	.7153
PT	1	.0348	.2509
CO	1	3.8131	27.5124**
CG	1	.4107	2.9631
TM	1	.2531	1.8264
MF	1	.0072	.0520
PT	1	1.7486	12.6163**
CO	1	2.8480	20.5488**
CG	1	.5303	3.8264*
TMxMF	1	.0991	.7153
TMxPT	1	.2303	1.6615
TMxCO	1	.0259	.1867
TMxCG	1	.3741	2.6991
MFxPT	1	.2781	2.0067
MFxCO	1	.0186	.1342
MFxCG	1	.0201	.1452
PTxCO	1	.2361	1.7023
PTxCG	1	.5800	4.1847**
COxCG	1	.1887	1.3615
Residual	107	.2763	
Subjects	3	4.7663	34.3899**
Lack-of-Fit	6	.2808	2.0260
Replications	98	.1386	
Total	127		

* $p \leq .05$
** $p \leq .01$

34

EXPERIMENT 1 PREDICTION TIME
LATERAL ERROR
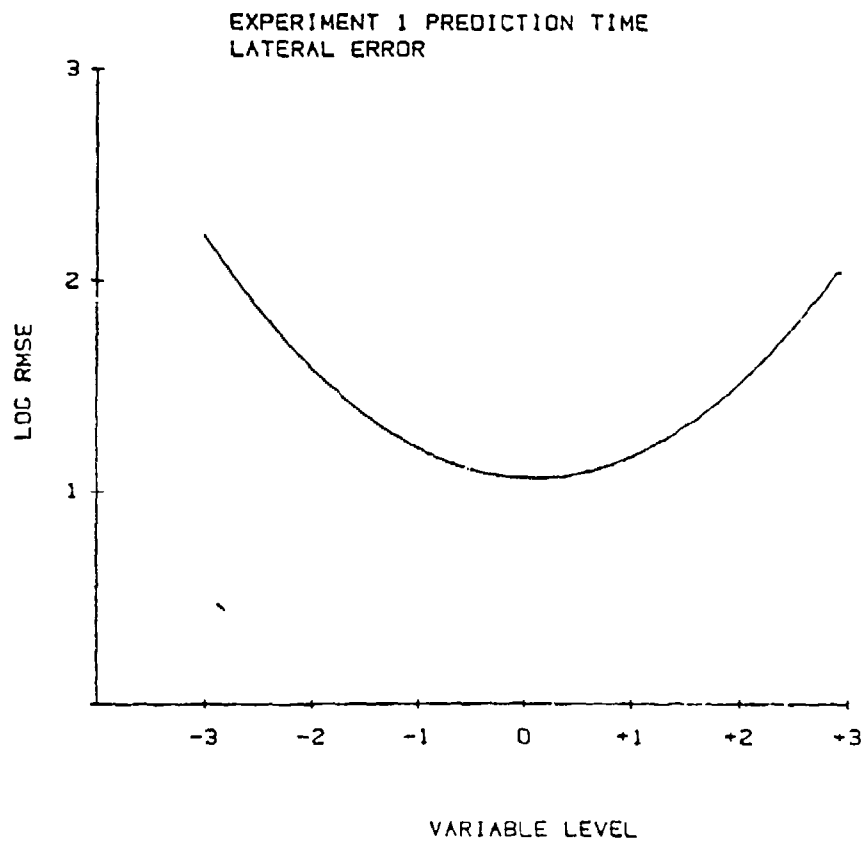
Figure A-1.   Takeoff Scenario: Lateral log RMSE as
a function of Prediction Time.

EXPERIMENT 1 CONTROL ORDER
LATERAL ERROR
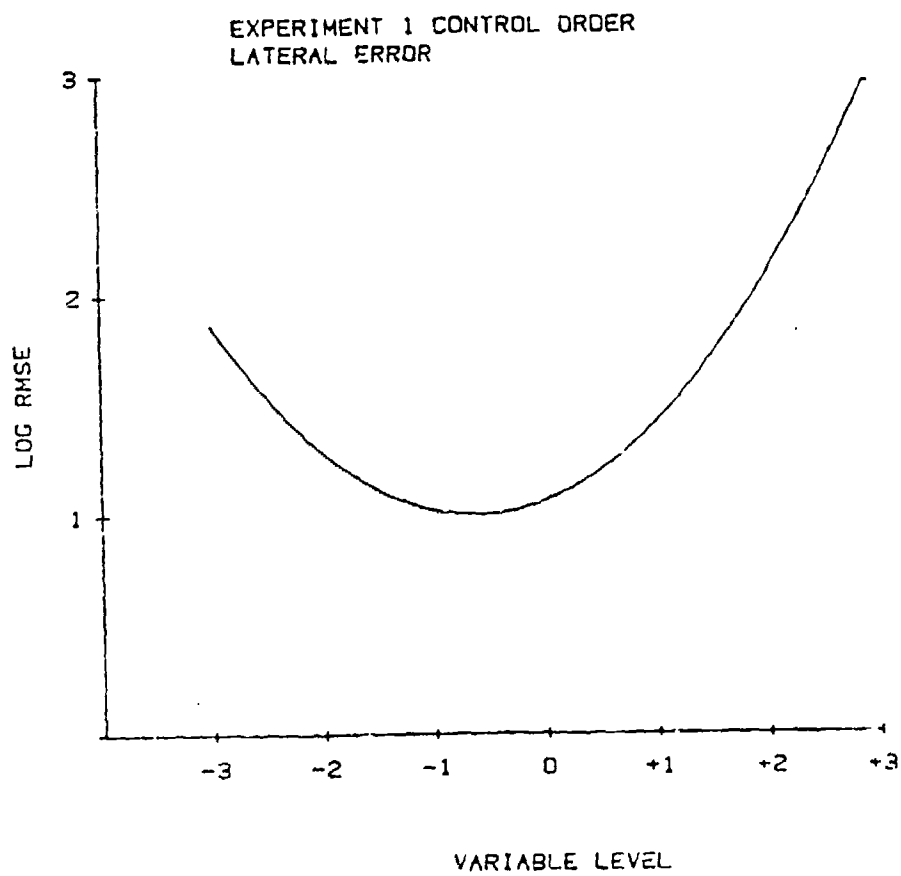
Figure A-2.   Takeoff Scenario: Lateral log RMSE as
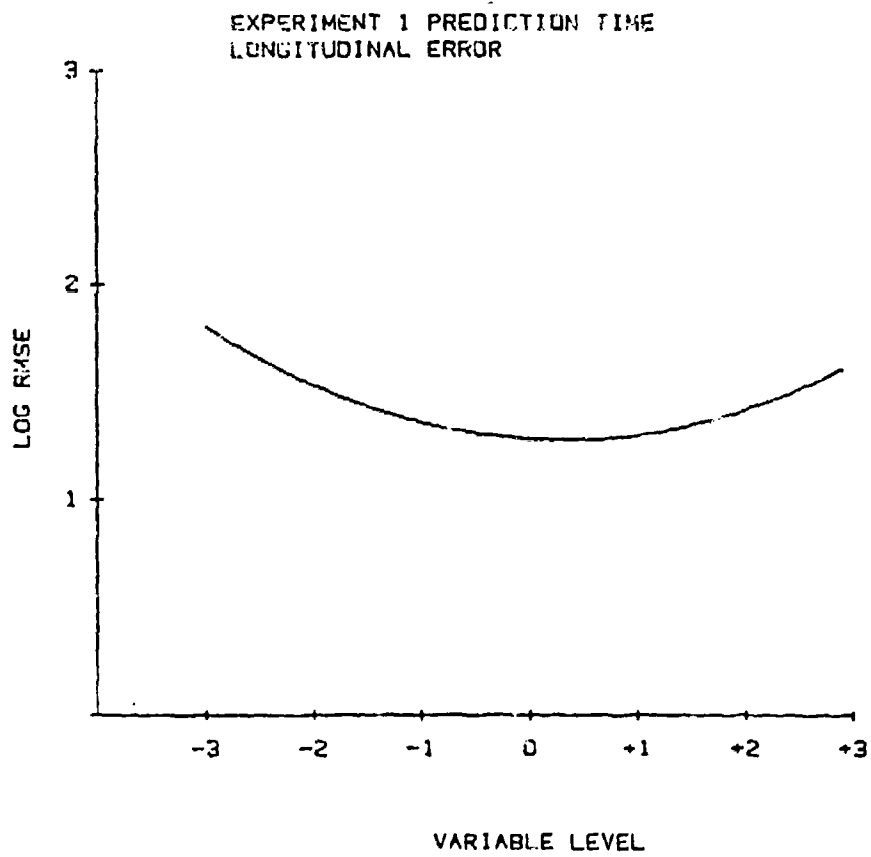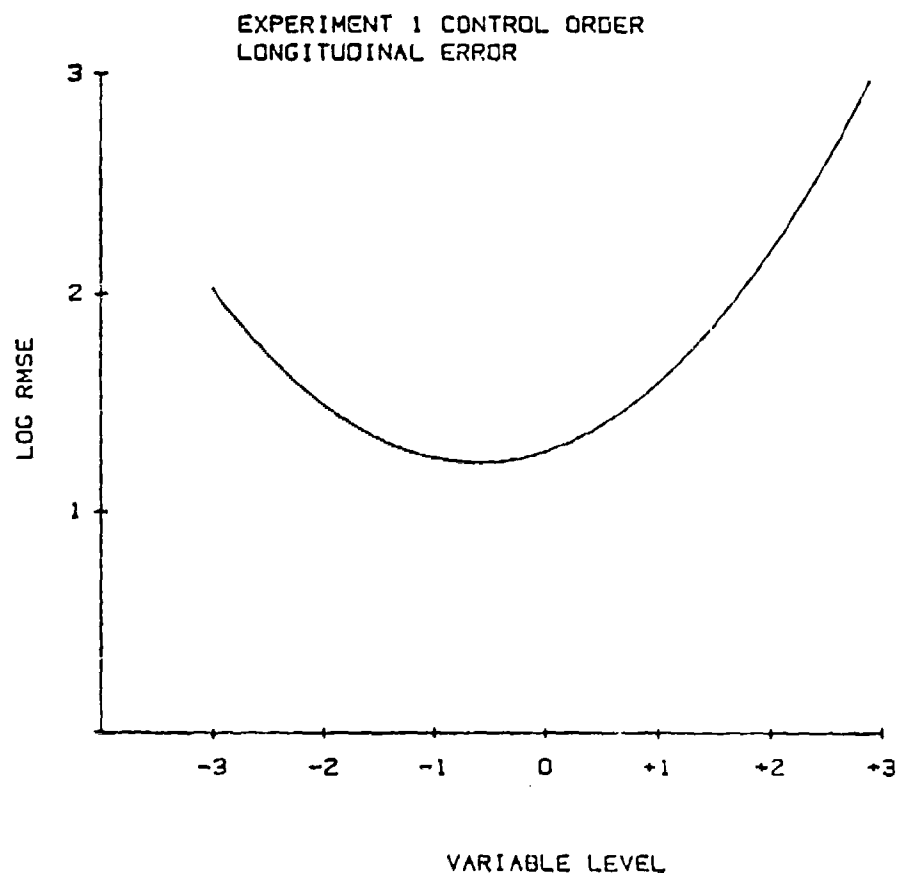a function of Control Order.

**EXPERIMENT 1 CONTROL GAIN
LATERAL ERROR**
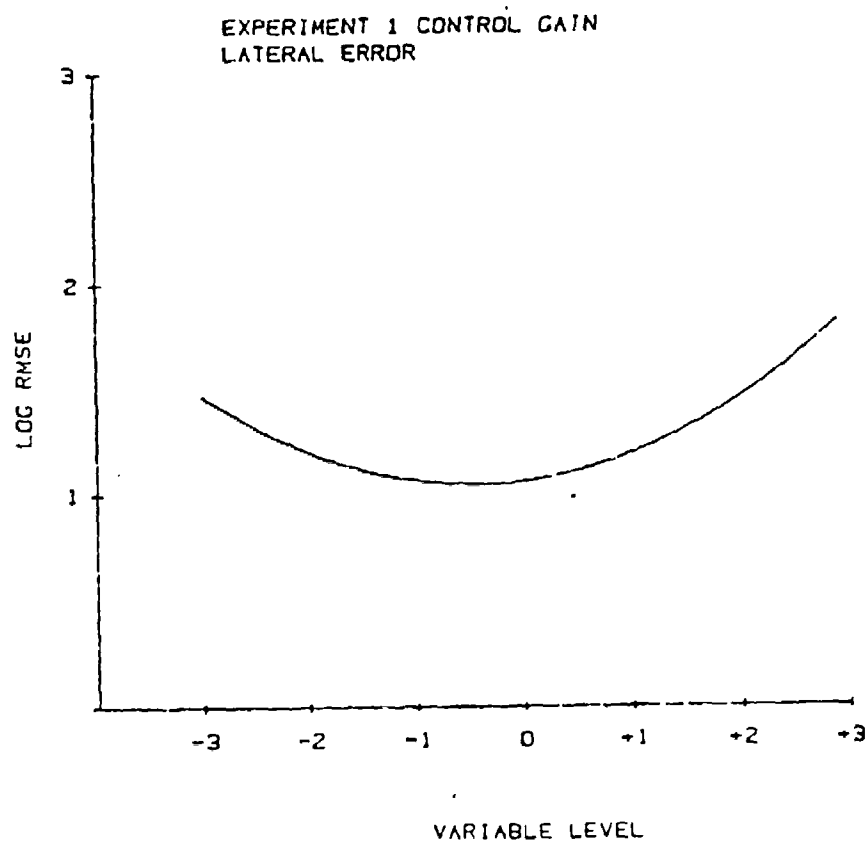
Figure A-3. Takeoff Scenario: Lateral log RMSE as
a function of Control Gain.
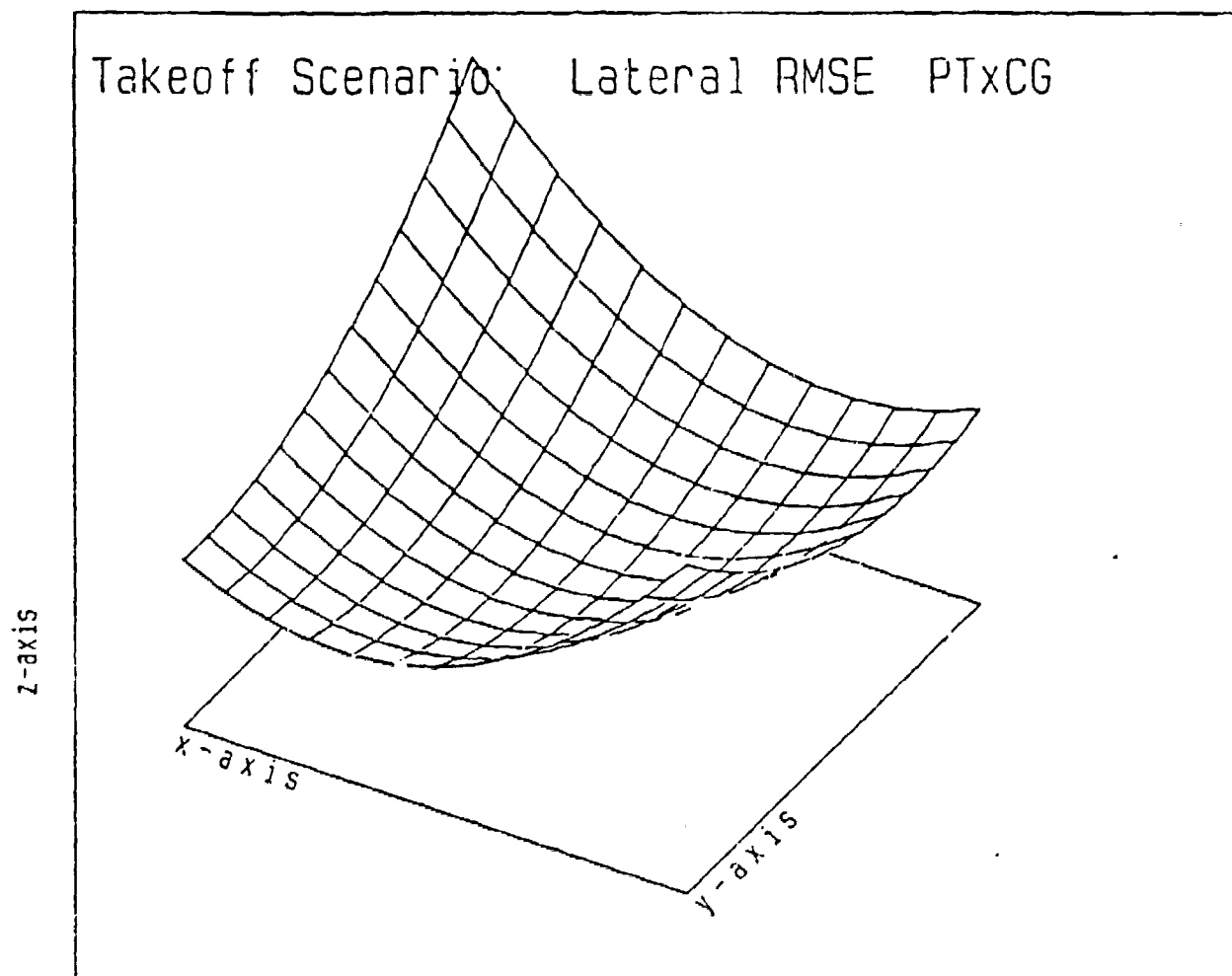
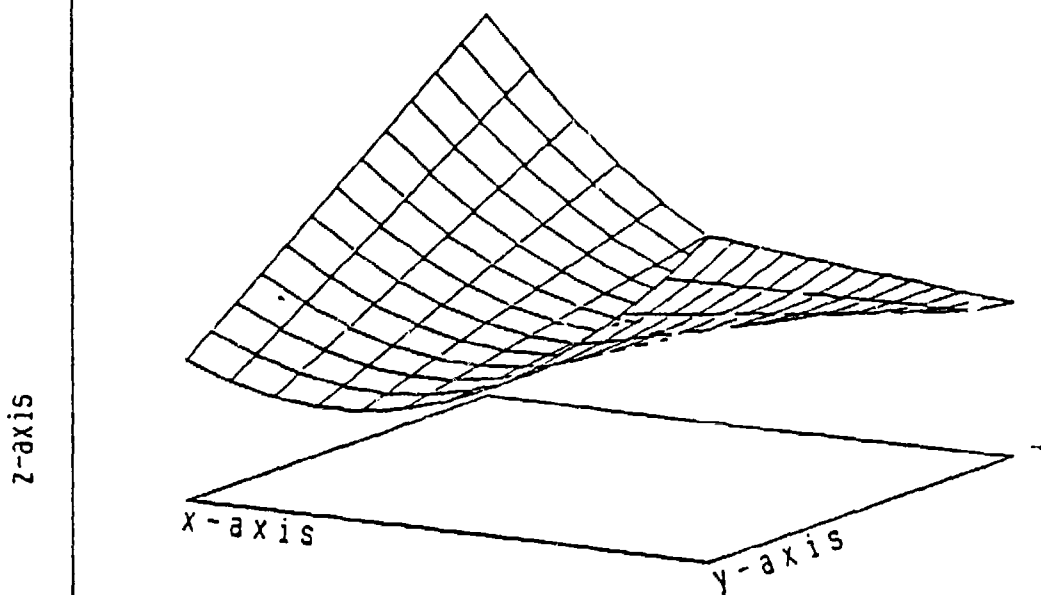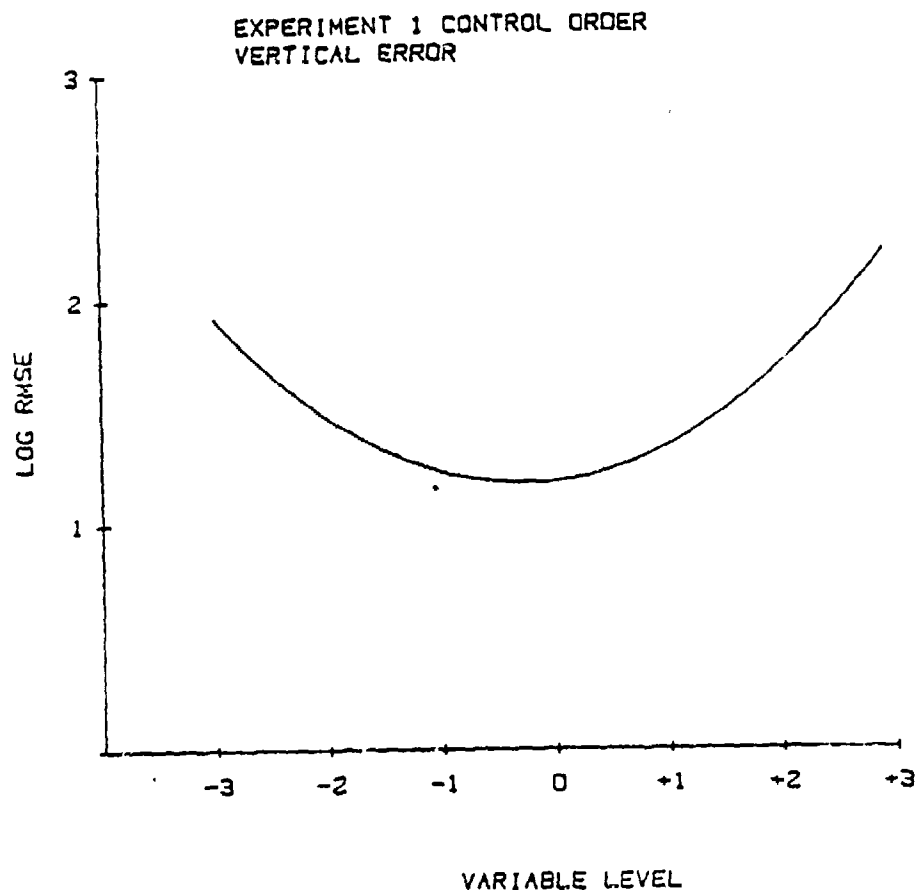Figure A-4. Takeoff Scenario: Lateral log RMSE as
a function of Prediction Time and Control Gain.

TABLE A-2
Summary of the Analysis of Variance for the Regression
Equation of Longitudinal Log RMS Error in the Takeoff Scenario

$$\log \text{RMSE,lon} = 1.28 - 0.02TM - 0.03MF - 0.03PT + 0.17CO + 0.05CG$$
$$- 0.01TM^2 + 0.06MF^2 + 0.05PT^2 + 0.14CO^2 + 0.05CG^2 + 0.01TMxMF$$
$$- 0.02TMxPT + 0.05TMxCO + 0.07TMxCG - 0.01MFxPT + 0.01MFxCO$$
$$+ 0.01MFxCG - 0.03PTxCO - 0.10PTxCG + 0.01COxCG.$$

Source	df	Mean Square	F
Regression	20	.4182	4.9964**
TM	1	.0530	.6330
MF	1	.1007	1.2032
PT	1	.0768	.9176
CO	1	2.9123	34.8045**
CG	1	.2641	3.1558
TM	1	.0073	.0876
MF	1	.3960	4.7321*
PT	1	.2771	3.3120*
CO	1	2.3238	27.7707**
CG	1	.3340	3.9911*
TMxMF	1	.0048	.0558
TMxPT	1	.0269	.3219
TMxCO	1	.1361	1.6261
TMxCG	1	.2961	3.5383*
MFxPT	1	.0026	.0315
MFxCO	1	.0069	.0826
MFxCG	1	.0012	.0145
PTxCO	1	.0478	.5712
PTxCG	1	.5825	6.9594**
COxCG	1	.0138	.1649
Residual	107	.1502	
Subjects	3	1.5808	18.8921**
Lack-of-Fit	6	.5223	6.2401**
Replications	98	.0837	
Total	127		

* $p \leq .05$
** $p \leq .01$

EXPERIMENT 1 MAGNIFICATION FACTOR
LONGITUDINAL ERROR

LOG RMSE

VARIABLE LEVEL
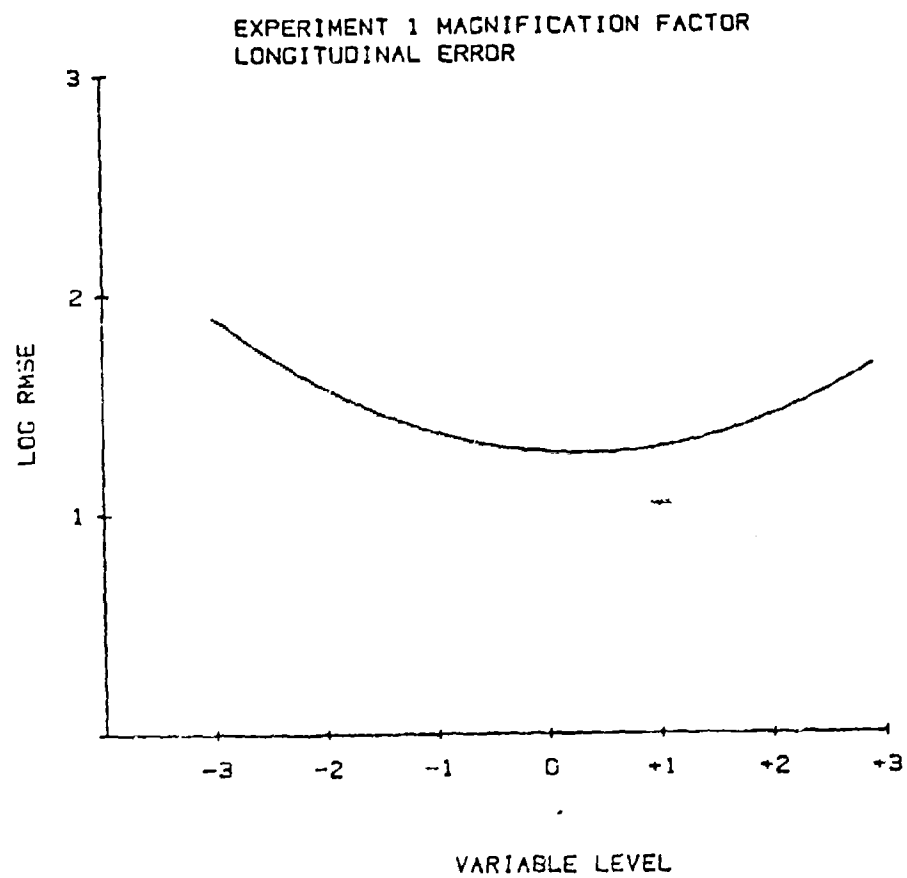
Figure A-5.   Takeoff Scenario: Longitudinal log RMSE as
a function of Magnification Factor.

EXPERIMENT 1 PREDICTION TIME
LONGITUDINAL ERROR

Figure A-6.   Takeoff Scenario: Longitudinal log RMSE as
a function of Prediction Time.

EXPERIMENT 1 CONTROL ORDER
LONGITUDINAL ERROR

LOG RMSE

VARIABLE LEVEL

Figure A-7. Takeoff Scenario: Longitudinal log RMSE as
a function of Control Order.
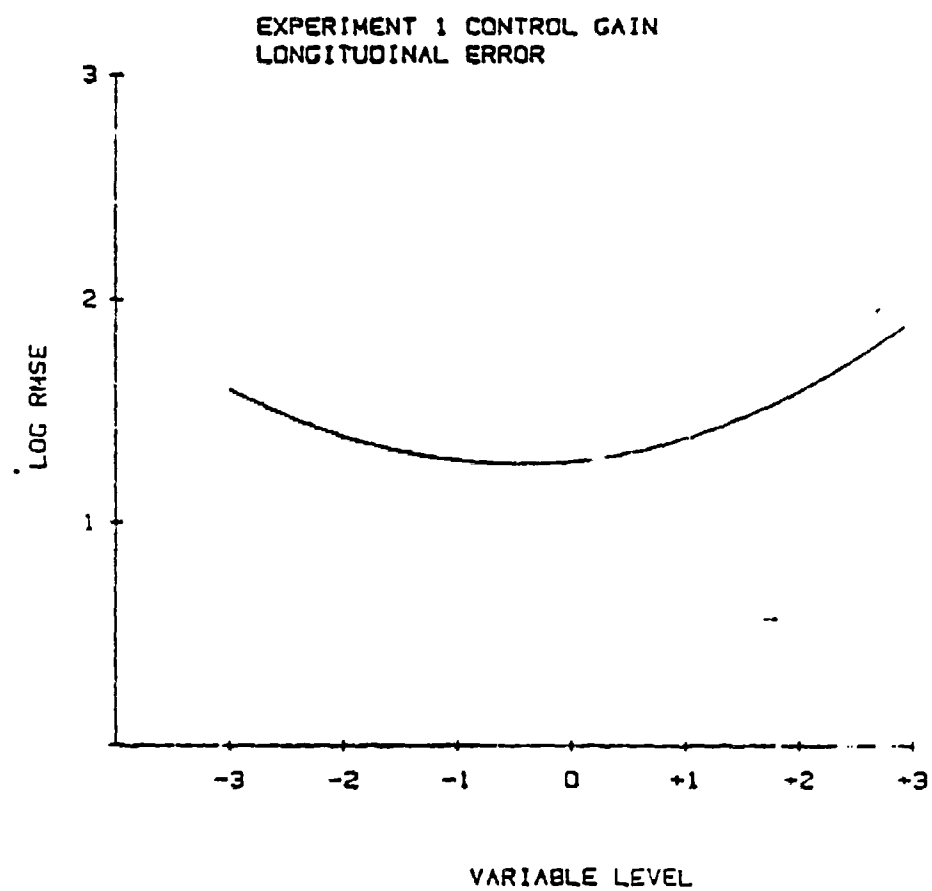
Figure A-8.   Takeoff Scenario: Longitudinal log RMSE as
a function of Control Gain.
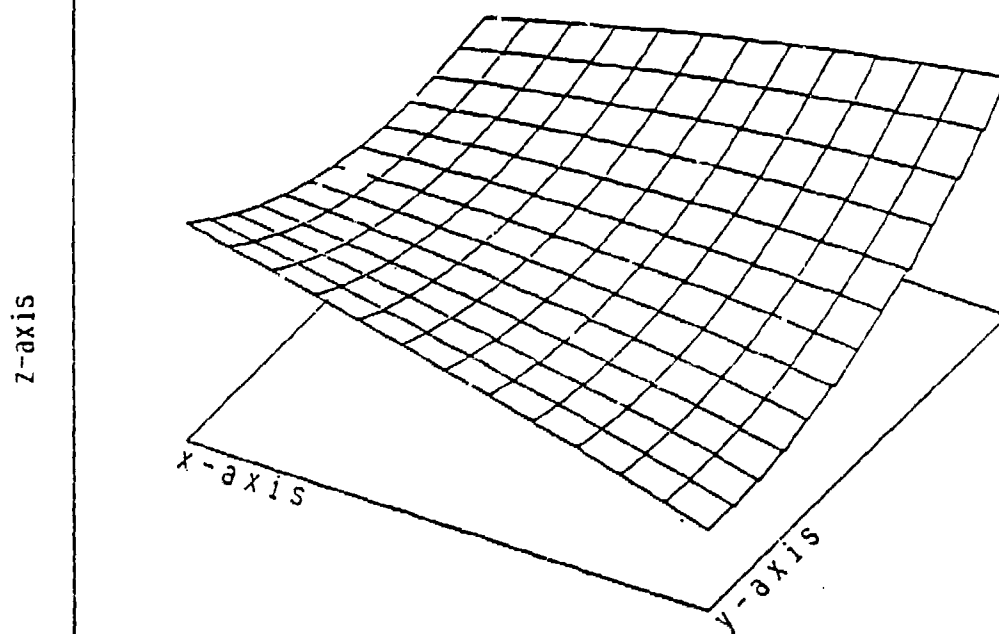
Figure A-9. Takeoff Scenario: Longitudinal log RMSE as
a function of Tracking Mode and Control Gain.

Figure A-10. Takeoff Scenario: Longitudinal log RMSE as
a function of Prediction Time and Control Gain.

TABLE A-3
Summary of the Analysis of Variance for the Regression
Equation of Vertical Log RMS Error in the Takeoff Scenario

$$\log RMSE, ver = 1.19 - 0.02TM + 0.03MF - 0.02PT + 0.06CO + 0.01CG$$
$$+ 0.01TM^2 + 0.02MF^2 + 0.02PT^2 + 0.10CO^2 - 0.03CG^2 - 0.03TMxMF$$
$$+ 0.00TMxPT - 0.01TMxCO + 0.02TMxCG - 0.00MFxPT + 0.01MFxCO$$
$$- 0.01MFxCG + 0.00PTxCO - 0.05PTxCG - 0.04COxCG.$$

Source	df	Mean Square	F
Regression	20	.1246	3.6327**
TM	1	.0535	1.5611
MF	1	.0699	2.0393
PT	1	.0397	1.1586
CO	1	.3300	9.6250**
CG	1	.0160	.4663
TM	1	.C032	.0937
MF	1	.0318	.9264
PT	1	.0327	.9547
CO	1	1.1959	34.8758**
CG	1	.0888	2.5909
TMxMF	1	.0558	1.6271
TMxPT	1	.0005	.0133
TMxCO	1	.0055	.1592
TMxCG	1	.0175	.5091
MFxPT	1	.0006	.0166
MFxCO	1	.C081	.2356
MFxCG	1	.0025	.0718
PTxCO	1	.0000	.0000
PTxCG	1	.1487	4.3353*
COxCG	1	.1183	3.4490*
Residual	107	.0636	
Subjects	3	.9459	27.5849**
Lack-of-Fit	6	.1020	2.9723**
Replications	98	.0343	
Total	127		

* $p \leq .05$
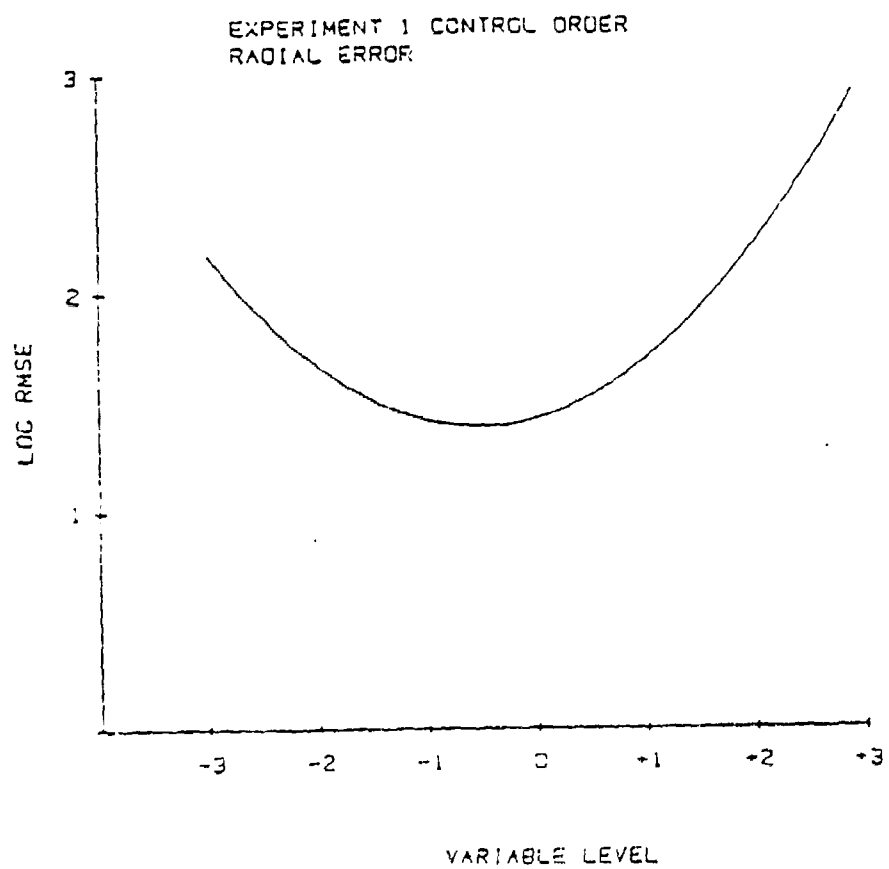** $p \leq .01$

46

EXPERIMENT 1 CONTROL ORDER
VERTICAL ERROR

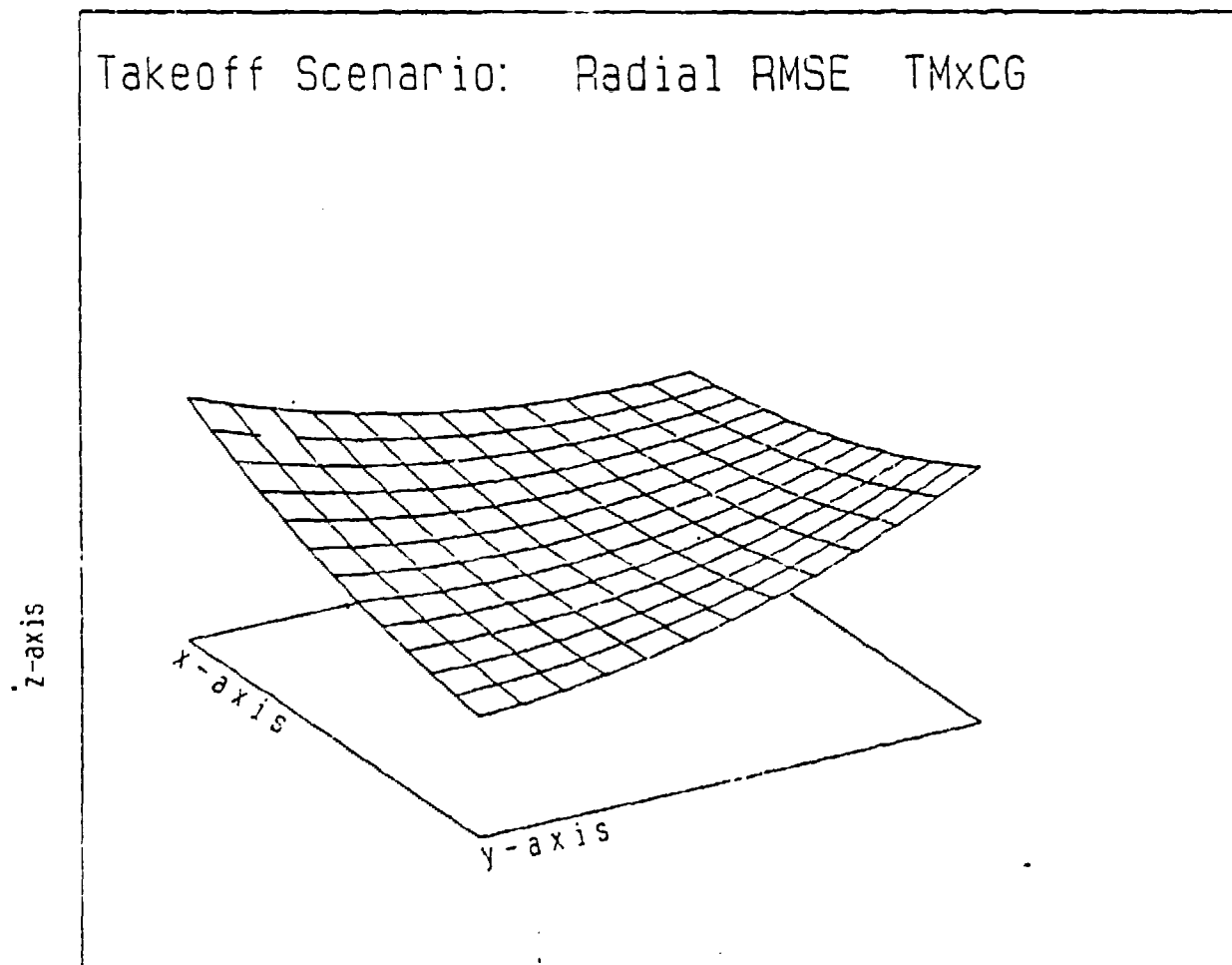Figure A-11. Takeoff Scenario: Vertical log RMSE as
a function of Control Order.
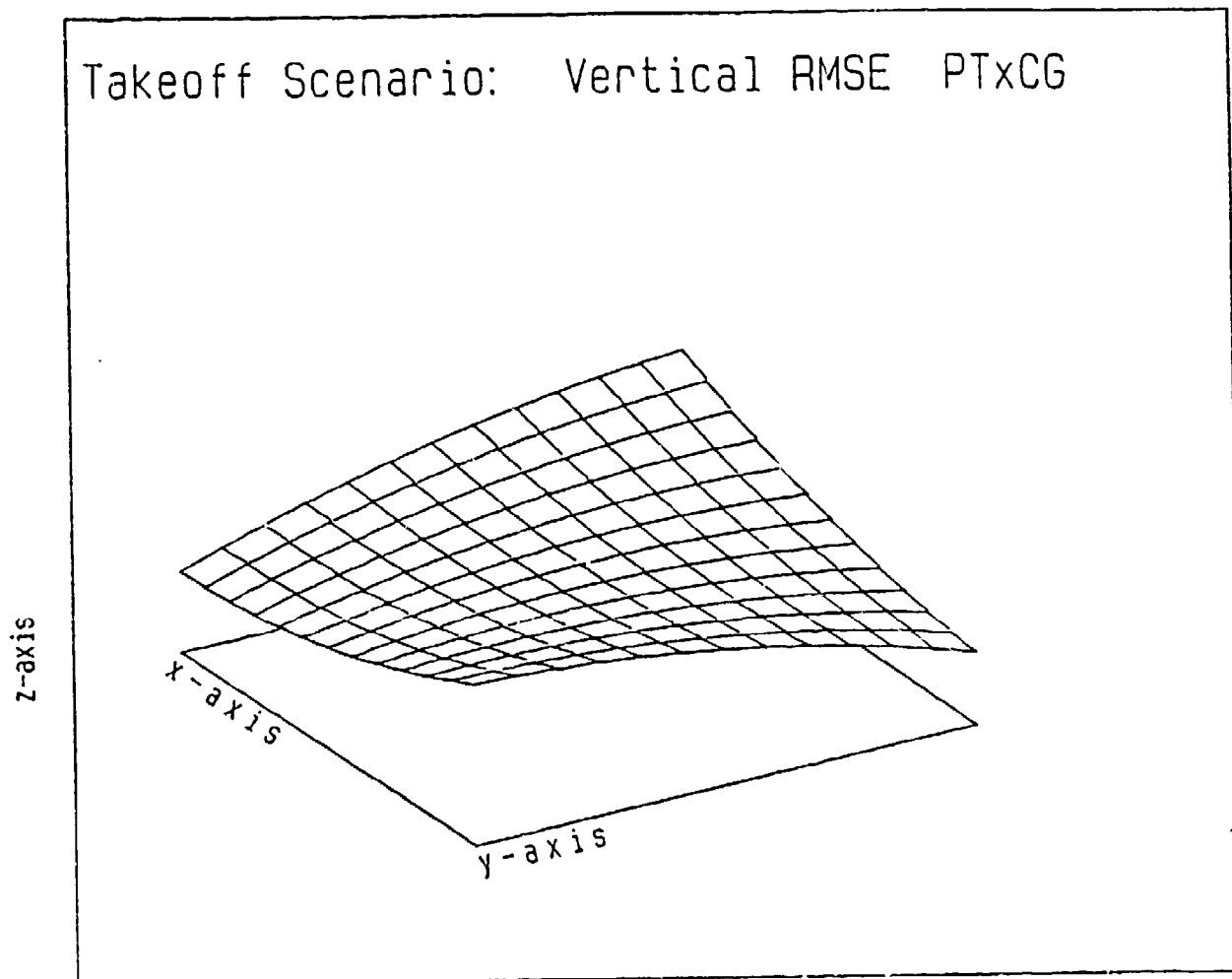
Figure A-12. Takeoff Scenario: Vertical log RMSE as
a function of Prediction Time and Control Gain.
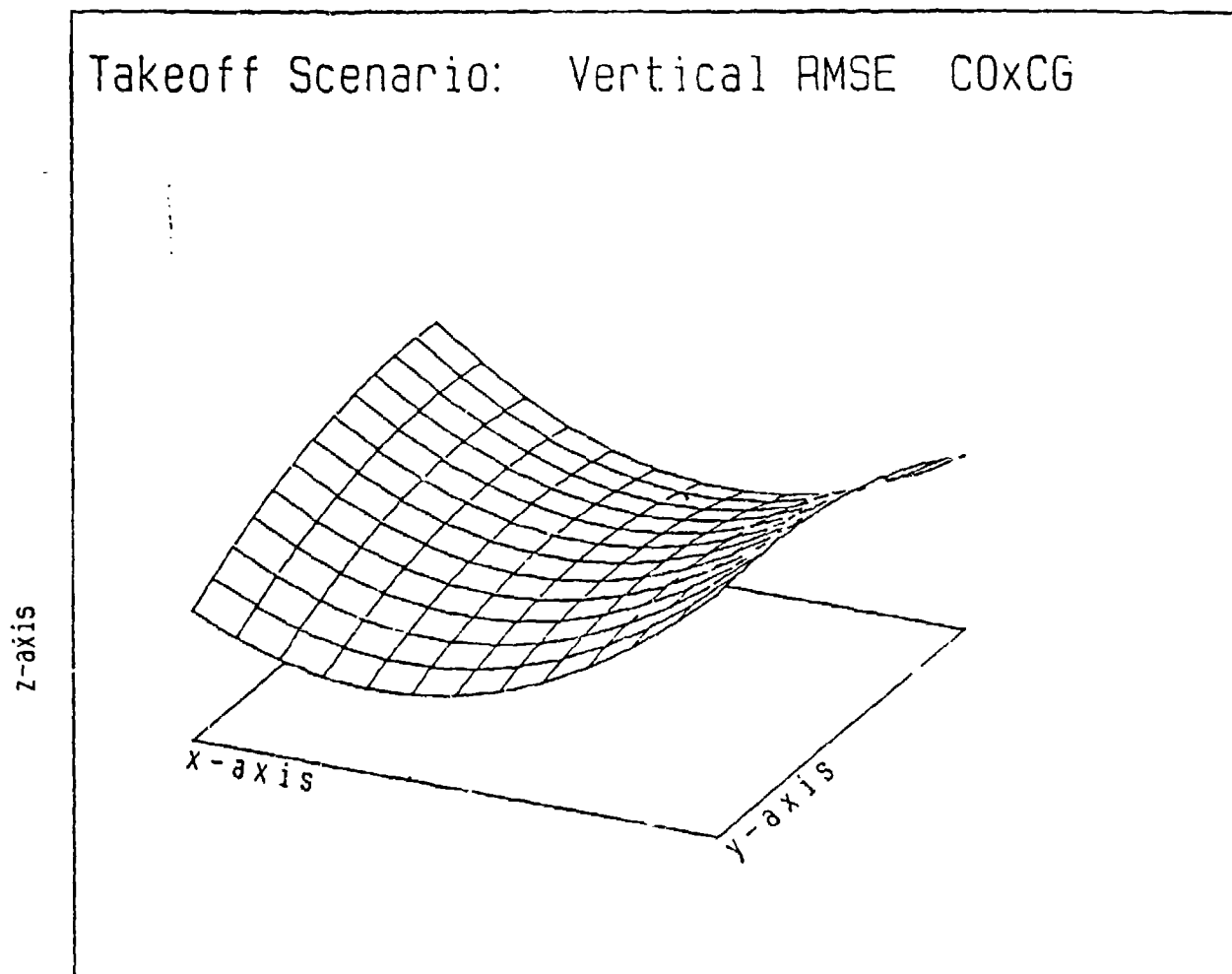
Figure A-13. Takeoff Scenario: Vertical log RMSE as
a function of Control Order and Control Gain.

TABLE A-4

Summary of the Analysis of Variance for the Regression
Equation of Radial Log RMS Error in the Takeoff Scenario

$\log \text{RMSE,rad} = 1.23 - 0.02TM - 0.01MF - 0.06PT + 0.14CO + 0.04CG$
$+ 0.02TM^2 + 0.03MF^2 + 0.06PT^2 + 0.13CO^2 + 0.03CG^2 + 0.01TMxMF$
$- 0.03TMxPT + 0.01TMxCO + 0.06TMxCG - 0.04MFxPT + 0.01MFxCO$
$- 0.01MFxCG + 0.01PTxCO - 0.07PTxCG - 0.05COxCG.$

Source	df	Mean Square	F
Regression	20	.3032	5.3474**
TM	1	.0593	1.0460
MF	1	.0161	.2837
PT	1	.1058	1.8647
CO	1	1.8345	32.3336**
CG	1	.1747	3.0786
TM	1	.0371	.6533
MF	1	.0977	1.7216
PT	1	.4210	7.4203*
CO	1	1.9705	34.7303**
CG	1	.1429	2.5188
TMxMF	1	.0079	.1394
TMxPT	1	.0574	1.0120
TMxCO	1	.0100	.1767
TMxCG	1	.2541	4.4793*
MFxPT	1	.1167	2.0570
MFxCO	1	.0036	.0637
MFxCG	1	.0083	.1456
PTxCO	1	.0065	.1146
PTxCG	1	.3590	6.3316*
COxCG	1	.1331	2.3474
Residual	107	.1193	
Subjects	3	1.8698	32.9551**
Lack-of-Fit	6	.2662	4.6949**
Replications	98	.0567	
Total	127		

* $p \le .05$
** $p \le .01$

EXPERIMENT 1 PREDICTION TIME
RADIAL ERROR
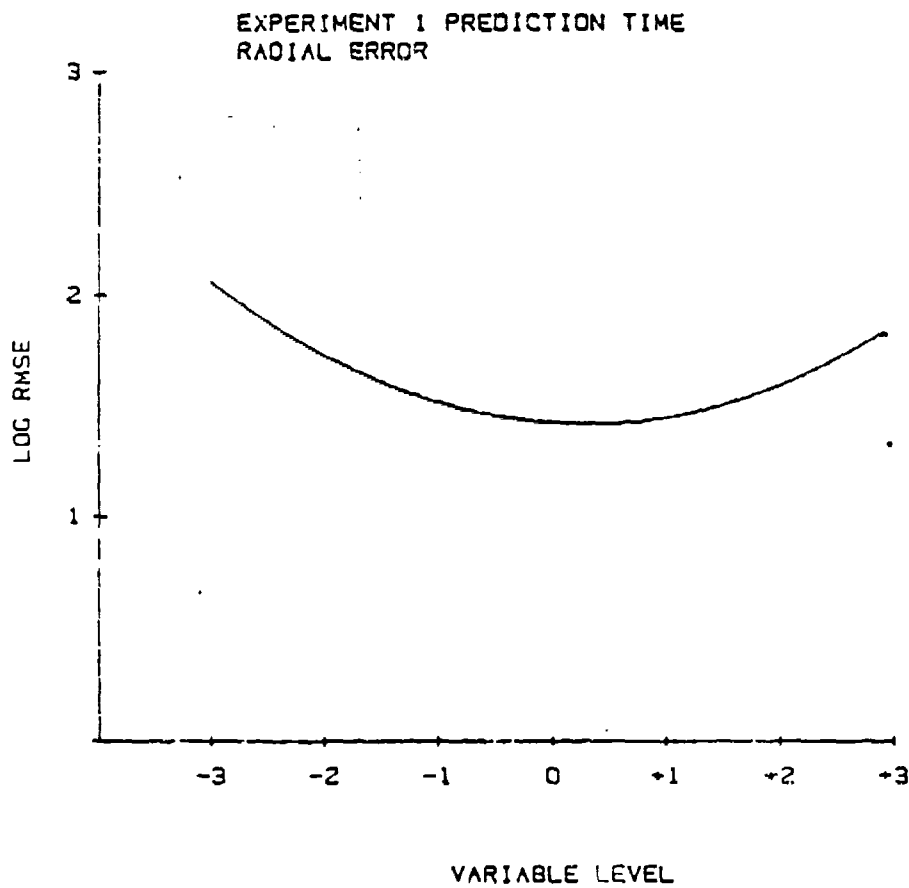
Figure A-14.   Takeoff Scenario: Radial log RMSE as a function
of Prediction Time.

EXPERIMENT 1 CONTROL ORDER
RADIAL ERROR

Figure A-15.   Takeoff Scenario: Radial log RMSE as a function
of Control Order.

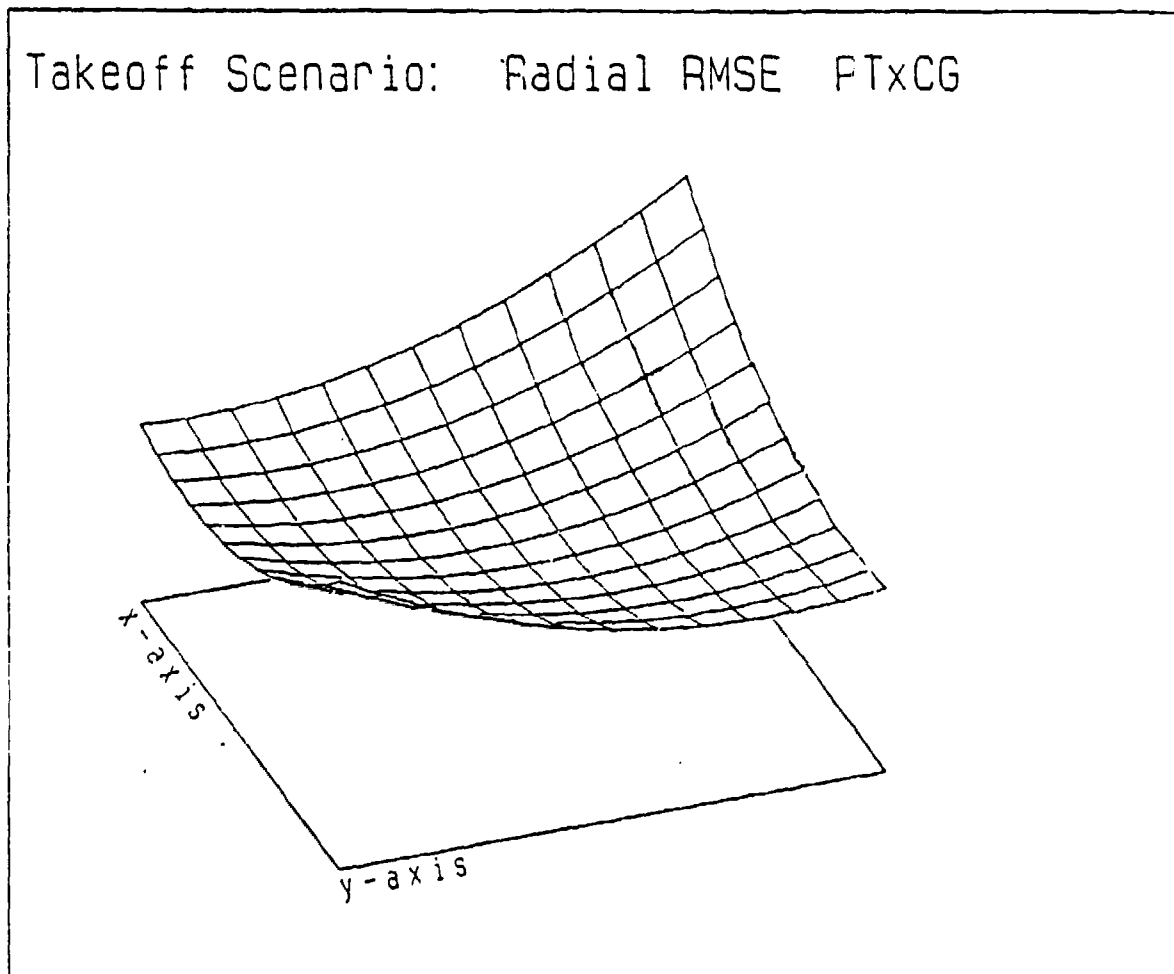Figure A-16. Takeoff Scenario: Radial log RMSE as a function of Tracking Mode and Control Gain.

Figure A-17. Takeoff Scenario: Radial log RMSE as a function
of Prediction Time and Control Gain.

TABLE A-5
Summary of the Analysis of Variance for the Regression
Equation of Lateral Log RMS Error in the Landing Scenario

$$\log \text{RMSE,lat} = 1.21 + 0.01TM - 0.06MF - 0.01PT + 0.14CO + 0.01CG$$
$$- 0.02TM^2 + 0.04MF^2 + 0.02PT^2 + 0.13CO^2 - 0.02CG^2 - 0.01TM\times MF$$
$$+ 0.01TM\times PT - 0.03TM\times CO + 0.01TM\times CG + 0.02MF\times PT - 0.04MF\times CO$$
$$- 0.01MF\times CG + 0.01PT\times CO - 0.00PT\times CG - 0.00CO\times CG.$$

Source	df	Mean Square	F
Regression	20	.2360	4.9043**
TM	1	.0119	.2473
MF	1	.3275	6.8041*
PT	1	.0210	.4358
CO	1	1.7671	36.7169**
CG	1	.0098	.2041
TM	1	.0556	1.1563
MF	1	.1677	3.4853
PT	1	.0683	1.4195
CO	1	1.8511	38.4612**
CG	1	.0537	1.1168
TMxMF	1	.0123	.2564
TMxPT	1	.0141	.2924
TMxCO	1	.0633	1.3155
TMxCG	1	.0098	.2042
MFxPT	1	.0193	.4007
MFxCO	1	.0948	1.9695
MFxCG	1	.0020	.0423
PTxCO	1	.0091	.1900
PTxCG	1	.0000	.0000
COxCG	1	.0000	.0000
Residual	107	.1454	
Subjects	3	2.5759	53.5209**
Lack-of-Fit	6	.5183	10.7687**
Replications	98	.0481	
Total	127		

* $p \leq .05$
** $p \leq .01$

55

EXPERIMENT 2 MAGNIFICATION FACTOR
LATERAL ERROR
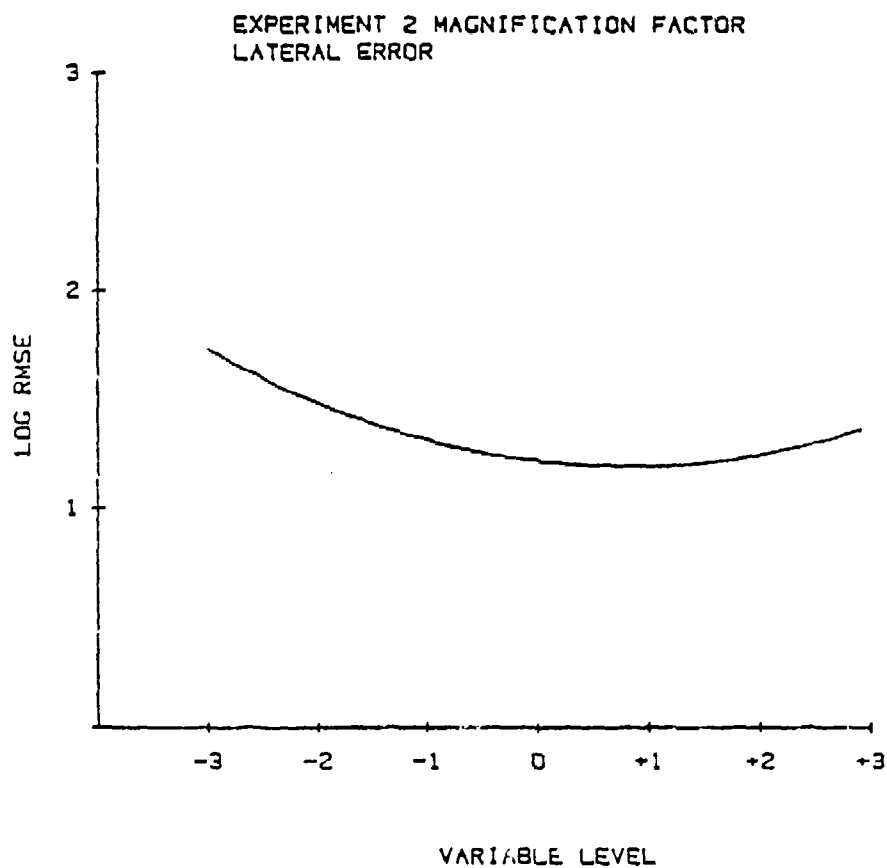
Figure A-18.   Landing Scenario: Lateral log RMSE as a function
of Magnification Factor.

EXPERIMENT 2 CONTROL ORDER
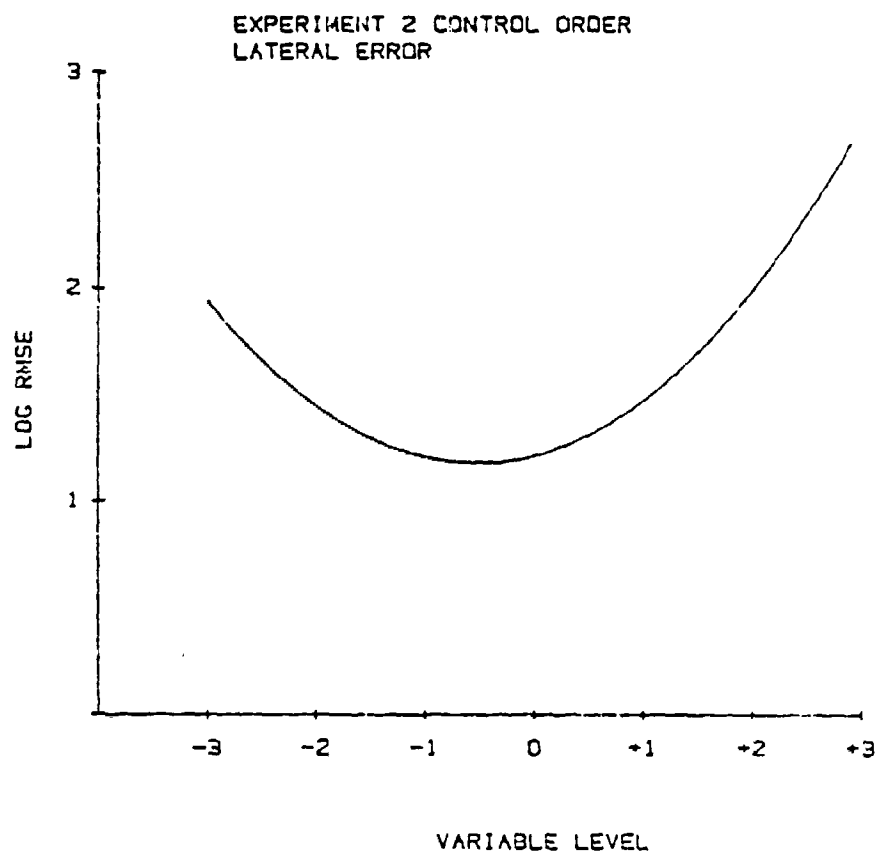**LATERAL ERROR**

Figure A-19. Landing Scenario: Lateral log RMSE as a function
            of Control Order.

TABLE A-6

Summary of the Analysis of Variance for the Regression
Equation of Longitudinal Log RMS Error in the Landing Scenario

$$\log \text{RMSE,lon} = 1.35 + 0.01TM + 0.01MF - 0.02PT + 0.08CO + 0.00CG$$
$$- 0.03TM^2 + 0.03MF^2 + 0.04PT^2 + 0.09CO^2 - 0.03CG^2 - 0.01TMxMF$$
$$+ 0.03TMxPT - 0.02TMxCO - 0.04TMxCG + 0.02MFxPT + 0.00MFxCO$$
$$+ 0.02MFxCG + 0.04PTxCO + 0.00PTxCG + 0.00COxCG.$$

Source	df	Mean Square	F
Regression	20	.1235	3.0444**
TM	1	.0161	.3974
MF	1	.0021	.0511
PT	1	.0344	.8488
CO	1	.5649	13.9263**
CG	1	.0004	.0099
TM	1	.1124	2.7707
MF	1	.1300	3.2062
PT	1	.1533	3.7801*
CO	1	.8583	21.1597**
CG	1	.1207	2.9758
TMxMF	1	.0015	.0365
TMxPT	1	.0574	1.4142
TMxCO	1	.0364	.8971
TMxCG	1	.0927	2.2859
MFxPT	1	.0154	.3791
MFxCO	1	.0000	.0008
MFxCG	1	.0378	.9327
PTxCO	1	.1161	2.8626
PTxCG	1	.0000	.0000
COxCG	1	.0000	.0001
Residual	107	.1192	
Subjects	3	2.5256	62.2670**
Lack-of-Fit	6	.2002	4.9351**
Replications	98	.0406	
Total	127		

* $p \leq .05$
** $p \leq .01$

EXPERIMENT 2 PREDICTION TIME
LONGITUDINAL ERROR
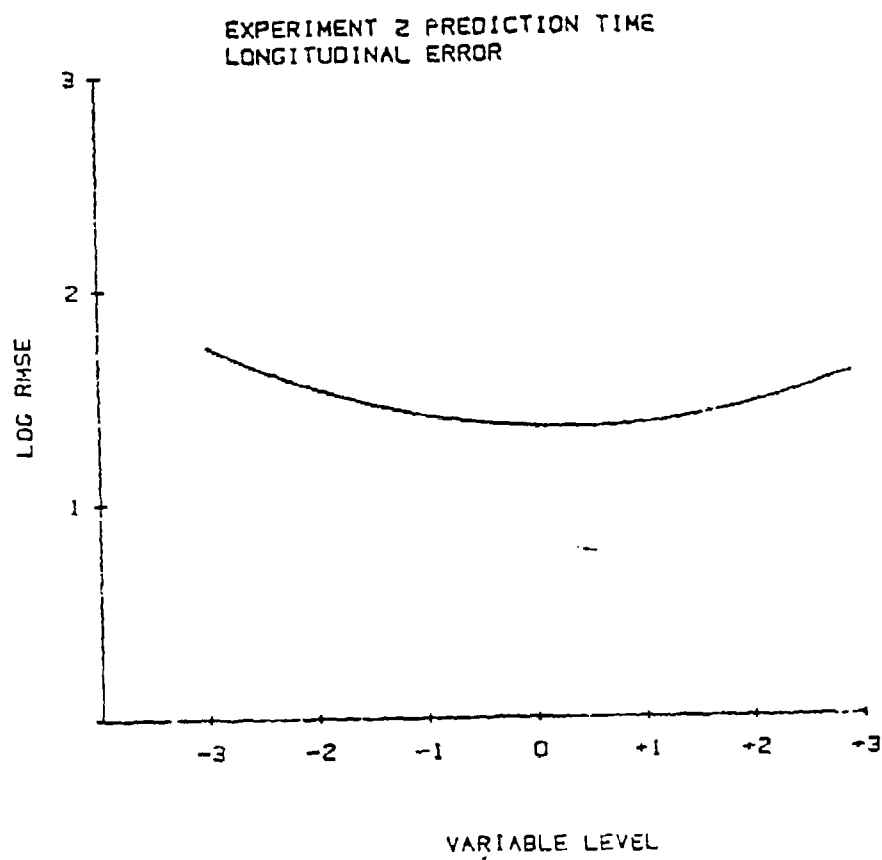
Figure A-20. Landing Scenario: Longitudinal log RMSE as a
function of Prediction Time.

EXPERIMENT 2 CONTROL ORDER
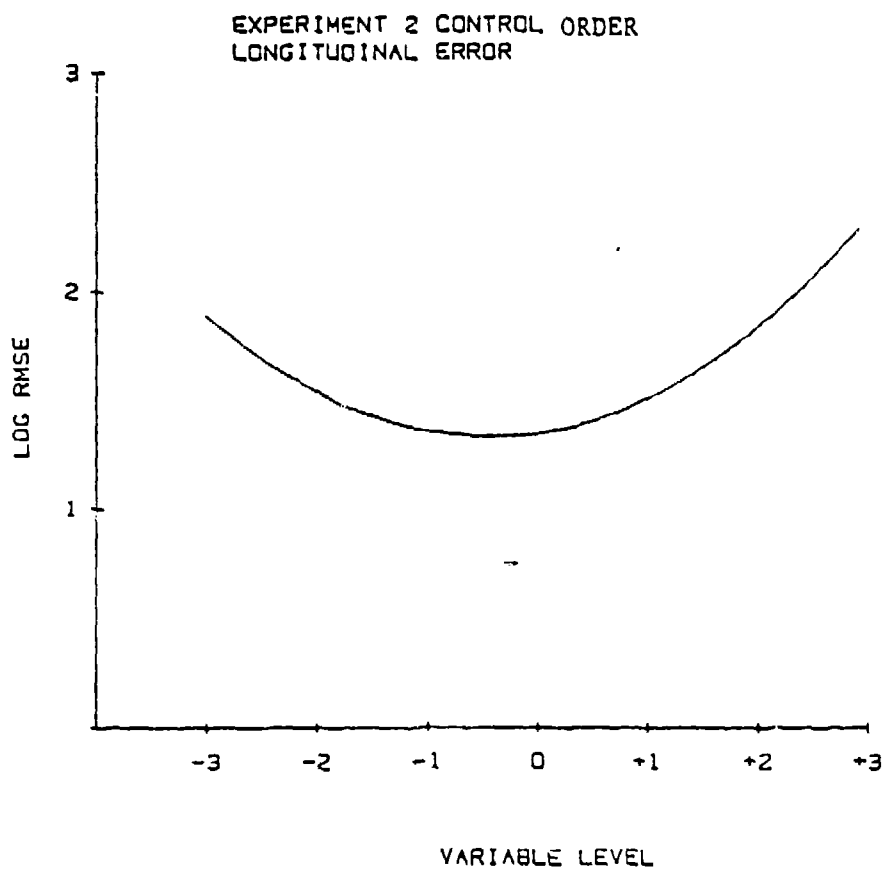LONGITUDINAL ERROR

LOG RMSE

VARIABLE LEVEL

Figure A-21.   Landing Scenario: Longitudinal log RMSE as a
function of Control Order.

TABLE A-7
Summary of the Analysis of Variance for the Regression
Equation of Vertical Log RMS Error in the Landing Scenario

$$\log \text{RMSE,ver} = 0.93 - 0.02TM + 0.01MF + 0.03PT + 0.06CO - 0.03CG$$
$$- 0.00TM^2 + 0.01MF^2 + 0.03PT^2 + 0.05CO^2 - 0.00CG^2 + 0.03TMxMF$$
$$- 0.01TMxPT - 0.01TMxCO - 0.01TMxCG + 0.00MFxPT - 0.01MFxCO$$
$$+ 0.01MFxCG - 0.02PTxCO + 0.01PTxCG - 0.02COxCG.$$

Source	df	Mean Square	F
Regression	20	.0583	2.2863*
TM	1	.0444	1.7389
MF	1	.0046	.1814
PT	1	.0900	3.5223*
CO	1	.3508	13.7320**
CG	1	.0763	2.9882
TM	1	.0001	.0051
MF	1	.0137	.5358
PT	1	.1149	4.4988*
CO	1	.2597	10.1667**
CG	1	.0004	.0154
TMxMF	1	.0703	2.7508
TMxPT	1	.0111	.4326
TMxCO	1	.0012	.0456
TMxCG	1	.0026	.1013
MFxPT	1	.0004	.0147
MFxCO	1	.0138	.5416
MFxCG	1	.0102	.4003
PTxCO	1	.0235	.9209
PTxCG	1	.0080	.3137
COxCG	1	.0344	1.3490
Residual	107	.0428	
Subjects	3	.6202	24.2812**
Lack-of-Fit	6	.0357	1.4000
Replications	98	.0255	
Total	127		

* $p \leq .05$
** $p \leq .01$

61

EXPERIMENT 2 PREDICTION TIME
VERTICAL ERROR

LOG RMSE

VARIABLE LEVEL
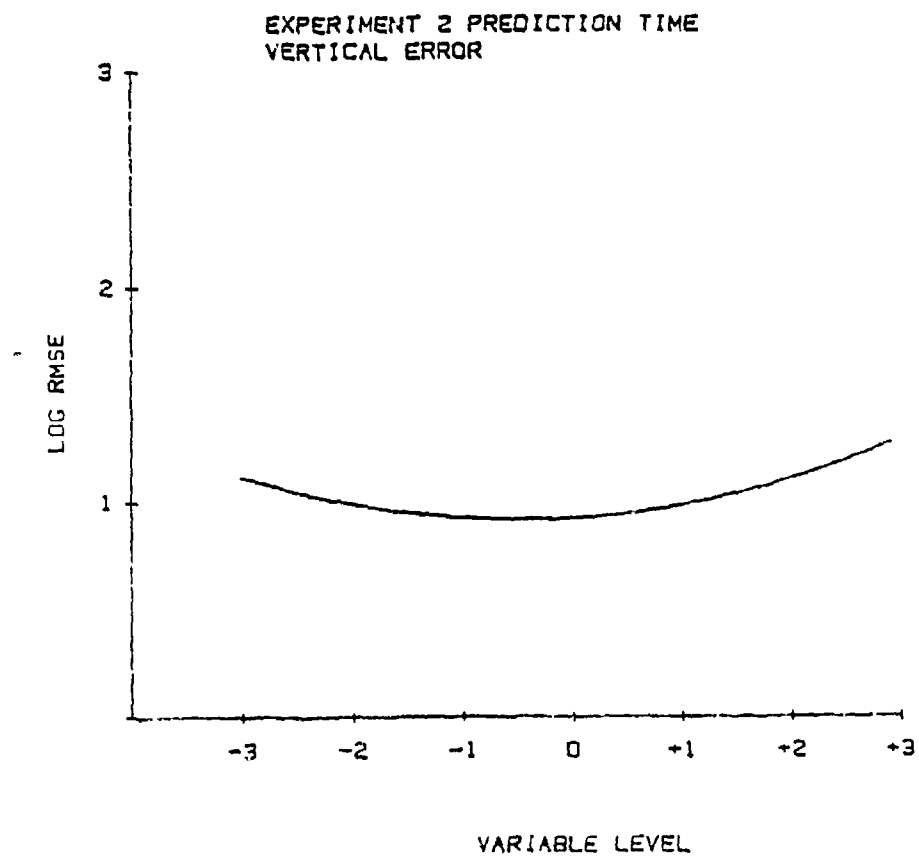
Figure A-22. Landing Scenario: Vertical log RMSE as a
function of Prediction Time.

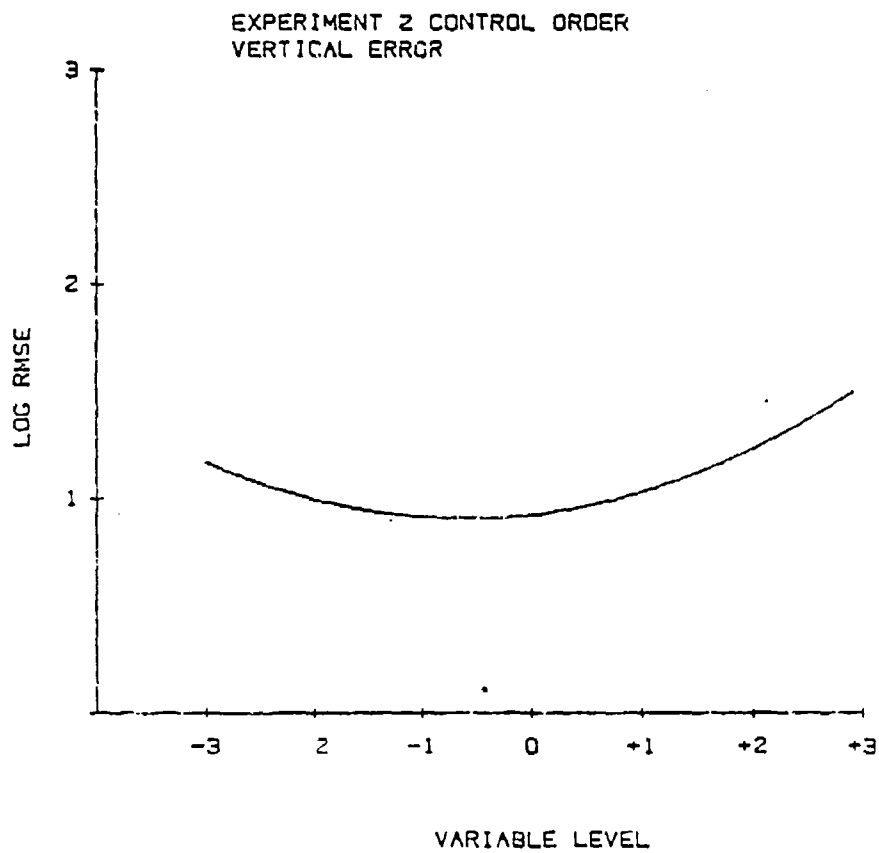EXPERIMENT 2 CONTROL ORDER
VERTICAL ERROR

Figure A-23. Landing Scenario: Vertical log RMSE as a
function of Control Order.

TABLE A-8
Summary of the Analysis of Variance for the Regression
Equation of Radial Log RMS Error in the Landing Scenario

$$\log \text{RMSE,rad} = 1.43 + 0.00\text{TM} - 0.03\text{MF} - 0.01\text{PT} + 0.11\text{CO} + 0.00\text{CG}$$
$$- 0.03\text{TM}^2 + 0.03\text{MF}^2 + 0.03\text{PT}^2 + 0.10\text{CO}^2 - 0.03\text{CG}^2 + 0.00\text{TMxMF}$$
$$+ 0.01\text{TMxPT} - 0.02\text{TMxCO} - 0.01\text{TMxCG} + 0.01\text{MFxPT} - 0.03\text{MFxCO}$$
$$+ 0.01\text{MFxCG} + 0.03\text{PTxCO} - 0.00\text{PTxCG} - 0.00\text{COxCG}.$$

Source	df	Mean Square	F
Regression	20	.1553	5.8977**
TM	1	.0000	.001
MF	1	.0711	2.001
PT	1	.0035	.1344
CO	1	1.1578	43.9575**
CG	1	.0004	.0163
TM	1	.1015	3.8527*
MF	1	.1181	4.4824*
PT	1	.0910	3.4536*
CO	1	1.1911	45.2202**
CG	1	.0807	3.0628
TMxMF	1	.0003	.0317
TMxPT	1	.0125	.4731
TMxCO	1	.0361	1.3688
TMxCG	1	.0101	.3844
MFxPT		.0118	.4480
MFxCO		.0400	1.5167
MFxCG	1	.0049	.1854
PTxCO	1	.0440	1.6723
PTxCG	1	.0001	.0041
COxCG	1	.0002	.0082
Residual	107	.0964	
Subjects	3	2.0893	79.3227**
Lack-of-Fit	6	.2440	9.2647**
Replications	98	.0263	
Total	127		

* $p \leq .05$
** $p \leq .01$
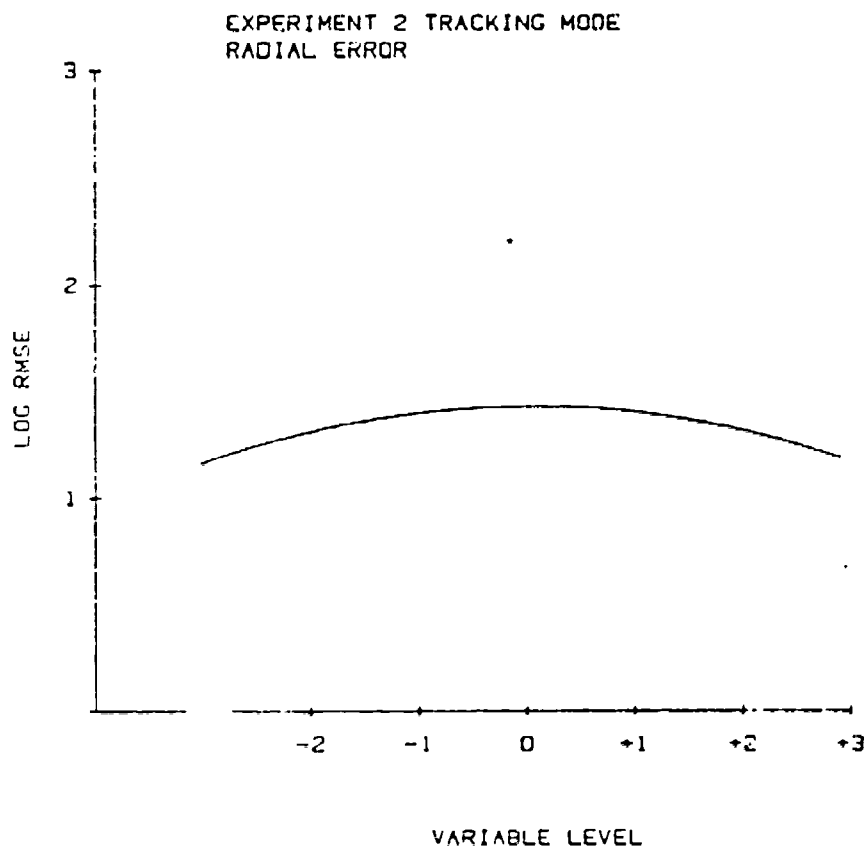
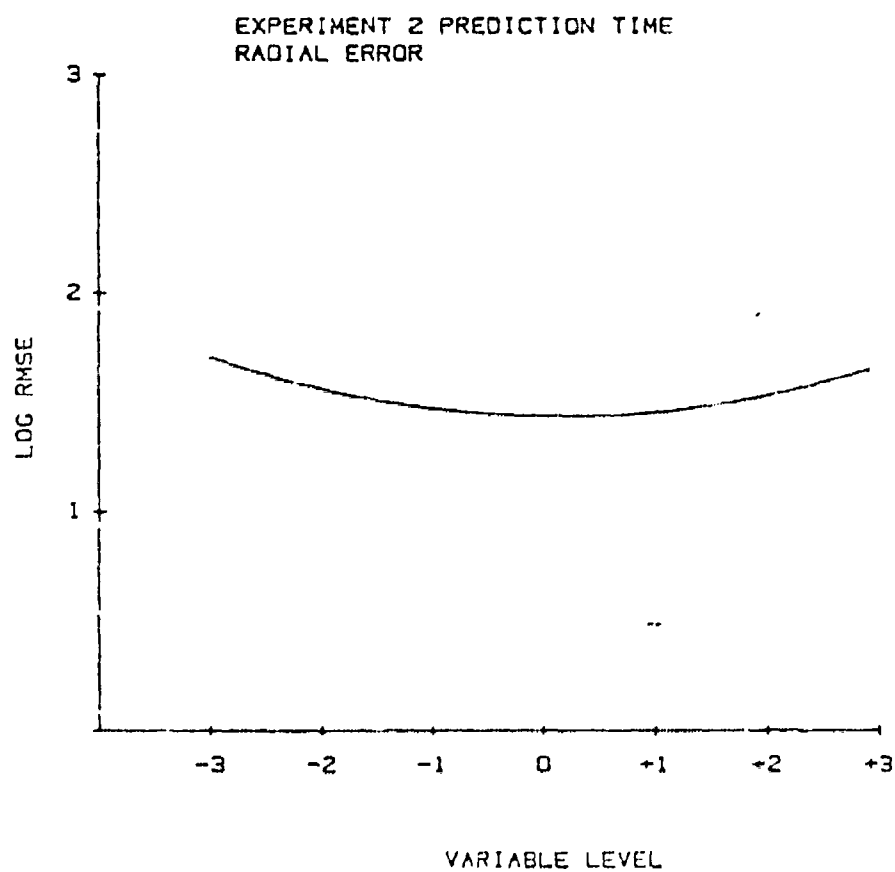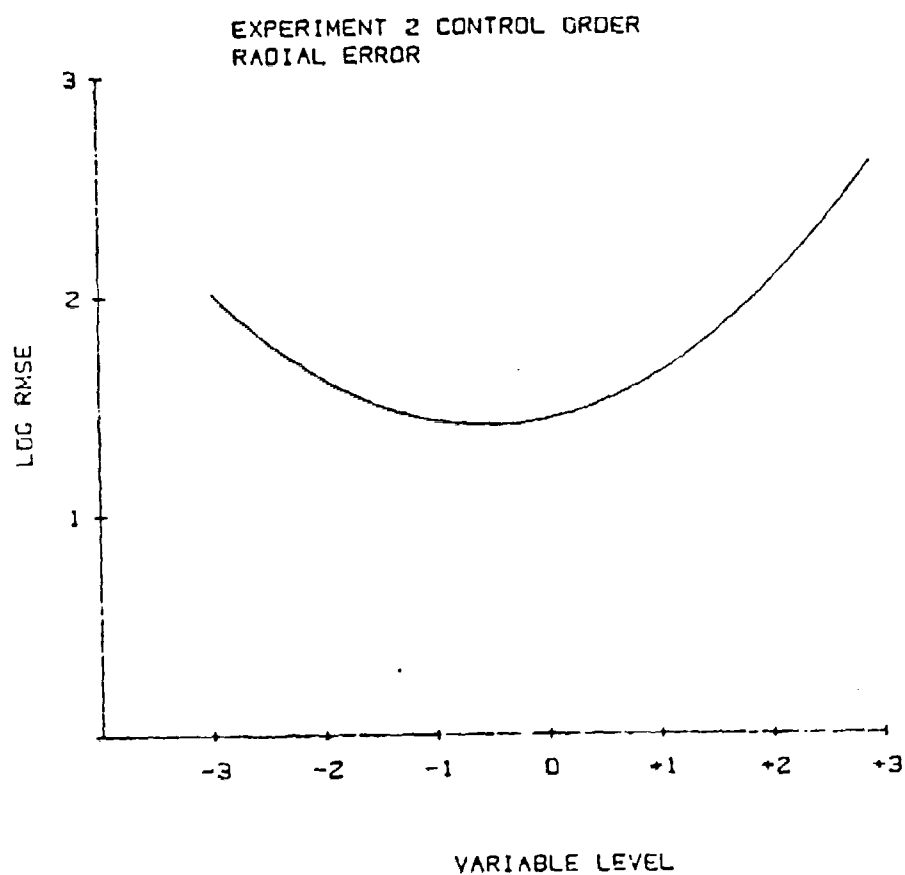Figure A-24. Landing Scenario: Radial log RMSE as a function of Tracking Mode.

EXPERIMENT 2 PREDICTION TIME
RADIAL ERROR

Figure A-25. Landing Scenario: Radial log RMSE as a
function of Prediction Time.

EXPERIMENT 2 CONTROL ORDER
RADIAL ERROR

LOG RMSE

VARIABLE LEVEL

Figure A-26.   Landing Scenario: Radial log RMSE as a
                function of Control Order.

TABLE A-9
Summary of the Analysis of Variance for the Regression
Equation of Lateral Log RMS Error in the SID Scenario

$$\log \text{RMSE,lat} = 1.08 + 0.04\text{TM} - 0.07\text{MF} - 0.08\text{PT} + 0.08\text{CO} + 0.02\text{CG}$$
$$- 0.01\text{TM}^2 + 0.01\text{MF}^2 + 0.02\text{PT}^2 + 0.10\text{CO}^2 - 0.01\text{CG}^2 + 0.08\text{TMxMF}$$
$$- 0.02\text{TMxPT} + 0.02\text{TMxCO} - 0.03\text{TMxCG} + 0.06\text{MFxPT} - 0.01\text{MFxCO}$$
$$+ 0.01\text{MFxCG} + 0.00\text{PTxCO} + 0.01\text{PTxCG} - 0.04\text{COxCG}.$$

Source	df	Mean Square	F
Regression	20	.2098	3.9407**
TM	1	.1876	3.5804*
MF	1	.5319	10.1508**
PT	1	.6844	13.0614**
CO	1	.6096	11.6332**
CG	1	.0304	.5799
TM	1	.0112	.2144
MF	1	.0111	.2114
PT	1	.0487	.9294
CO	1	1.0941	20.8794**
CG	1	.0046	.0884
TMxMF	1	.4512	8.6097**
TMxPT	1	.0157	.2994
TMxCO	1	.0270	.5148
TMxCG	1	.0680	1.2975
MFxPT	1	.2421	4.6195*
MFxCO	1	.0119	.2267
MFxCG	1	.0028	.0526
PTxCO	1	.0007	.0142
PTxCG	1	.0015	.0286
COxCG	1	.0867	1.6546
Residual	107	.0626	
Subjects	3	.1086	2.0725
Lack-of-Fit	6	.2067	3.9447**
Replications	98	.0524	
Total	127		

* $p \leq .05$
** $p \leq .01$

EXPERIMENT 3 TRACKING MODE
LATERAL ERROR
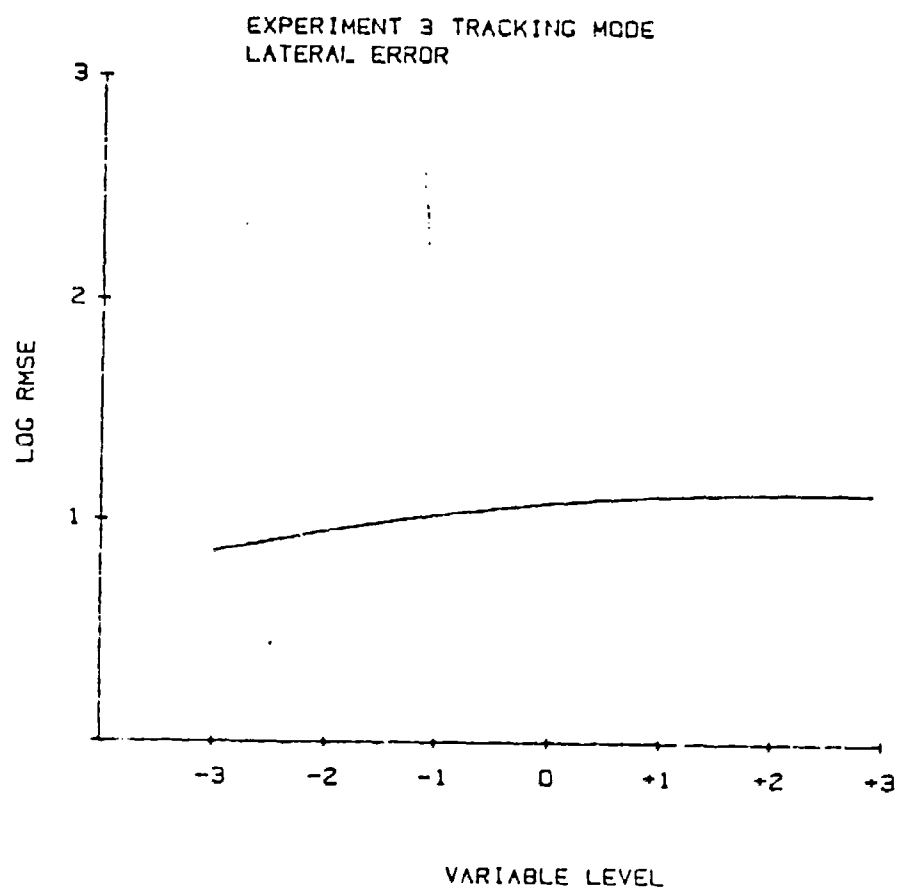
Figure A-27.   SID Scenario: Lateral log RMSE as a function
of Tracking Mode.

EXPERIMENT 3 MAGNIFICATION FACTOR
LATERAL ERROR
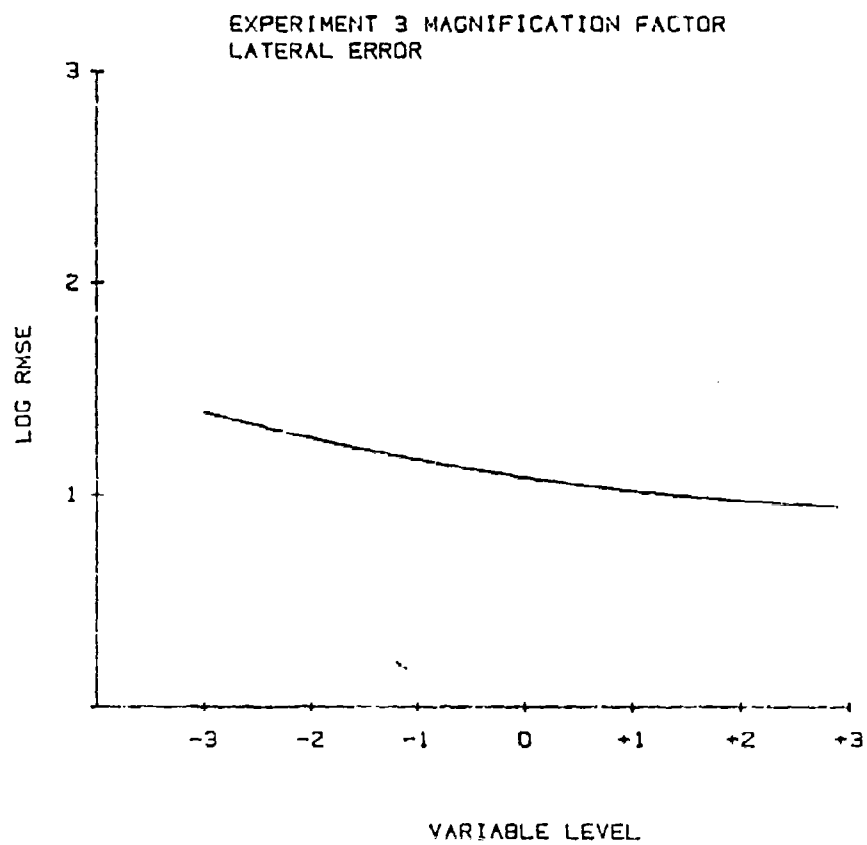
Figure A-28.   SID Scenario: Lateral log RMSE as a function
of Magnification Factor.

EXPERIMENT 3 PREDICTION TIME
LATERAL ERROR
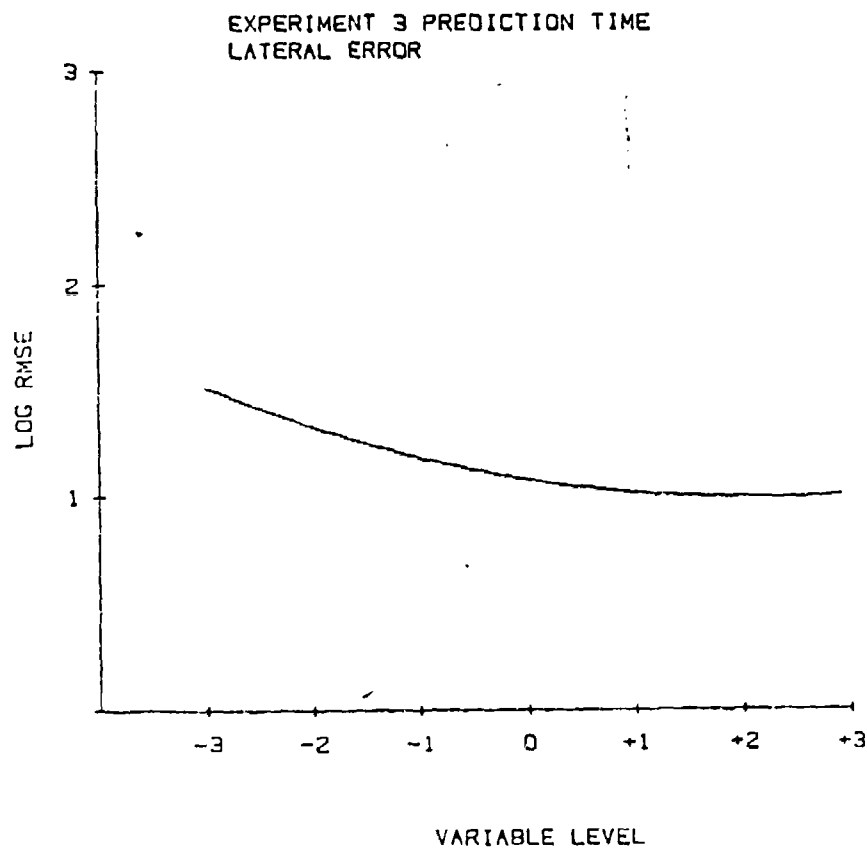
Figure A-29. SID Scenario: Lateral log RMSE as a function of Prediction Time.

EXPERIMENT 3 CONTROL ORDER
LATERAL ERROR
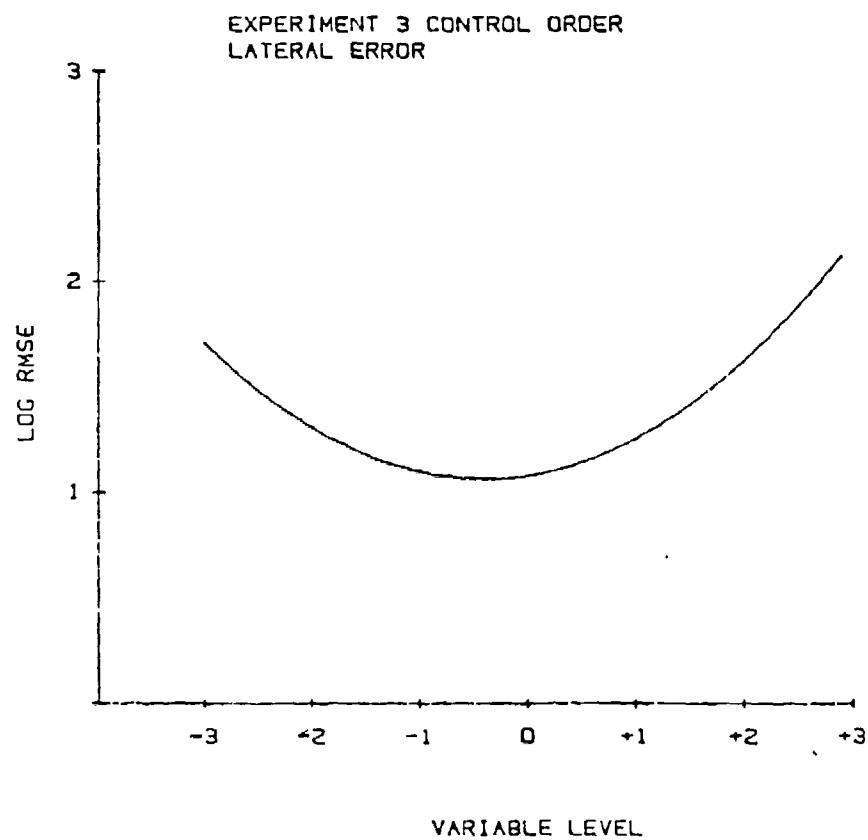
Figure A-30. SID Scenario: Lateral log RMSE as a function of Control Order.
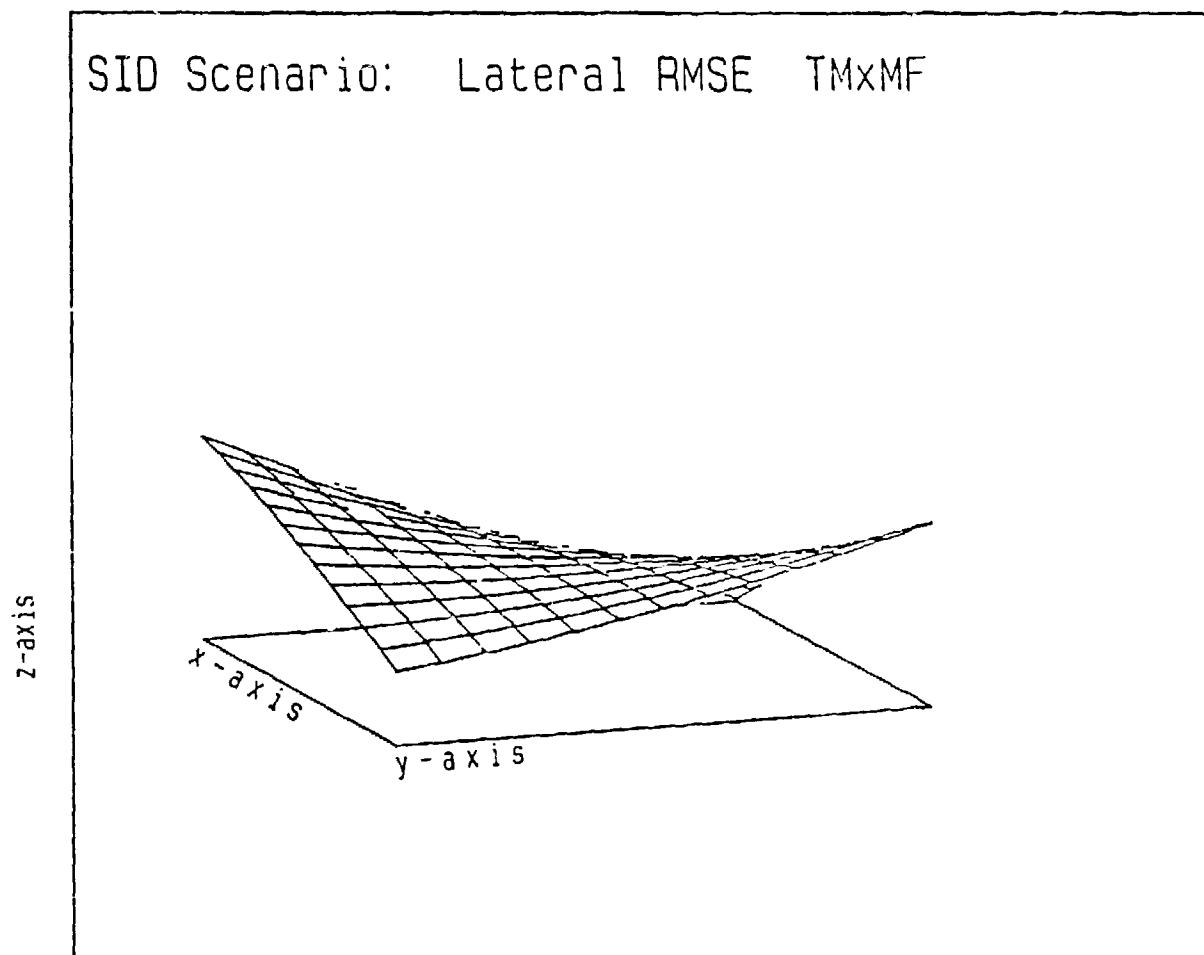
Figure A-31.   SID Scenario: Lateral log RMSE as a function
of Tracking Mode and Magnification Factor.

SID Scenario: Lateral RMSE   MFxPT
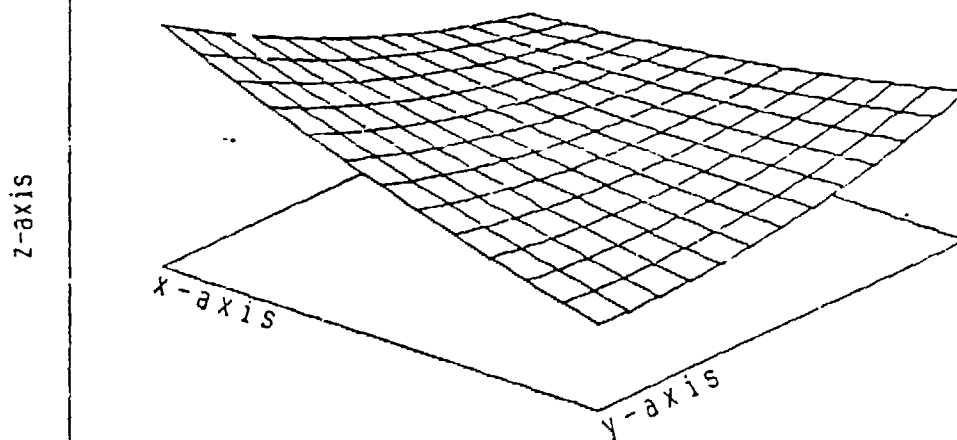
Figure A-32.   SID Scenario: Lateral log RMSE as a function
of Magnification and Prediction Time.

TABLE A-10
Summary of the Analysis of Variance for the Regression
Equation of Longitudinal Log RMS Error in the SID Scenario

$$\log \text{RMSE,lon} = 1.14 + 0.05\text{TM} - 0.06\text{MF} - 0.04\text{PT} + 0.01\text{CO} + 0.02\text{CG}$$
$$- 0.00\text{TM}^2 + 0.01\text{MF}^2 + 0.03\text{PT}^2 + 0.08\text{CO}^2 + 0.02\text{CG}^2 + 0.04\text{TMxMF}$$
$$- 0.00\text{TMxPT} - 0.02\text{TMxCO} - 0.02\text{TMxCG} + 0.05\text{MFxPT} - 0.03\text{MFxCO}$$
$$- 0.02\text{MFxCG} - 0.06\text{PTxCO} - 0.05\text{PTxCG} - 0.02\text{COxCG}.$$

Source	df	Mean Square	F
Regression	20	.1256	3.5182**
TM	1	.2017	5.6500*
MF	1	.3838	10.7526**
PT	1	.1643	4.6043*
CO	1	.0073	.2059
CG	1	.0470	1.3166
TM	1	.0013	.0378
MF	1	.0032	.0900
PT	1	.1309	3.6659*
CO	1	.5507	15.5044**
CG	1	.0354	.9909
TMxMF	1	.0805	2.2554
TMxPT	1	.0000	.0014
TMxCO	1	.0359	1.0061
TMxCG	1	.0193	.5394
MFxPT	1	.1584	4.4381*
MFxCO	1	.0458	1.2831
MFxCG	1	.0218	.6116
PTxCO	1	.1951	5.4674*
PTxCG	1	.1606	4.4986*
COxCG	1	.0390	1.0924
Residual	107	.0402	
Subjects	3	.0416	1.1879
Lack-of-Fit	6	.1122	3.1429**
Replications	98	.0357	
Total	127		

* $p \leq .05$
** $p \leq .01$

EXPERIMENT 3 TRACKING MODE
LONGITUDINAL ERROR
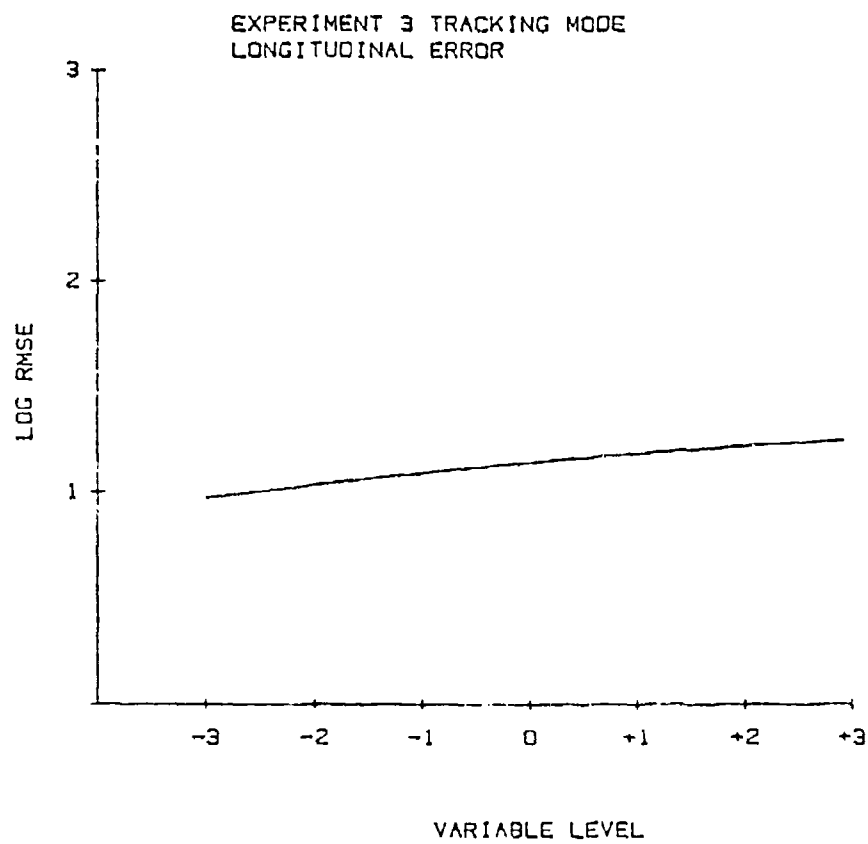
Figure A-33.   SID Scenario: Longitudinal log RMSE as a function
of Tracking Mode.

EXPERIMENT 3 MAGNIFICATION FACTOR
LONGITUDINAL ERROR
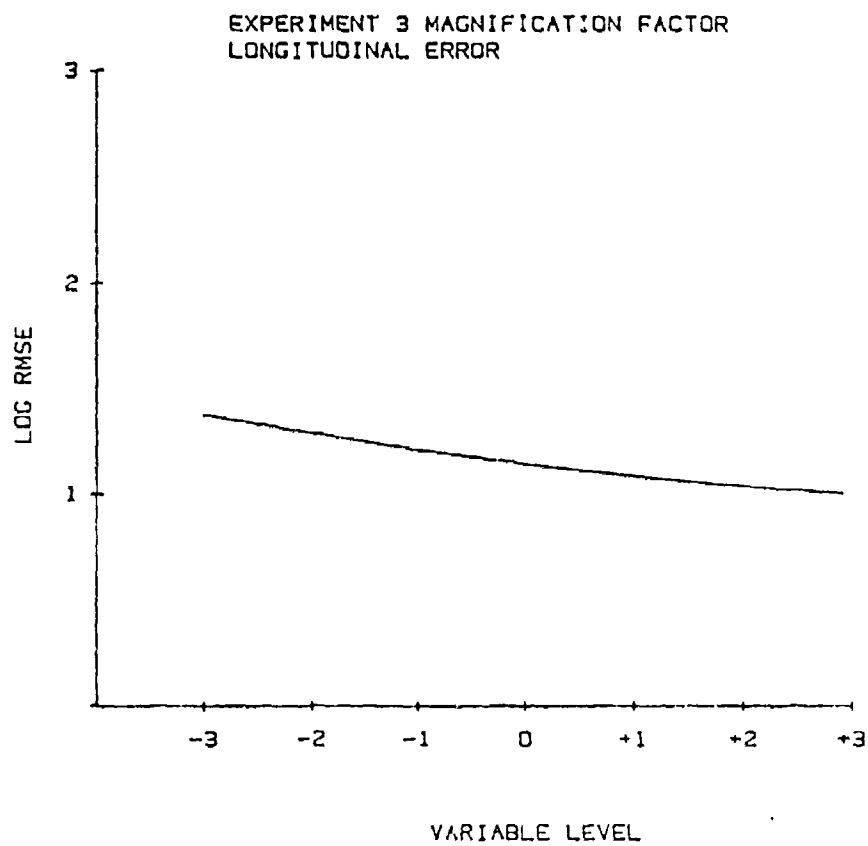
Figure A-34.   SID Scenario: Longitudinal log RMSE as a function
of Magnification Factor.

EXPERIMENT 3 PREDICTION TIME
LONGITUDINAL ERROR
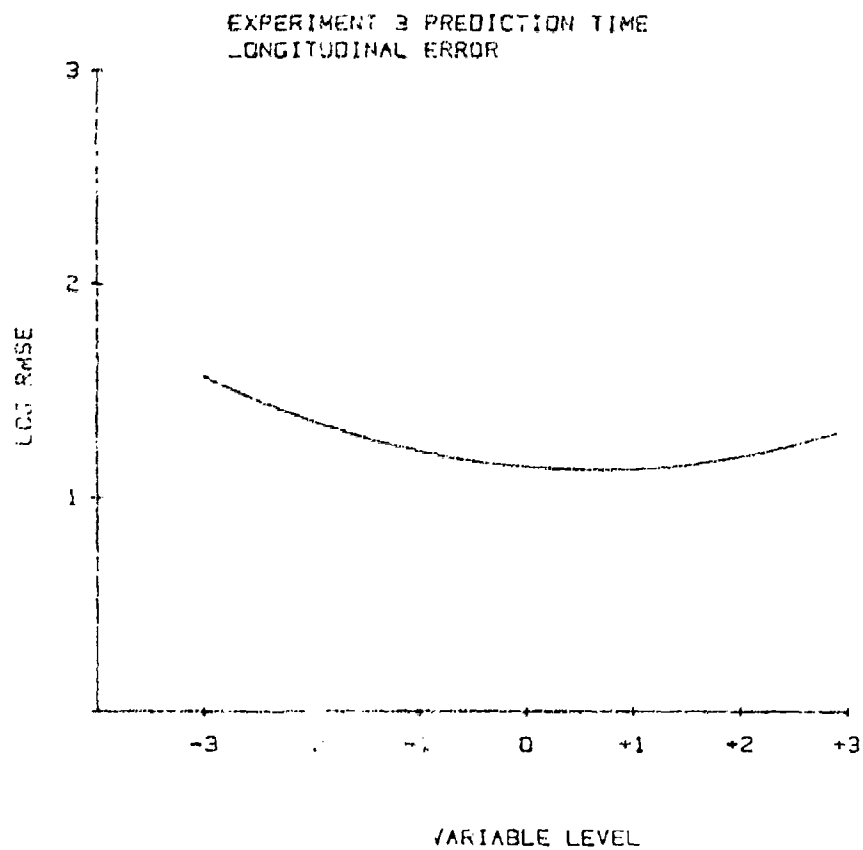
Figure A-35.   SID Scenario: Longitudinal log RMSE as a function
of Prediction Time.

EXPERIMENT 3 CONTROL ORDER
LONGITUDINAL ERROR
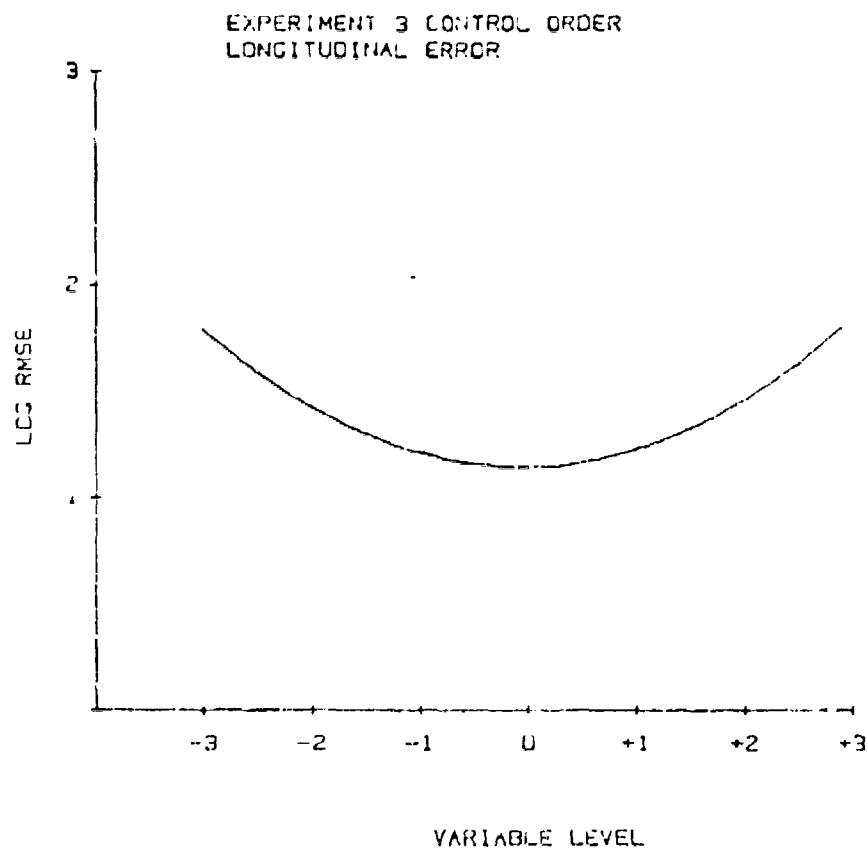
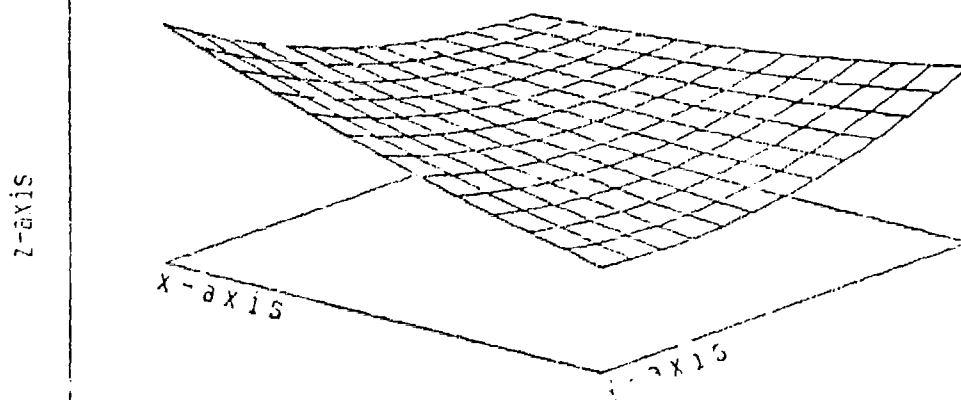Figure A-36. SID Scenario: Longitudinal log RMSE as a   for
of Control Order.

Figure A-57. SID Scenario: Longitudinal log RMSE as a function
of Magnification Factor and Prediction Time.

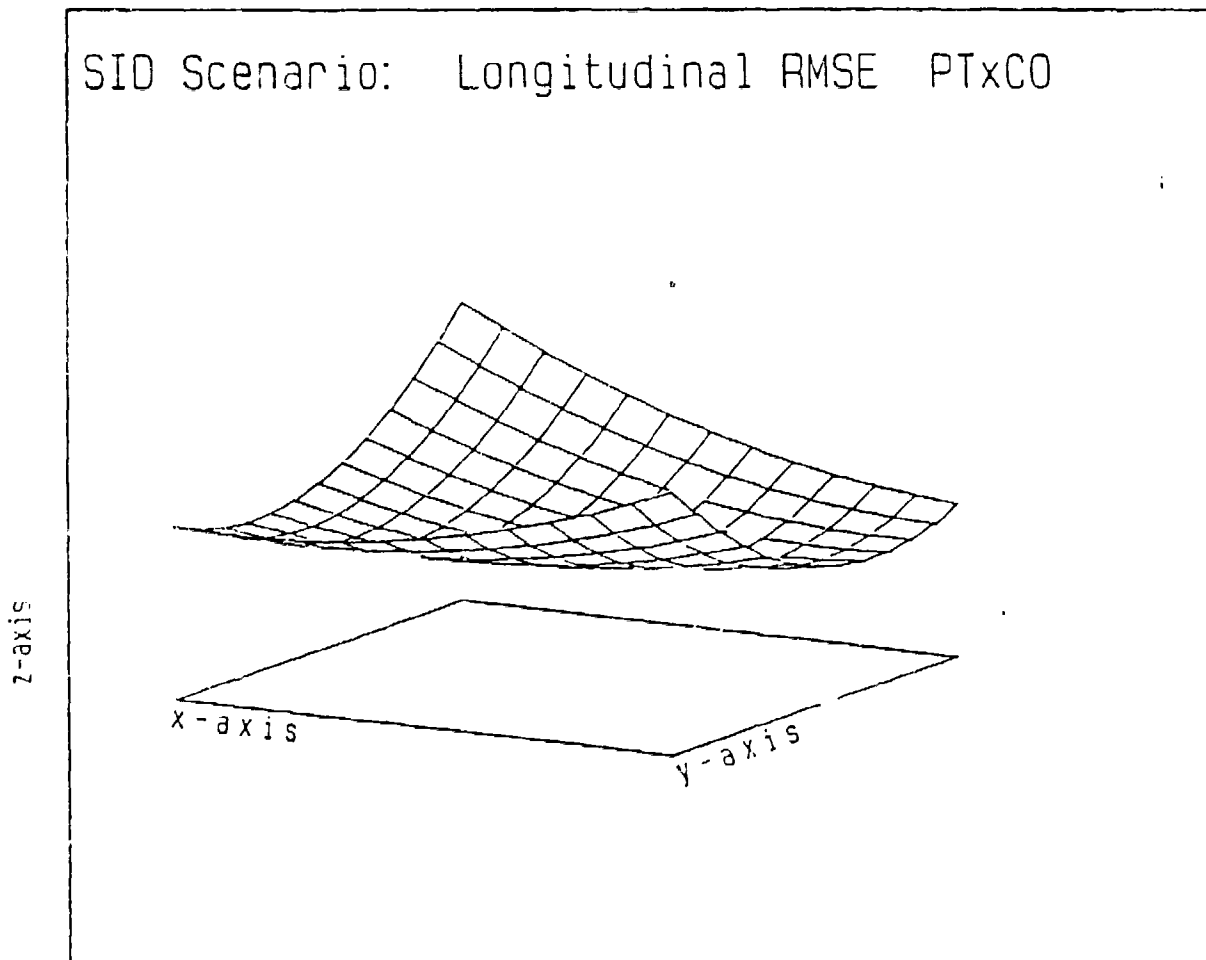SID Scenario: Longitudinal RMSE   PTxCO

z-axis

x-axis

y-axis

Figure A-38.   SID Scenario: Longitudinal log RMSE as a function
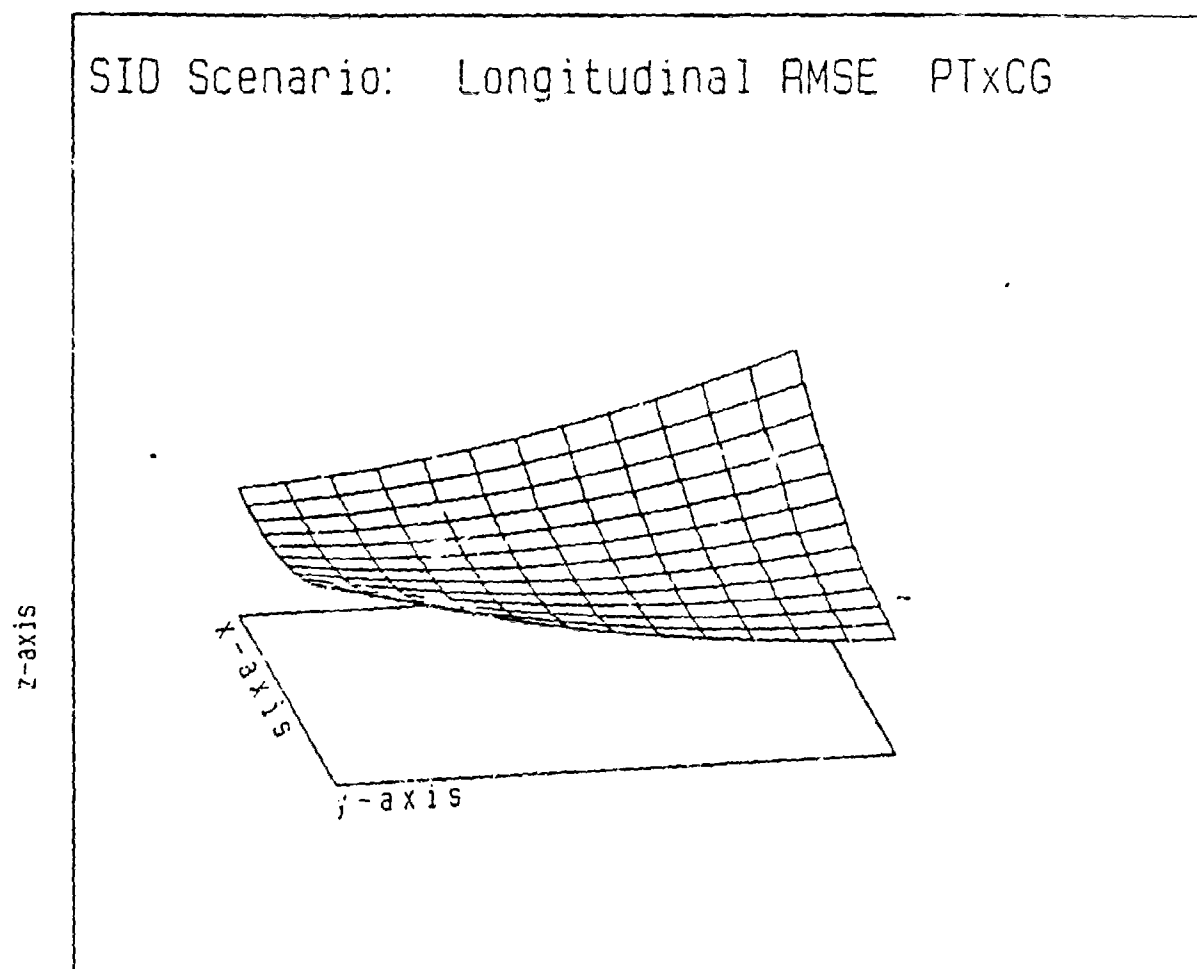of Prediction Time and Control Order.

Figure A-39. SID Scenario: Longitudinal log RMSE as a function
of Prediction Time and Control Gain.

TABLE A-11

Summary of the Analysis of Variance for the Regression
Equation of Vertical Log RMS Error in the SID Scenario

$\log \text{RMSE,ver} = 1.10 - 0.02\text{TM} + 0.01\text{MF} - 0.01\text{PT} + 0.00\text{CO} + 0.02\text{CG}$
$+ 0.00\text{TM}^2 + 0.01\text{MF}^2 - 0.01\text{PT}^2 + 0.08\text{CO}^2 + 0.01\text{CG}^2 - 0.04\text{TMxMF}$
$+ 0.01\text{TMxPT} - 0.03\text{TMxCO} - 0.00\text{TMxCG} + 0.03\text{MFxPT} - 0.02\text{MFxCO}$
$+ 0.00\text{MFxCG} - 0.04\text{PTxCO} + 0.00\text{PTxCG} + 0.01\text{COxCG}.$

Source	df	Mean Square	F
Regression	20	.0686	1.3251
TM	1	.0547	1.0601
MF	1	.0077	.1486
PT	1	.0101	.1954
CO	1	.0003	.0052
CG	1	.0339	.6567
TM	1	.0002	.0041
MF	1	.0241	.4662
PT	1	.0260	.5035
CO	1	.8003	15.5055**
CG	1	.0123	.2385
TMxMF	1	.1221	2.3654
TMxPT	1	.0021	.0414
TMxCO	1	.0658	1.2746
TMxCG	1	.0009	.0183
MFxPT	1	.0421	.8162
MFxCO	1	.0222	.4301
MFxCG	1	.0001	.0012
PTxCO	1	.0923	1.7875
PTxCG	1	.0002	.0039
COxCG	1	.0059	.1143
Residual	107	.0714	
Subjects	3	.3047	7.0651**
Lack-of-Fit	6	.2486	4.8178**
Replications	98	.0516	
Total	127		

---

* $p \leq .05$
** $p \leq .01$

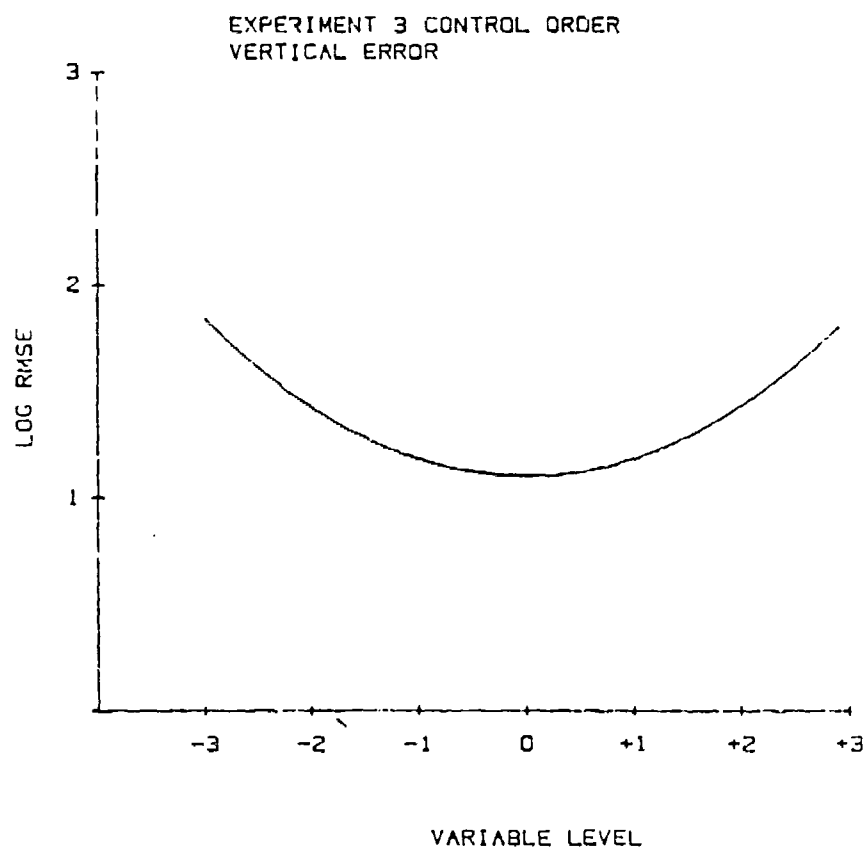EXPERIMENT 3 CONTROL ORDER
VERTICAL ERROR

VARIABLE LEVEL

Figure A-40. SID Scenario: Vertical log RMSE as a function
of Control Order.

TABLE A-12
Summary of the Analysis of Variance for the Regression
Equation of Radial Log RMS Error in the SID Scenario

$$\log \text{RMSE, rad} = 1.32 + 0.02TM - 0.05MF - 0.05PT + 0.04CO + 0.02CG$$
$$- 0.00TM^2 + 0.00MF^2 + 0.02PT^2 + 0.09CO^2 + 0.02CG^2 + 0.03TM \times MF$$
$$- 0.01TM \times PT - 0.01TM \times CO - 0.02TM \times CG + 0.06MF \times PT - 0.02MF \times CO$$
$$- 0.01MF \times CG - 0.04PT \times CO - 0.02PT \times CG - 0.01CO \times CG.$$

Source	df	Mean Square	F
Regression	20	.1122	4.0215**
TM	1	.0480	1.7229
MF	1	.2411	8.6509**
PT	1	.2174	7.8025**
CO	1	.1348	4.8358*
CG	1	.0577	2.0693
TM	1	.0008	.0275
MF	1	.0003	.0121
PT	1	.0516	1.8523
CO	1	.9598	34.7998**
CG	1	.0310	1.1126
TMxMF	1	.0725	2.6008
TMxPT	1	.0083	.2980
TMxCO	1	.0065	.2347
TMxCG	1	.0367	1.3176
MFxPT	1	.2008	7.2056**
MFxCO	1	.0227	.8141
MFxCG	1	.0018	.0629
PTxCO	1	.0968	3.4733*
PTxCG	1	.0384	1.3763
COxCG	1	.0068	.2437
Residual	107	.0354	
Subjects	3	.0248	.8900
Lack-of-Fit	6	.1641	5.8817**
Replications	98	.0279	
Total	127		

* $p \leq .05$
** $p \leq .01$

EXPERIMENT 3 MAGNIFICATION FACTOR
RADIAL ERROR

LOG RMSE

VARIABLE LEVEL
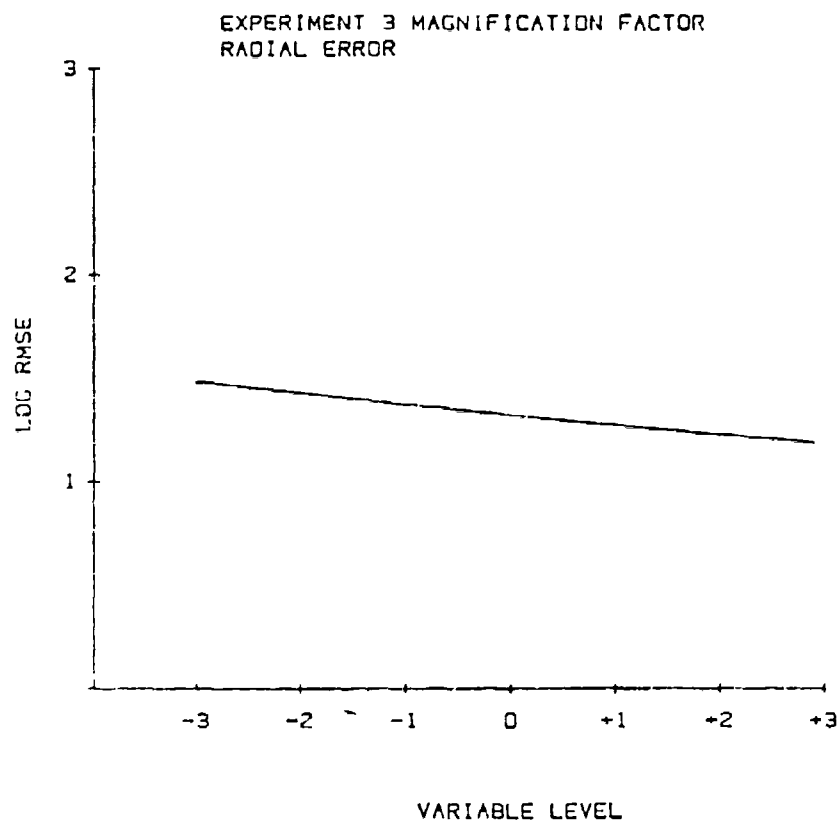
Figure A-41.   SID Scenario: Radial log RMSE as a function
                of Magnification Factor.

EXPERIMENT 3 PREDICTION TIME
RADIAL ERROR

LOG RMSE

VARIABLE LEVEL

Figure A-42.   SID Scenario: Radial log RMSE as a function
              of Prediction Time.

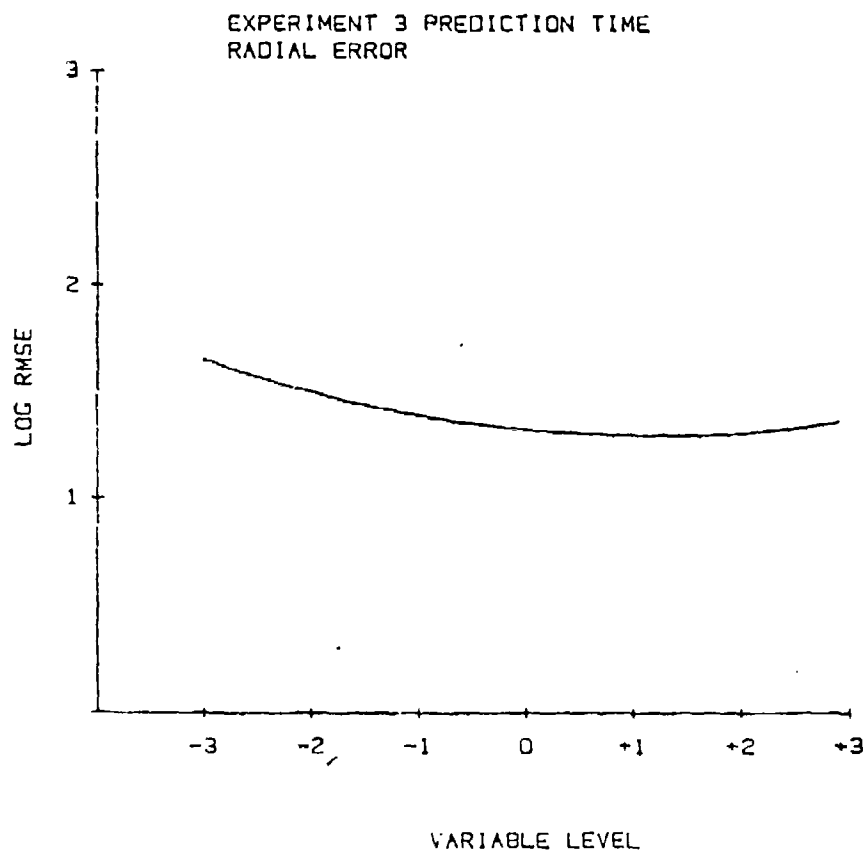EXPERIMENT 3 CONTROL ORDER
RADIAL ERROR
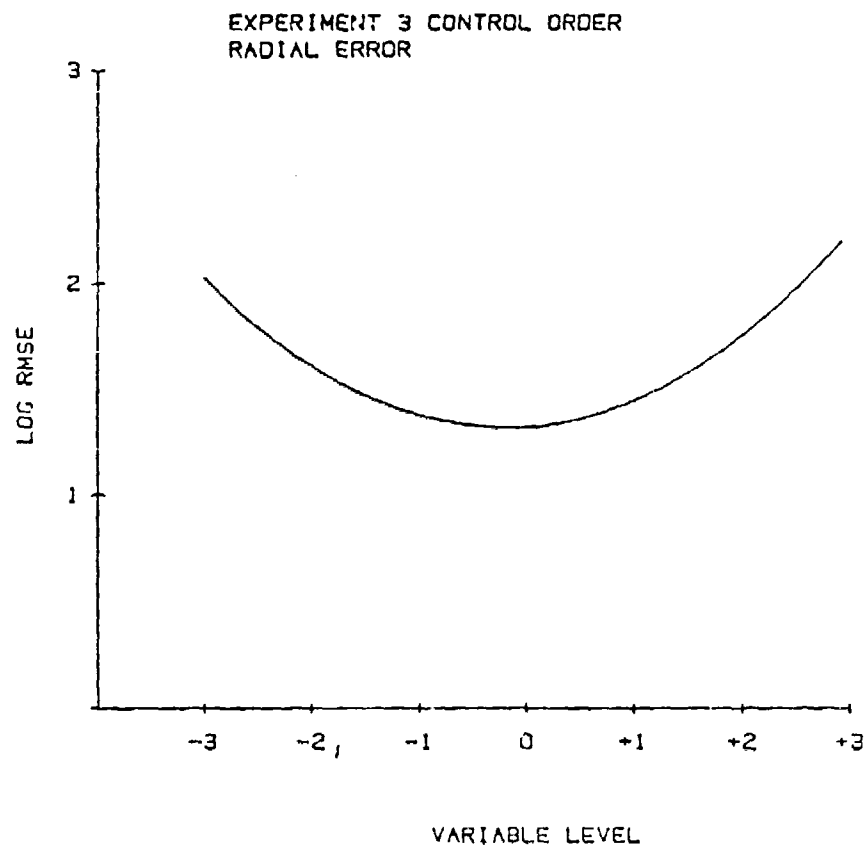
VARIABLE LEVEL

Figure A-43.   SID Scenario: Radial log RMSE as a function
of Control Order.
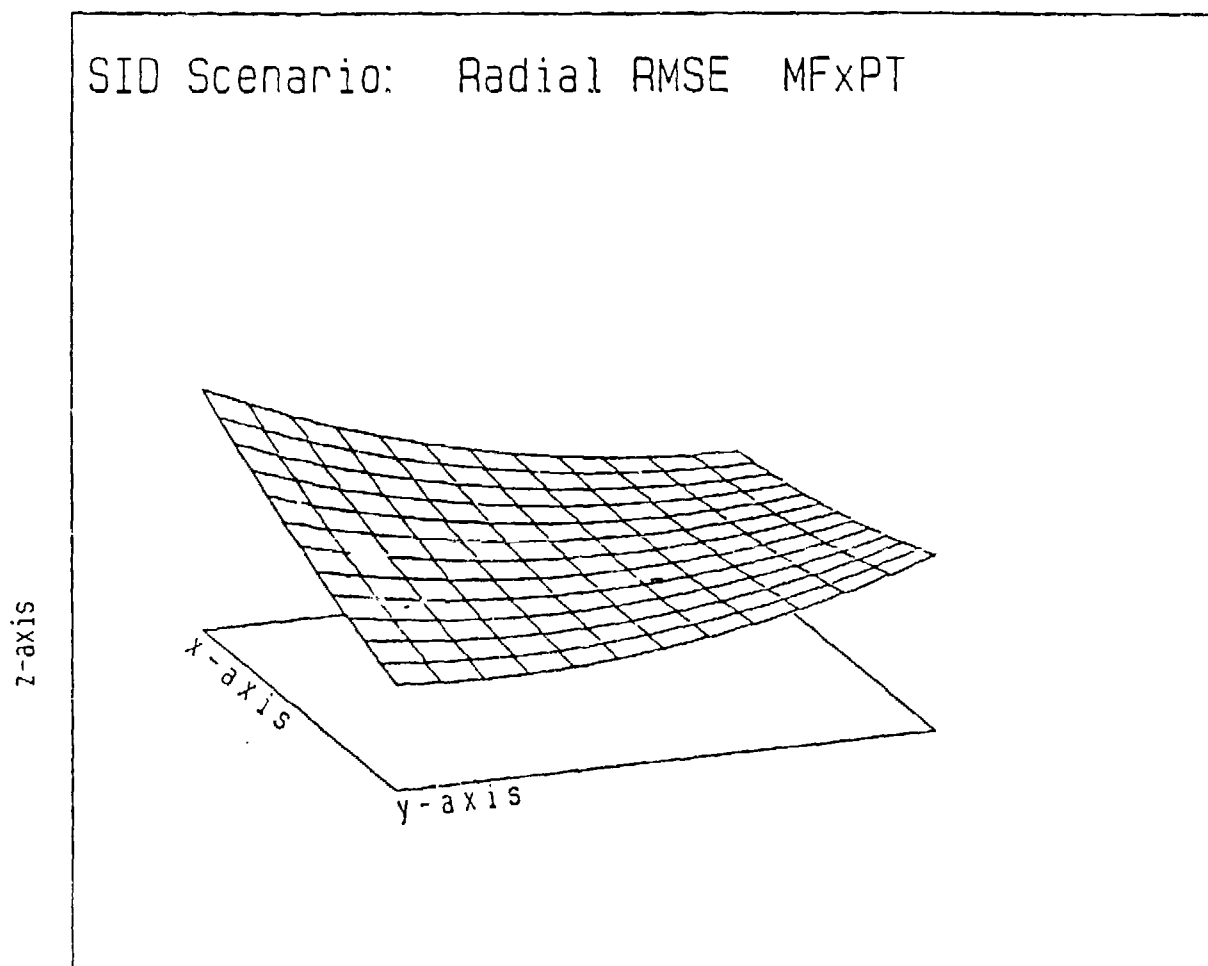
Figure A-44.   SID Scenario: Radial log RMSE as a function
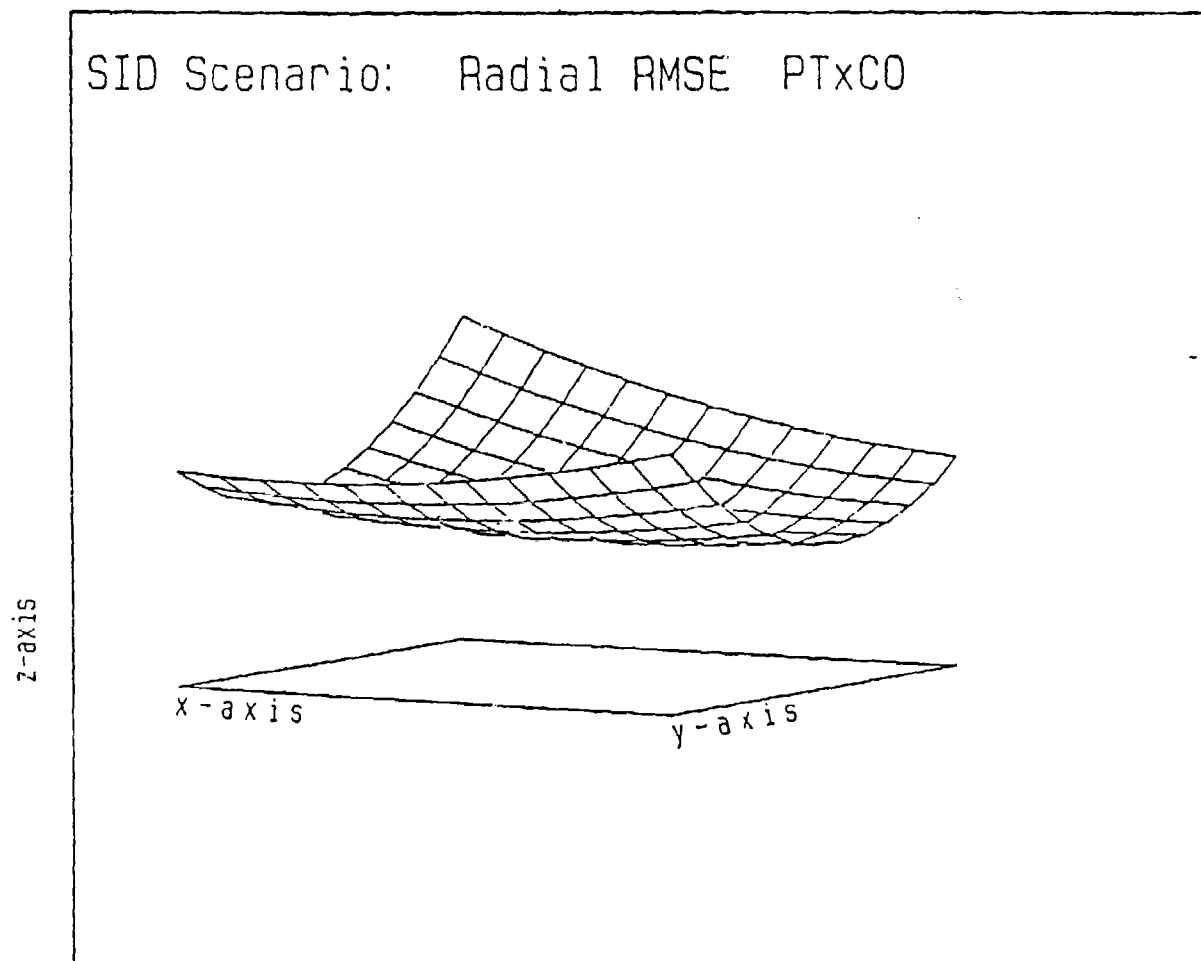   of Magnification Factor and Prediction Time.

Figure A-45.   SID Scenario: Radial log RMSE as a function
                of Prediction Time and Control Order.

REFERENCES

Bauerschmidt, D. K., and Roscoe, S. N. (1960). A comparative evaluation of a pursuit moving-airplane steering display. IRE Transactions on Human Factors in Electronics, HFE-1(2), 62-66.

Beringer, D. B. (1979). The design and evaluation of complex systems: A pilot-computer touch interface for complex navigation tasks. Unpublished doctoral dissertation, University of Illinois at Urbana-Champaign.

Beringer, D. B., Williges, R. C., and Roscoe, S. N. (1975). The transition of experienced pilots to a frequency-separated aircraft attitude display. Human Factors, 17, 401-414.

Blodgett, R. B. (1957). The advantages in industrial research of looking at the effects of many variables at the same time. Statistical Methods in the Chemical Industry, 17, 35-52.

Box, G. E. P., and Wilson, K. B. (1951). On the experimental attainment of optimum conditions. Journal of the Royal Statistical Society, 18, 1-45.

Box, G. E. P., and Hunter, J. S. (1957). Experimental designs for the exploration and exploitation of response surfaces. In V. Chew (Ed.), Experimental designs in industry (pp. 138-190). New York: Wiley.

Clark, C. (1976). Mixed-factors central-composite designs: A theoretical and empirical comparison (Tech. Report ARL-76-13/AFOSR-76-6). Savoy, IL: University of Illinois at Urbana-Champaign, Aviation Research Laboratory.

Clark, C., and Williges, R. C. (1972). Central-composite response surface methodology design and analyses (Tech. Report ARL-72-10/AFOSR-72-5). Savoy, IL: University of Illinois at Urbana-Champaign, Aviation Research Laboratory.

Clark, C., and Williges, R. C. (1973). Response surface methodology central-composite design modifications for human performance research. Human Factors, 15, 295-310.

Cragle, R. G., Myers, R. M., Waugh, R. K., Hunter, J. S., and Anderson, R. L. (1955). The effects of various levels of sodium citrate, glycerol, and equilibration time on survival of bovine spermatozoa after storage at -79 C. Journal of Dairy Sciences, 38, 508-512.

Day, B. B. (1949). Application of statistical methods to research and development in engineering. Review of the International Statistical Institute, 3, 129-135.

Davies, O. L., and Hay, W. A. (1950). The construction and uses of fractional factorial designs in industrial research. Biometrics, 6, 233-249.

Meyer, D. L. (1963). Response surface methodology in education and psychology. The Journal of Experimental Education, 31, 329-336.

Poulton, E. C. (1974). Tracking skill and manual control. New York: Academic Press.

Randle, R. J., Roscoe, S. N., and Petitt, J. (1980). Effects of accommodation and magnification on aimpoint estimation in a simulated landing task (Tech. Paper NASA-TP-1635). Washington, DC: National Aeronautics and Space Administration.

Roscoe, S. N. (1980). Aviation psychology. Ames, IA: Iowa State University Press.

Roscoe, S. N. (1982). Human factors affecting pilot performance in vertical and translational instrument flight: Phase II interim scientific report (Tech. Report BEL-82-2/ONR-82-2). Las Cruces, NM: New Mexico State University, Behavioral Engineering Laboratory.

Roscoe, S. N., and Eisele, J. E. (1980). Visual cue requirements in contact flight simulators. In S. N. Roscoe. Aviation psychology (pp. 217-226). Ames, IA: Iowa State University Press.

Roscoe, S. N., Hull, J. C., Simon, P. M., and Corl L. (1981). Human factors affecting pilot performance in vertical and translational instrument flight: Phase I interim scientific report (Tech. Report BEL-81-1/ONR-81-1). Las Cruces, NM: New Mexico State University, Behavioral Engineering Laboratory.

Roscoe, S. N., Tatro, J. S., and Trujillo, E. J. (1984). The role of human factors in VTOL aircraft display technology. DISPLAYS Technology and Applications, 5, 149-153.

Scanlan, L. A. (1975a). Apparent motion quality and target detection on a visually time-compressed display (Tech. Report ARL-75-16/AFOSR-75-6). Savoy, IL: University of Illinois at Urbana-Champaign, Aviation Research Laboratory.

Scanlan, L. A. (1975b). Visual time compression: Spatial and temporal cues. Human Factors, 17, 337-345.

Scanlan, L. A., and Roscoe, S. N. (1980). Time-compressed displays for target detection In S. N. Roscoe. Aviation psychology (pp. 108-124). Ames, IA: Iowa State University Press.

Simon, C. W. (1970). The use of central-composite designs in human factors engineering experiments (Tech. Report AFOSR-70-6). Culver City, CA: Hughes Aircraft Company.

Simon, C. W. (1973). Economical multifactor designs for human factors engineering experiments (Tech. Report P73-326A). Culver City, CA: Hughes Aircraft Company.

Simon, C. W. (1977). Design, analysis, and interpretation of screening studies for human factors engineering research. (Tech. Report CWS-03-77B). Westlake Village, CA: Canyon Research Group.

Tatro, J. S., Corl, L., and Roscoe, S. N. (1983). Human factors affecting pilot performance in vertical and translational instrument flight: Phase III technical report (Tech. Report BEL-83-1/ONR-83-1). Las Cruces, NM: New Mexico State University, Behavioral Engineering Laboratory.

Tatro, J. S., and Roscoe, S. N. (1985). An integrated display for vertical and translational flight: Eight factors affecting pilot performance. Human Factors, (in press).

Wilburn, N. T. (1963). Application of fractional factorials in screening of variables affecting the performance of dry process zinc battery electrodes. In S. S. Wilks. Proceedings of the Eighth Conference on the Design of Experiments in Army Research, Development, and Testing. Washington, DC: Walter Reed Army Institute of Research.

Williges, R. C., and Simon, C. W. (1971). Applying response surface methodology to problems of target acquisition. Human Factors, 13, 511-519.

DISTRIBUTION LIST

CAPT Paul R. Chatelier
Office of the Deputy Under Secretary
of Defense
OUSDRE (E&LS)
Pentagon, Room 3D129
Washington, DC 20301

Engineering Psychology Programs
Office of Naval Research
Code 442EP
800 North Quincy Street
Arlington, VA 22217-5000 (3 copies)

Aviation & Aerospace Technology
Programs
Code 210
Office of Naval Research
800 North Quincy Street
Arlington, VA 22217-5000

CAPT P. M. Curran
Code 270
Office of Naval Research
800 North Quincy Street
Arlington, VA 22217-5000

Information Sciences Division
Code 433
Office of Naval Research
800 North Quincy Street
Arlington, VA 22217-5000

CDR Kent S. Hull
Helicopter/VTOL Human Factors
Office
MS 239-21
NASA/Ames Research Center
Moffett Field, CA 94035

Special Assistant for Marine
Corps Matters
Code 100M
Office of Naval Research
800 North Quincy Street
Arlington, VA 22217-5000

Mr. R. Lawson
ONR Detachment
1030 East Green Street
Pasadena, CA 91106-2485

Director
Technical Information
Division
Code 2627
Naval Research Laboratory
Washington, DC 20375-5000

Naval Training Equipment
Center
ATTN: Technical Library
Orlando, FL 32813

Human Factors Department
Code N 71
Naval Training Equipment
Center
Orlando, FL 32813

Dr. Gary Poock
Operations Research
Department
Naval Postgraduate School
Monterey, CA 93940

Dr. A. L. Slafkosky
Scientific Advisor
Commandant of the Marine
Corps
Code RD-1
Washington, DC 20380

Dr. Michael Letsky
Office of the Chief of Naval
Operations (OP-01B7)
Washington, DC 20350

Professor Douglas E. Hunter
Defense Intelligence College
Washington, DC 20374

CDR C. Hutchins
Code 55
Naval Postgraduate School
Monterey, Ca 93940

Human Factors Technology
Administration
Office of Naval Technology
Code MAT 0722
800 North Quincy Street
Arlington, VA 22217-5000

CDR Tom Jones
Naval Air Systems Command
Human Factors Programs
NAVAIR 330J
Washington, DC 20361

Commander
Naval Air Systems Command
Crew Station Design
NAVAIR 5313
Washington, DC 20361

Aircrew Systems Branch
Systems Engineering Test
Directorate
U. S. Naval Test Center
Patuxent River, MD 20670

CAPT Robert Biersner
Naval Biodynamics Laboratory
Michoud Station
Box 29407
New Orleans, LA 70189

Dr. George Moeller
Human Factors Engineering
Branch
Naval Submarine Base
Submarine Medical Research Lab.
Groton, CT 06340

Head
Aerospace Psychology Department
Naval Aerospace Medical
Research Lab
Pensacola, FL 32508

Dr. Robert Blanchard
Code 17
Navy Personnel Research and
Development Center
San Diego, CA 92152-6800

LCDR T. Singer
Human Factors Engineering
Division
Naval Air Development Center
Warminster, PA 18974

Mr. Stephen Merriman
Human Factors Engineering
Division
Naval Air Development Center
Warminster, PA 18974

LT Dennis McBride
Human Factors Branch
Pacific Missile Test Center
Point Mugu, CA 93042

LCDR R. Carter
Office of Chief of Naval
Operations (OP-01B)
Washington, DC 20350

CDR W. Moroney
Naval Air Development Center
Code 602
Warminster, PA 18974

Human Factors Branch
Code 3152
Naval Weapons Center
China Lake, CA 93555

Dr. Eugene E. Gloye
ONR Detachment
1030 East Green Street
Pasadena, CA 91106-2485

Dr. Edgar M. Johnson
Technical Director
U.S. Army Research Institute
Alexandria, BA 22333-5600

Technical Director
U.S. Army Human Engineering
Laboratory
Aberdeen Proving Ground, MD 21005

Director, Organizations and
Systems Research Laboratory
U.S. Army Research Institute
5001 Eisenhower Avenue
Alexandria, BA 22333-5600

Dr. A. Fregly
U.S. Air Force Office of
Scientific Research
Life Science Directorate, NL
Bolling Air Force Base
Washington, DC 20332-6448

Mr. Charles Bates, Director
Human Engineering Division
USAF AMRL/HES
Wright-Patterson AFB, OH 45433

Dr. Earl Alluisi
Chief Scientist
AFHRL/CCN
Brooks Air Force Base, TX 78235

Dr. Edward R. Jones
Chief, Human Factors Engineering
McDonnell-Douglas Astronautics Co.
St. Louis Division
Box 516
St. Louis, MO 63166

Dr. Robert Wherry
Analytics, Inc.
2500 Maryland Road
Willow Grove, PA 19090

Dr. M. C. Montemerlo
Information Sciences &
Human Factors Code RC
NASA HQS
Washington, DC 20546

Dr. Stanley Deutsch
NAS-National Research Council
(COHF)
2101 Constitution Avenue, N.W.
Washington, DC 20418

Defense Technical Information
Center
Cameron Station, Bldg. 5
Alexandria, VA 22314
(12 copies)